Jurassic belemnite geochemistry from Cabo Mondego (Bajocian-Bathonian, Portugal) and Albstadt-Pfeffingen (Bathonian-Callovian, Germany)

Submitted by Jack Thomas Rhodes Wilkin to the University of Exeter

as a thesis for the degree of

Master of Research in Geology

In July 2021

Word count: 19,140

I certify that all material in this thesis which is not my own work has been identified and that no material has previously been submitted and approved for the award of a degree by this or any other University.

Signature: 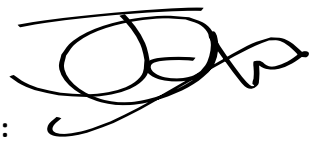

Contribution Statements

List of techniques, equipment and persons who contributed to this work.

Technique	Equipment	Who?	Location
Collection of Material (Cabo Mondego)	-	Christoph Korte, Maria Paulsen, Micha Ruhl, Ricardo Silva, Clemens Ullmann, Madeleine Vickers, Iben Winter, Weimu Xu.	Cabo Mondego
Collection of Material (Albstadt-Pfeffingen)	-	Christoph Korte, Malgorzata Rizzi, Gerd Dietl	Albstadt-Pfeffingen
Cathodoluminescence	Cold Cathodoluminescence Microscope	Jack Wilkin	University of Exeter, Chemical, Imaging & Mineralogical Facility
Trace Element Analysis	Agilent 5110 VDV Inductively Coupled Optical Emission Spectrometer	Clemens Ullmann, Jack Wilkin	University of Exeter, Wet Chemistry Lab
Stable Isotope Analysis	Sercon 20-22 Gas Source Isotope Ratio Mass Spectrometer	Clemens Ullmann, Jack Wilkin	University of Exeter, Stable Isotope Facility
Strontium Isotope Analysis	Sector VG 54 TIMS	Malgorzata Rizzi	University of Copenhagen
Brachiopod Data	Mass Spectrometer and ICP-OES	Maria Paulsen	University of Copenhagen
Data Interpretation	-	Jack Wilkin	-

Abstract

Here, I have investigated the stable isotope ($\delta^{13}C$, $\delta^{18}O$) and elemental composition (Mg/Ca, Sr/Ca, Fe/Ca, Mn/Ca) of Jurassic belemnites from Cabo Mondego in Portugal (Bajocian-Bathonian) and Albstadt-Pfeffingen in southern Germany (Bathonian-Callovian). Both localities are stratigraphically significant, with Cabo Mondego representing the Auxiliary Stratotype Section and Point (ASSP) for the Bathonian Stage and Albstadt-Pfeffingen being a potential Global Stratotype Section and Point (GSSP) for the Callovian Stage.

Variations in the stable carbon-isotope ratios of macrofossil calcite can reflect changes in fluxes between reservoirs in the palaeo carbon cycle. Cabo Mondego is an important site to link changes in stable isotope ratios directly to ammonite zones and subzones, and thereby allow chronostratigraphic calibration. An abrupt positive $\delta^{13}C$ isotope shift is observed in the belemnite stable isotope record from the *bomfordi* Subzone below the Bajocian-Bathonian boundary. The $\delta^{13}C$ shift appears not to have been caused by temperature changes as $\delta^{18}O$ ratios remain stable throughout the studied section, nor is there a change in the $\delta^{13}C$ values of coeval brachiopods. One possible cause of this shift in carbon-isotope ratios is a faunal turnover. Faunal turnovers of ammonites and belemnites are observed elsewhere in Europe within the *bomfordi* Subzone.

The potential of the Jurassic section at Albstadt-Pfeffingen (Baden-Württemberg, Germany) to become a GSSP, an internationally agreed reference point which defines the lower boundary of a stage on the geologic timescale, for the base of the Middle Jurassic Callovian Stage, makes detailed investigations, especially regarding the completeness of the strata, important. The ammonite assemblages of this section have already been studied in detail, but few chemostratigraphic data from the Bathonian and Lower Callovian fossils of the site have been published. Belemnite rostra are relatively abundant in the section and have undergone little diagenetic alteration according to chemical and optical screening techniques, making them a suitable target for isotopic analysis. Chemostratigraphic signals in the rostra across the Bathonian-Callovian boundary show comparatively little change in $\delta^{13}C$ values, but a gradual decrease in $\delta^{18}O$ may indicate a warming trend into the Callovian. Notably, a distinct step-change in $^{87}Sr/^{86}Sr$ ratios across the stage boundary suggests an unconformity, or at least strongly condensed part of the section, confirming strong doubts on the site's suitability as a GSSP.

Acknowledgements

The author would like to thank:

Professor Stephen P. Hesselbo (Camborne School of Mines) and Dr Clemens V. Ullmann (Camborne School of Mines) for being my project supervisors during my time at the University of Exeter and helping me with this research.

Dr Sev Kender (Camborne School of Mines and British Antarctic Survey) for allowing me to work as a Postgraduate Teaching Assistant on the first-year undergraduate Palaeontology and Stratigraphy unit and allowing me to work on sediment cores from West Antarctica which will become the basis of future PhD research.

Stephen Pendray (Camborne School of Mines) for making the thin section slides.

Dr Sam Broom-Fendley (Camborne School of Mines) for teaching me how to do cathodoluminescence microscopy and Dr Gavyn Rollinson for helping with laboratory access, especially during the Covid-19 Pandemic.

Professor Christoph Korte (University of Copenhagen) for providing the belemnites from Albstadt-Pfeffingen.

Dr Malgorzata Rizzi (University of Copenhagen) and Dr Gerd Dietl (Staatliches Museum für Naturkunde Stuttgart) for helping with Albstadt-Pfeffingen.

Dr Micha Ruhl (Trinity College Dublin) and Dr Maria Helena Henriques (University of Coimbra) for helping with Cabo Mondego.

Professor James McArthur (University College London) for providing the LOWESS FIT 5 curve.

Dr Alena Ebinghaus (University of Aberdeen), Wendell Ricketts (Fossil News), Mike Fredericks (Prehistoric Times), Jon Trevelyan (Deposits Magazine) and Peter Doyle (Geology Today) for publishing my articles.

Contents

List of Figures 6
List of Tables 9
Aims/Objectives of Research 10
Chapter 1 Introduction 11
1.1 The Rostrum 11
1.2 $\delta^{18}O$ 15
1.3 $\delta^{13}C$ 20
1.4 Pitfalls in Belemnite Geochemistry for Palaeoenvironmental Reconstruction. 24
1.4.1 Scatter in Geochemical Proxies 24
1.4.2 Salinity 25
1.4.3 Vital Effects and Fractionation (oxygen) 26
Chapter 2: Geological Settings 29
2.1 Cabo Mondego 29
2.1.1 Sedimentology and Palaeoenvironments 29
2.1.2 Stratigraphic Significance 30
2.1.3 Palaeontology 32
2.1.4 Previous Geochemical Work 33
2.2 Albstadt-Pfeffingen 33
2.2.1 Sedimentology and Palaeoenvironment 33
2.2.2 Global Boundary Stratotype Section and Points 35
2.2.3 Stratigraphic Significance 37
2.3.4 Palaeontology 38
Chapter 3: Methodology 39
3.1 Rationale 39
3.2 Sample Collection 39
3.2.1 Sample Collection (Cabo Mondego) 39
3.2.2 Sample Collection (Albstadt-Pfeffiengen) 41
3.3 Laboratory Techniques 44
3.3.1 Sample Preparation 44
3.3.2 Cathodoluminescence and Petrography 45
3.3.3 Elemental Analyses 45
3.3.4 Oxygen and Carbon Isotopes 46
3.3.5 $^{87}Sr/^{86}Sr$ Ratios 48
Chapter 4: Results 49
4.1 Cabo Mondego 49
4.1.1 Carbon and Oxygen Isotopes 49
4.1.2 El/Ca Ratios 52

4.1.3 Belemnite Rostrum Cross-section Measurements (Cabo Mondego) 56
4.2 Albstadt-Pfeffingen 59
4.2.1 Carbon and oxygen isotopes 59
5.2.2 El/Ca Ratios 62
4.2.3 Cathodoluminescence and Petrography 64
4.2.4 $^{87}Sr/^{86}Sr$ Ratios 66
Chapter 5: Sample Preservation 67
5.1 Elemental Contamination 67
5.1.1 Alternation Indicators 67
5.1.2 El/Ca Ratios (Cabo Mondego) 68
5.1.3 El/Ca Ratios (Albstadt-Pfeffingen) 70
5.2 Cathodoluminescence and Petrology 72
Chapter 6: Discussion 73
6.1 Carbon Isotope Excursion at Cabo Mondego. 73
6.1.2 Hypothesis 2: Faunal Turnover 74
6.2 Strontium stratigraphy at Albstadt-Pfeffingen 77
6.2.1 Strontium Chemostratigraphy 77
6.2.2 $^{87}Sr/^{86}Sr$ Values During the Middle Jurassic 79
6.2.3 Step Change in Strontium Data 80
6.2.4 Disparity with Previous Work 82
6.3 Mg/Ca and Sr/Ca as Palaeothermometers 84
6.4 Middle Jurassic Climates 90
6.4.1 Palaeotemperatures 90
6.4.2 Carbon Isotope Trend 94
Chapter 7: Conclusions 97
References 98

List of Figures

Figure 1.1: Diagram showing belemnite anatomy. Author's own work…11

Figure 1.2: Close up of belemnite rostrum from Albstadt-Pfeffingen (specimen: APF-118) in thick section (50 µm) showing the radially orientated fibrous calcite crystals. Author's own work. Scale bar: 0.5 mm…13

Figure 1.3: Thick section (50 µm) of a belemnite rostrum from Albstadt-Pfeffingen (specimen APF-105) clearly showing the growth rings. Author's own work. Scale bar: 1 mm....13

Figure 1.4: Comparison of $\delta^{18}O_{seawater}$ values from recent Atlantic and Pacific oceans. From Hoefs (2009, p. 146), originally from Delaygue *et al* (2000)…19

Figure 1.5: $\delta^{13}C$ gradient at different water depths depending on C fractionation in surface waters and subsequent remineralization on the way to the seafloor. From Wilkin (2018)...23

Figure 2.1: The stratigraphy of the Cabo Mondego Formation. Unpublished graphic by Micha Ruhl…31

Figure 2.2: (A) the Aalenian-Bajocian GSSP and (B) the Bajocian-Bathonian ASSP. Photograph by Maria Helena Henriques. From Rocha *et al*. (2014)…31

Figure 2.3: Lithology of Albstadt-Pfeffingen. Redrawn from Callomon and Dietl (1990)…34

Figure 2.4: The ammonite *Kepplerites* (*Kepplerites*) *aigii* (specimen SMNS-70349(; a) ventral view; b) lateral view, from Albstadt-Lautlingen, a site closely associated with Albstadt-Pfeffingen. From Mönnig and Dietl (2017)...38

Figure 3.1: Ammonite biostratigraphy from Cabo Mondego (Section 2). Taken from Fernández-López *et al*. (2006a)…40

Figure 3.2: Middle Jurassic geology of southern Germany. A star indicates the location of the studied section. Redrawn from Dimter and Smelror (1990). Insert shows global palaeogeography of the Middle Jurassic modified from Ullmann *et al*. (2013a)…41

Figure 3.3: Field photograph showing the collection area matched to lithostratigraphy from field notes provided by Christoph Korte. The *keppleri* Horizon is subdivided into the higher (h.) and lower (l.) *keppleri*…42

Figure 3.4: The lithology of the studied section used in this paper (right) compared to the original Albstadt-Pfeffingen beds (left) redrawn from Callomon and Dietl (2000) and Beher *et al*. (2010)…43

Figure 3.5: Stratigraphic positions of belemnites that were analysed at the Camborne School of Mines (Cornwall, Penryn) for minor elements and stable isotopes…44

Figure 4.1: Stable isotope data from belemnite calcite, Cabo Mondego, Portugal showing positive $\delta^{13}C$ shift in belemnite data, but no such carbon isotope excursion can be observed in the coeval brachiopod data. Lithographical succession based on Fernández-López *et al*. (2006a). Unpublished graphic provided by Dr Micha Ruhl…51

Figure 4.2 Correlations between $\delta^{13}C$ and $\delta^{18}O$ from Cabo Mondego. Y-axis = $\delta^{13}C$; X-axis = $\delta^{18}O$. A) entire section; B) pre-carbon isotope excursion (correlative coefficient = 0.04); C) post-carbon isotope excursion showing a weak negative correlation (correlative coefficient = -0.35)…52

Figure 4.3: Cross plot showing belemnite rostrum "circularity" throughout the studied section. The rostrum become more oval after the carbon isotope excursion (cf. Figure 4.1)…56

Figure 4.4: Cross plot of $\delta^{18}O$ values and circularity index Belemnites with higher $\delta^{13}C$ values have less circular rostrum cross sections. Correlation coefficient = -0.75…56

Figure 4.5: Cross plot of $\delta^{18}O$ values and circularity index. (Top) there is very weak correlation between $\delta^{18}O$ values and the rostrum "circularity (correlation coefficient = 0.33). (Bottom) when low $\delta^{18}O$ values, those <-1.5, the correlation coefficient increases to 0.63…58

Figure 4.6: Profile of the studied section across the Bathonian-Callovian boundary showing $\delta^{18}O$, $\delta^{13}C$ and $^{87}Sr/^{86}Sr$ ratios. $^{87}Sr/^{86}Sr$ ratios show a noticeable decrease at the bottom of the l*. keppleri* Horizon, which may represent a possible unconformity, while $\delta^{13}C$ values show little variation, a gradual trend of decreasing $\delta^{18}O$ values can also be observed…59

Figure 4.7: Cross plot of $\delta^{18}O$, and $\delta^{13}C$ values showing possible, though weak, positive correlation which may be caused by fractionation due to water depth. correlation coefficient = 0.37…61

Figure 4.8: Light microscope (left) and cathodoluminescence (right) photographs of three belemnite rostra (A. APF-105; B. APF-108; C. APF-118) from Albstadt-Pfeffingen. Areas with the most diagenetic alternation, shown in yellows and oranges, are found along the margins, apical region, and prominent cracks and growth bands. Scale bar = 1mm…65

Figure 5.1: Specimens from the lower part of the section are more prone to elevated Mn and Fe ratios but no such trend is observed in Sr/Ca ratios at Cabo Mondego…68

Figure 5.2: Scatterplots of oxygen isotope ratios versus Fe/Ca (correlation coefficient = -0.25) and Mn/Ca ratios (correlation coefficient = -0.63). $\delta^{18}O$ results above the diagenetic cut off point of Mn/Ca >0.2 mmol/mol were excluded from later analysis. A strong negative correlation between Mn/Ca and $\delta^{18}O$ values suggests that both were changing as a response to diagenetic overprinting and is, potentially, more reliable for identifying diagenesis in the studied section. A potential diagenetic trend in Mn/Ca is based on an observation made in Korte and Hesselbo (2011)…70

Figure 5.3: (A) Scatterplots of oxygen isotopes versus Fe/Ca concentrations (correlation coefficient = 0.29). The diagenetic cut-off point of Fe/Ca for samples was 1.0 mmol/mol. (B) Scatterplots of oxygen isotopes versus Mn/Ca concentrations (correlation coefficient = -0.03). The diagenetic cut-off point of Mn/Ca for samples was 0.2 mmol/mol…71

Figure 5.4: Fe/Ca compared to stratigraphy at Albstadt-Pfeffingen. The increase in Fe/Ca between 8-12 cm below the top of the *keppleri* Subzone can likely be explained by an increase in iron content in the sediment...72

Figure 6.1: Matching results of belemnite $^{87}Sr/^{86}Sr$ ratios from Albstadt-Pfeffingen and Wierzbowski *et al*. (2017) with LOWESS Fit 5 data for Jurassic strontium-isotope data. The significant step-change in $^{87}Sr/^{86}Sr$ values between 28 and 21 cm may indicate an unconformity…80

Figure 6.2: Rate of change in seawater $^{87}Sr/^{86}Sr$ ratio per 1 Ma during the Middle-Late Jurassic. Redrawn from Wierzbowski *et al.* (2017)…82

Figure 6.3: Measured $^{87}Sr/^{86}Sr$ ratios from Albstadt-Pfeffingen in belemnites around the Bathonian-Callovian boundary. From Callomon and Dietl (2000)…83

Figure 6.4: Sections of Upper Bathonian and Lower Callovian beds in southern Germany; Klingenbachtal near Bisingen-Thanhein, Zollernalb, modified after Dietl (1981), Albstadt-Pfeffingen, village centre, construction pit 1986, modified after Dietl (1990), Achalm near Eningen, Alte Steige, modified after Terzidis (1966) and Buck *et al*. (1966). Abbreviations: *FK: Fuscus Bank (Lower Bathonian); MO: Macrocephalenoolith; BM: Basis-Mergellage* (Upper Bathonian). Redrawn from Mönnig and Dietl (2017)…84

Figure 6.5: Cross-plots of Mg/Ca and Sr/Ca against and $\delta^{18}O$ for Pliensbachian–Toarcian belemnites from Yorkshire of the UK (data of McArthur *et al*., 2000), southern Germany (data from Bailey *et al*., 2003) and northern Spain (data from Rosales *et al*., 2004a). From Li (2011)…86

Figure 6.6: Cross plots of Sr/Ca and Mg/Ca versus $\delta^{18}O$ values from Cabo Mondego and Albstadt-Pfeffingen…88

Figure 6.7: A). Mg/Ca ratios versus $\delta^{18}O$ values of well-preserved belemnite rostra shows no correlation between Mg/Ca ratios and $\delta^{18}O$ values. B). No correlation is observed between Sr/Ca and $\delta^{18}O$. However, when data from different taxa are combined, it can give a false correlation. Diamonds= *Hibolithes sp.*, circular= *Cylindroteuthis sp.*, square= *Lagonibelus sp*. From Wierzbowski and Rogov (2010)…89

Figure 6.8: Palaeotemperature estimates from Cabo Mondego (orange), the Polish Jura Chain (grey), and Albstadt-Pfeffingen (blue). Polish data taken from Wierzbowski and Joachimski (2007) and stratigraphy based on Wierzbowski *et al*. (2017)…94

Figure 6.9: $\delta^{13}C$ values from Cabo Mondego (blue), the Polish Jura (grey), and Albstadt-Pfeffingen (orange). Polish data taken from Wierzbowski and Joachimski (2007) and stratigraphy based on Wierzbowski *et al*. (2017)…96

List of Tables

Table 1: Description of the different elements of the belemnite rostrum…12

Table 2: Requirements for establishing a GSSP revised from Remane *et al*. (1996) according to the International Commission on Stratigraphy (ICS) procedures. Adapted from Gradstein and Ogg (2012)…36

Table 3: Standards used for elemental analysis…47

Table 4: Stable isotope data from Cabo Mondego…50-1

Table 5: Minor element data from Cabo Mondego…53-5

Table 6: Gas source IRMS standards from Cabo Mondego. Abbreviations: *CAR = Carrara Marble; NCA = Namibia Carbonatite*…55

Table 7: Belemnite "circularity". The closer to 1 the specimens cross-section than the more circular the rostrum cross section…57

Table 8: Stable isotope data ($\delta^{13}C$ and $\delta^{18}O$) from Albstadt-Pfeffingen. Top of *kep.* refers to the *keppleri* Horizon…60

Table 9: Gas source data from Albstadt-Pfeffingen. Abbreviations: *CAR = Carrara Marble; NCA = Namibia Carbonatite.* Highlighted gas was lost, caused fractionation so was therefore excluded…61

Table 10: Minor element data from Albstadt-Pfeffingen. Top of *kep.* refers to the *keppleri* Horizon…62-4

Table 11: Strontium isotope data and associated minor elements from Albstadt-Pfeffingen. Analysis performed at the University of Copenhagen by Dr Malgorzata Rizzi…66

Table 12: Element incorporation into belemnite calcite. Mn^{2+} and Fe^{2+} can substitute for Ca^{2+} only under post-oxic/anoxic conditions so also indicate alternation. From Li (2011)...67

Aims/Objectives of Research

This research investigates the stratigraphy and palaeoclimate for the Middle Jurassic of south Germany and Portugal, principally via stable isotopes and elemental proxies derived from belemnite rostra.

To achieve this aim the following objectives were accomplished:

1. Evaluate the use of belemnites, stable isotope and elemental/Ca ratios as palaeoclimatic indicators.
2. Execute a palaeogeographical and sedimentological overview of the Cabo Mondego and Albstadt-Pfeffingen sections.
3. Obtain stable isotopes ($\delta^{13}C$ and $\delta^{18}O$) and trace elements (Sr, Mn, Fe, S, and P) from belemnite rostra from both localities.
4. Discuss the positive carbon isotope excursion at Cabo Mondego.
5. Discuss the GSSP at Albstadt-Pfeffingen.
6. Discuss the validity of Mg/Ca and Sr/Ca from Middle Jurassic belemnite calcite as a palaeo-proxy palaeotemperature proxy.
7. Produce palaeotemperature estimates for each site based on $\delta^{18}O$ data.

Chapter 1 Introduction

Belemnites (Belemnitida) are marine cephalopods that lived during the Mesozoic. Although the typical belemnite best resembles the extant squid *Loligo,* modern squids possess a flexible, unmineralised internal skeleton composed of chitin called a gladius. Belemnites, in contrast, had an inflexible bullet-shaped calcified internal skeleton consisting of 3 parts: a rostrum or guard to the posterior (the term rostrum will be used throughout this work), the phragmocone in the middle, and the pro-ostracum to the anterior (Figure 1.1; Hoffmann and Stevens, 2020).

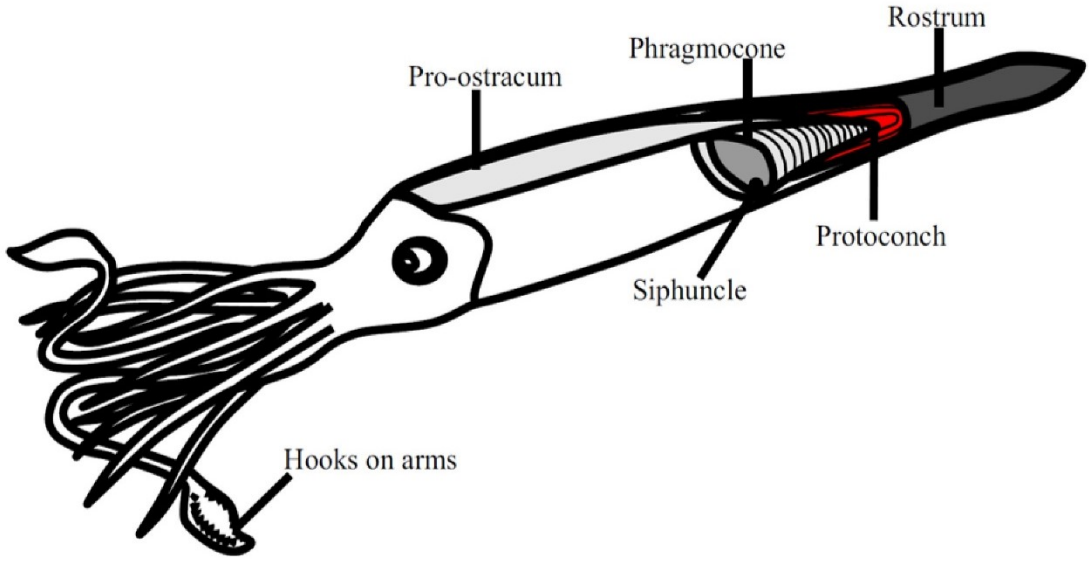

Figure 1.1: Diagram showing belemnite anatomy. Author's own work.

1.1 The Rostrum

The rostrum was a bullet-shaped cylinder of solid calcite which tapered posteriorly to a point and was indented anteriorly by the alveolus, a conical cavity that housed the phragmocone (Clarkson, 1993). The rostrum is made of low-Mg calcite, a mineral relatively resistant to diagenetic alteration, making them ideal for geochemical research (Veizer, 1983; Ullmann and Korte, 2015). The rostrum was the largest and most posterior part of the belemnite internal skeleton and is the most preserved part of the animal. The rostrum, therefore, is the most significant part of the belemnite skeleton for systematics. The rostrum likely acted

as a counterbalance to the head and arms while swimming (Doyle, 1985; Monks *et al*., 1996). The surface of the rostrum is generally smooth and unornamented though some genera had granulated surfaces (Clarkson, 1993). The different components of the rostrum are listed and described in Table 1.

Table 1: Description of the different elements of the belemnite rostrum.

Element	Description
Alveolus	Conical region at the anterior of the rostrum housing the phragmocone
Apex	Most posterior part of the rostrum
Apical line	The axis of the rostrum marking the position of the apex during successive growth stages
Grooves	Depressions on the surface of the rostrum
Radial structures	Radiating arrangement of fibrous calcite crystals

When the rostrum is broken transversely, the internal structure can be observed. The rostrum is composed of radially orientated fibrous calcite crystals arranged at right-angles to the surface, radiating from the central zone of the apical line (Ullmann *et al*., 2015; Benito *et al*., 2016; Figure 1.2). Concentric patterns, also observed in horizontal cross-sections, are interpreted as growth rings (Figure 1.3). The paler layers are made up of nearly pure calcite, but the darker layers are discoloured by the presence of organic matter (e.g., Müller-Stoll, 1936; Sælen, 1989; Hoffmann *et al*., 2016). The axis of this growth, shown by the apical line, is not in the centre of the rostrum but is instead placed towards the ventral margin (Clarkson, 1993), making it possible to orient the rostrum.

These growth rings were described by Müller-Stoll (1936) as “laminae pelucidae” and “laminae obscurae”, referring to the successions of clear calcite and intermittent growth boundaries separating them. The two terms, “laminae pelucidae” and “laminae obscurae”, were later replaced by Sælen (1989) with growth rings/lines as Sælen hypothesised that these “rings” may represent

seasonal growth bands – however they may also represent feeding patterns or be related to stress, so further research is needed. Oxygen isotope ($\delta^{18}O$) measurements across these bands have been interpreted as seasonal variations in temperature (Urey *et al*., 1951). Based on the assumption of daily formation of growth increments, Wierzbowski (2013) postulated a one-year life span for mesohibolitid belemnites, comparable to those of extant coleoids, and one or two years for the larger *Megateuthis* (Dunca *et al*., 2006).

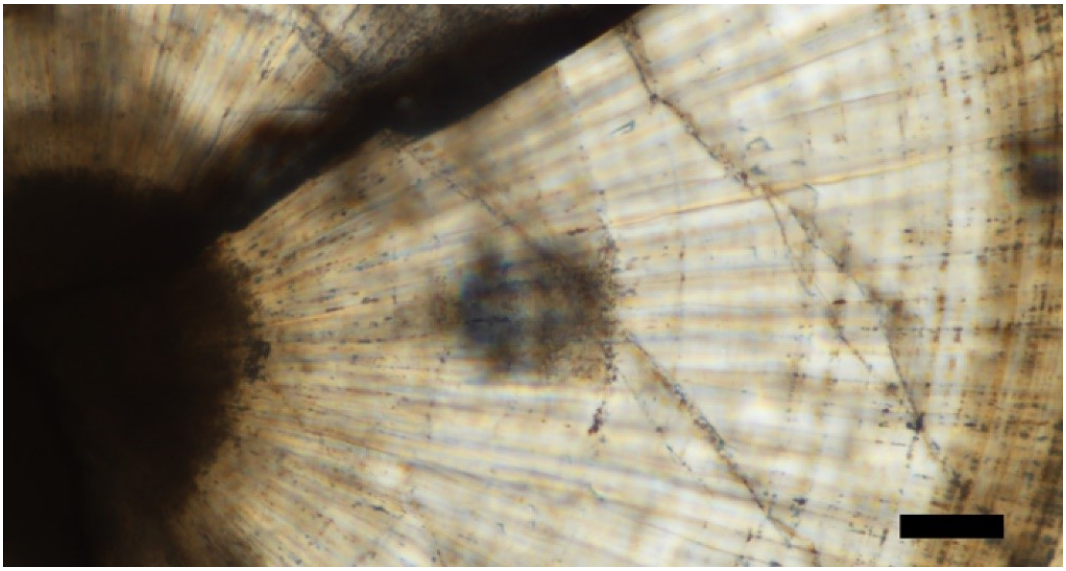

Figure 1.2: Close up of belemnite rostrum from Albstadt-Pfeffingen (specimen: APF-118) in thick section (50 µm) showing the radially orientated fibrous calcite crystals. Author's own work. Scale bar: 0.5 mm.

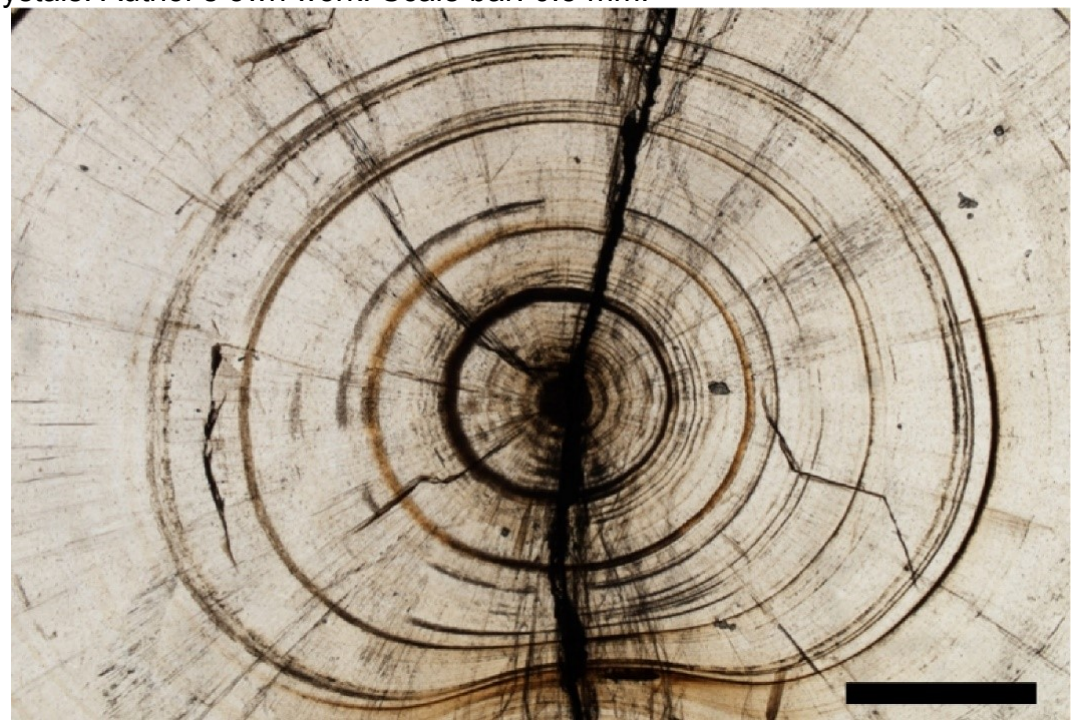

Figure 1.3: Thick section (50 µm) of a belemnite rostrum from Albstadt-Pfeffingen (specimen APF-105) clearly showing the growth rings. Author's own work. Scale bar: 1 mm.

However, a contrasting hypothesis states that the concentric rings resulted from the post-mortem decay of organic matter (Sælen, 1989). Scanning Electron Microscope studies (Veizer, 1974; Sælen, 1989) have suggested that belemnite rostra originally formed as radial low-Mg calcite crystals with variable amounts of organic matter within individual crystals in a pattern resembling that of concentric rings. After death it is hypothesized that the organic matter decayed, leaving behind void space, which was then infilled by secondary calcite (Sælen, 1989). Later authors (e.g., Hoffmann *et al*., 2016) hypothesized that the rostrum was not comprised of distinct types of alternating laminae, but rather small changes in organic matter content.

Spaeth (1971, 1973, 1975) reported non-mineralised, organic and porous parts in the belemnite rostrum suggesting that belemnite rostra had a sponge-like ultrastructure, with primary porosity of up to 20%, comparable to the cuttlebone of *Sepia*. Other authors also found evidence of primary porosity in belemnite rostra, with both Veizer (1974) and Bandel and Spaeth (1988) reporting 10% primary porosity. Geochemical analysis by Ullmann *et al.* (2015) reported 40% porosity along the central area of the belemnite rostrum near the apical line. Moreover, Hoffmann *et al*. (2016) argue for as much as 50-90% primary porosity for the bulk of the belemnite rostrum.

In contrast to the generally accepted notion that the belemnite rostrum was made of calcite, several authors (e.g., Kabanov, 1967; Dauphin, 1984; Dauphin *et al*., 2007) have questioned the mineralogy of the belemnite rostrum, instead proposing that it was originally made of aragonite, a more unstable form of calcium carbonate ($CaCO_3$), and later transformed into calcite. It is noted by several authors (e.g., Martín-García *et al.,* 2019, and references therein), that the unstable nature of aragonite is susceptible to diagenetic transformation into the more stable calcite, which leads to mineralogical, textural, and geochemical alterations. Despite the debate surrounding the original composition of the belemnite skeleton (see Dauphin, 1984; Dauphin *et al*., 2007), most authors (e.g., Hall and Kennedy, 1967; Wierzbowski and Joachimski, 2009; Ullmann *et al.,* 2015 and others) now agree that the rostrum was originally calcite while the phragmocone was made of aragonite (Richter *et al.,* 2011).

1.2 $\delta^{18}O$

Oxygen (O), by mass, is the most abundant element on Earth, forming the most common components of the hydrosphere, biosphere, and lithosphere. Oxygen naturally occurs, with decreasing abundance, as one of three stable isotopes: ^{16}O (99.755%), ^{18}O (0.206%), and ^{17}O (0.039%); Schoeller, 1999; Faure and Mensing, 2005; Pederzani and Britton, 2018). It is the ratio of ^{18}O to ^{16}O that is usually used in palaeoclimatological studies which is reported as $\delta^{18}O$.

Temperature is a primary representation of the state of the climate, and the temperature of the oceans is critical as the oceans are the single most important component of the Earth's climate system. Oxygen isotope analyses of marine carbonate fossils could substantiate the modelled palaeoclimate evolution by providing palaeotemperature data. Geochemical systems used for calculating palaeotemperatures are called palaeothermometers (e.g. Urey *et al.,* 1951*; Veizer*, 1974; Podlaha *et al.,* 1986; Popp *et al*., 1986; Veizer *et* al., 1986; Anderson *et al*., 1994; Carpenter and Lohmann, 1995; Showers *et al*., 2002; Brand *et al*., 2003, 2013; Bailey *et al*., 2003; Rosales *et* al., 2004a,b; Hesselbo *et al*., 2007; McArthur *et al*., 2007 a,b; Wierzbowski and Joachimiski, 2007; 2009; Li *et al*., 2011, 2012, 2013; Ullmann *et al.,* 2013a,b, 2015, 2017; Ullmann and Korte, 2015; and others).

The ratio of ^{16}O and ^{18}O in biogenic calcite is a function of the isotopic composition of the ambient water, its temperature and potential isotopic disequilibrium effects during calcite formation (Ullmann *et al*., 2015). The ratio of ^{16}O to ^{18}O decreases as both temperatures and evaporation rates increase. In general, an increase in temperature of a little more than 4°C corresponds to a reduction in $\delta^{18}O$ of about 1‰ in an ocean with constant isotopic composition of the water (Shackleton, 1987; Bender, 2013).

Because the oxygen isotopic proxy is based on thermodynamic principles, we expect it to be relatively unaffected by secondary kinetic factors. However, there are reasons to suspect that other non-temperature dependent factors such as ontogenetic variations and seawater carbonate ions can affect the isotope ratios (see Lea, 2003). Despite such issues, oxygen isotope ratios are one of the most widely used and reliable palaeotemperature proxies (Faure and Mensing,

2005 and references throughout). Isotope ratios of oxygen are typically expressed using the Delta notation normally with the Standard Mean Ocean Water as a reference. The standard used for $\delta^{18}O$ in carbonate is however the Vienna Pee Dee belemnite (VDPB; see Brand *et al.,* 2014).

The fractionation factor describes isotopic fractionation between minerals and water (α; Faure and Mensing, 2005):

$$\alpha(A-B)=\frac{R_A}{R_B}$$

R is the isotopic ratio (e.g., $^{18}O/^{16}O$ or $^{13}C/^{12}C$) and *A* and *B* are the mineral and water. The following equation is used to calculate the δ-value of oxygen (Faure and Mensing, 2005):

$$\delta^{18}O=\left(\frac{\left(\frac{^{18}O}{^{16}O}\right)_{Sample}}{\left(\frac{^{18}O}{^{16}O}\right)_{standard}}-1\right)*1000$$

The $\delta^{18}O$ and $\delta^{13}C$ values are measured in units per thousand, or 'per mil' (‰), relative to the standard (Grossman, 2012a, b). For example, a $\delta^{18}O$ value of 1.0‰ means that the sample has an $^{18}O/^{16}O$ ratio that is 0.1% greater than the standard, or a $\delta^{13}C$ value of -25‰ means that the sample has a $^{13}C/^{12}C$ ratio that is 2.5% lower than that of the standard (Ravelo and Hillaire-Marcel, 2007).

Some fossil groups, principally marine forms, with skeletal elements composed of calcium carbonate, can be used to measure, rather than interpret, palaeotemperatures directly. $CaCO_3$ and phosphates combine dissolved inorganic carbon in the form of bicarbonate (HCO_3^-) from the water to make their shells, skeletons, and tests in a process called marine biogenic calcification using the following equation (Zondervan *et al.,* 2001):

$$Ca^{2+}_{(aq)} + 2HCO_3^-{}_{(aq)} \rightarrow CaCO_{3(s)} + CO_2 + H_2O$$

The oxygen isotopic composition ($\delta^{18}O$) of marine biogenic calcite is presumed to reflect calcification temperature, and the isotopic composition of the

ambient seawater at the time the organism lived. Whereas the tests of planktonic and benthic foraminifera and the hard parts of coccoliths are essential sources for stable isotopes from open marine environments throughout the Cenozoic and beyond (see Zachos *et al.,* 2001), much of what is known about Mesozoic, particularly Jurassic and Cretaceous, palaeoceanography has been inferred from the calcareous rostra of belemnites. Belemnite research in Mesozoic marine successions has concentrated on the calcitic rostrum, therefore, more likely to preserve the original isotopic signature from the Jurassic and Cretaceous (e.g., Veizer, 1974; Dutton *et al.,* 2007; Li *et al.*, 2012, 2013; Ullmann *et al*., 2015, 2017 and others).

Recent cephalopods secrete their calcite close to isotopic equilibrium with ambient seawater (e.g., Taylor and Ward, 1983; Rosales *et al*., 2004b; Rexfort and Mutterlose, 2006). However, McArthur *et al.* (2000) concluded that since belemnites are extinct, it is unrealistic to calculate absolute palaeotemperatures from their $\delta^{18}O$ values. Temperature changes related to migrations and seasonal variations can also be detected using oxygen isotopes (Rexfort and Mutterlose, 2006, 2009), hence the importance of acquiring multiple samples from the same specimen.

Calcite fossils have played an essential role in palaeoenvironmental studies since Urey *et al.* (1947) first proposed that past ocean water temperatures could be reconstructed using a carbonate-based oxygen isotope thermometer. Belemnite $\delta^{18}O$ was first employed as a palaeothermometer by Urey *et al.* (1951) using the palaeotemperature equation developed in Epstein *et al.* (1953). The specimens used in Urey *et al*. (1951) were judged to be well-preserved by the authors. However, the belemnites used in that study appear to have undergone significant diagenesis as the author sampled pristine calcite but also prominent growth bands (Urey *et al.,* 1951), sites that are now known to be highly susceptible to diagenetic alteration. In our study, prominent growth bands were avoided with samples taken from only the pristine calcite between the concentric bands. Therefore, the palaeotemperature estimates presented by Urey *et al.* (1951) and their interpretation that cyclical isotopic signatures represented seasonal temperature variations is questionable, and the $\delta^{18}O$ data may suggest a diagenetic rather than an environmental/climatic origin for this cyclicity.

The three pre-requirements of using $\delta^{18}O$ derived palaeotemperatures are outlined by Spaeth *et al*. (1971) and Stevens and Clayton (1971):

1). The equilibrium fractionation of oxygen isotopes is achieved between belemnites and ambient water.

2) The rostrum must be well-preserved enough to be able to retain the primary palaeo-environmental signals.

3) The isotopic composition of the original seawater should be known.

The first point can be defended based on the study of cuttlefish (Rexfort and Mutterlose, 2006). For the second point, diagenesis can be well-constrained by applying petrographic, cathodoluminescence, and elemental analysis, which will be discussed later. And thirdly, the $\delta^{18}O_{seawater}$ in which the belemnites once lived is difficult to assess accurately. Because the Mesozoic has generally been thought of as ice-free, a $\delta^{18}O_{seawater}$ of -1‰ SMOW is widely used (Shackleton and Kennet, 1975; Pirrie and Marshall, 1990). However, in recent years, the theory of an entirely ice-free Mesozoic has been challenged by several authors (e.g., Price, 1999; Korte *et al*., 2015).

Furthermore, chemical studies on the Atlantic and Pacific Oceans (e.g., Delaygue *et al*., 2000) have found that the surface water $\delta^{18}O$ values shift with latitude with the mid latitudes having higher $\delta^{18}O$ than the high latitudes (Figure 1.4). Delaygue *et al.* (2000) used an oceanic general circulation model to determine a relationship between $\delta^{18}O_{seawater}$ values and surface water salinity. Because Mesozoic $\delta^{18}O_{seawater}$ values might have varied similarly, it can be assumed that an average value of -1‰ SMOW would not be representative for a wide range of palaeolatitudes. This insufficient knowledge of Mesozoic seawater $\delta^{18}O$ values brings some uncertainty regarding belemnite reliability as a palaeotemperature proxy.

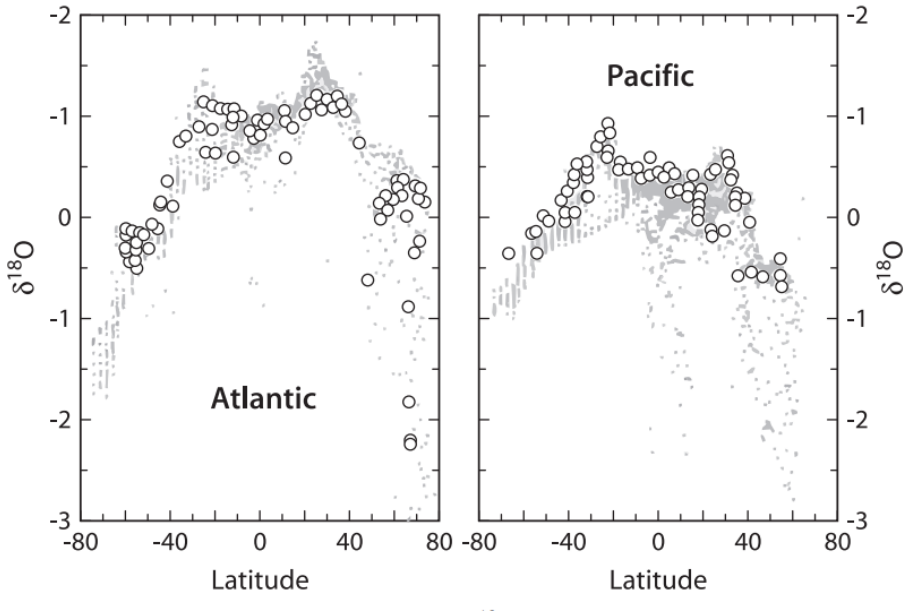

Figure 1.4: Comparison of $\delta^{18}O_{seawater}$ values from recent Atlantic and Pacific oceans. From Hoefs (2009, p. 146), originally from Delaygue *et al* (2000).

High-resolution studies of single rostra have been conducted to derive information about seasonal temperature variability. Despite being widely used in chemostratigraphy and palaeoenvironmental studies, much of the internal variability of geochemical signatures within a given rostrum is not fully understood (Ullmann *et al*., 2015).

To calculate palaeotemperatures from $\delta^{18}O$ values, several different equations can be used, for example:

- Anderson and Arthur (1983): T (°C) =16.0-4.14 (δc- δw) +0.13 (δc- δw)^2
- Epstein *et al.* (1953): T (°C) =16.5-4.3 (δc- δw) +0.14 (δc- δw)^2
- Sharp (2007): T (°C) =15.75-4.3 (δc- δw) +0.14 (δc- δw)^2

Following advice from Dr Clemens Ullmann (personal communication, February 25, 2019), the original Epstein equation is not used as the formula used is now known to give inaccurate results. This was due to a minor error that was induced by neglecting the instrumental fractionation during analysis. This slight methodological error was later corrected by Sharp (2007). Thus, Sharp (2007) will be used to calculate palaeotemperatures later in this work.

1.3 $\delta^{13}C$

Carbon (C) is the sixth most abundant element in the solar system (Anders and Ebihara, 1982) and plays an essential role in the geochemical processes that occur near the Earth's surface in sedimentary, metamorphic, and igneous rocks (Faure and Mensing, 2005). Findings by Craig (1953, 1957) form the baseline for carbon-isotope geochemistry and stratigraphy.

The isotopic composition of carbon is expressed by the $\delta^{13}C$ values, defined as (Faure and Mensing, 2005):

$$\delta^{13}\mathrm{C} = \left(\frac{\left(\frac{^{13}\mathrm{C}}{^{12}\mathrm{C}}\right)_{Sample}}{\left(\frac{^{13}\mathrm{C}}{^{12}\mathrm{C}}\right)_{standard}} - 1 \right) * 1000$$

where the standard is the V-PDB (PeeDee Belemnite). When the $\delta^{13}C$ values are positive, the sample is enriched with ^{13}C relative to the standard, while negative $\delta^{13}C$ values imply depletion in ^{13}C relative to the standard. The $\delta^{13}C$ values in marine carbonates are close to zero because of the V-PDB. Standards themselves are typically marbles and carbonates (Catling and Kasting, 2017).

Several authors have summarised the isotopic geochemistry of carbon (e.g., Farmer and Baxer, 1976; Deines, 1980) and by Faure and Mensing (2005, p.753-802). The fractionation factor for C isotopes is defined as (Faure and Mensing, 2005):

$$\alpha \frac{a}{b}(^{13}C) = \frac{R_a}{R_b}$$

where *a* and *b* are carbon bearing compounds in isotopic equilibrium, and *R* is the $^{13}C/^{12}C$ ratio.

The carbon isotopic composition of belemnites through time is thought to reflect changes in the carbon cycle linked to changes in oceanic productivity, atmospheric CO_2, and metabolic fractionation (e.g., Podlaha *et al.*, 1998; Wierzbowski, 2002; Wierzbowski and Joachimski, 2009; Korte and Hesselbo,

2011). The difference between nektonic and benthic species $\delta^{13}C$ values increase when biomass production in the surface waters increases due to an increase in nutrients. The loss of C from the surface of the water is compensated by the addition of CO_2 from the atmosphere (Shackleton *et al.*, 1983). Decreasing atmospheric CO_2 concentrations in turn can result in the cooling of the global average temperature. Such a scenario leads to a positive feedback loop in the global climate system as a decrease in water surface temperature increases the solubility of CO_2 in the oceans, which causes additional loss of CO_2 in the atmosphere, further decreasing global temperatures.

There have been numerous negative carbon isotope excursions (nCIEs) throughout geological history, which are interpreted as episodes of major carbon release, or upwelling of deep-ocean water rich in isotopically light carbon derived from the decomposition of organic matter which can be detected using belemnite geochemistry (see Wierzbowski, 2004). The study of such events is crucial as it helps connect past carbon cycling and climate variability. The study of nCIEs is important as it parallels current global warming trends. As of 2019, anthropogenic fossil fuel emissions have already caused the isotopic composition of atmospheric CO_2 ($\delta^{13}C_{CO_2}$) to decline by ~1.5 ‰ (Vervoort *et al.*, 2019), a development known as the Suess Effect first described by Suess (1955). According to Norris *et al.* (2013), current anthropogenic warming will be recorded as an nCIE in future sedimentological records. Multiple nCIEs in the geological record may be associated with coeval increases in average global temperatures, ocean acidification and even extinction events (e.g., Kaiho *et al.,* 2009; Erba *et al.,* 2010; Stanley, 2010). In many cases, belemnite carbonate is the only source of geochemical data from some sites dating to the Jurassic and Cretaceous (references provided throughout). These effects are being observed in the early twenty-first century (e.g., Thomas *et al.,* 2004; Hansen *et al.*, 2006; Pandolfi *et al.*, 2011), hence showing the importance of having a deep-time perspective concerning anthropogenic climate change.

Positive excursions, conversely, are caused by the burial of large amounts of isotopically light organic matter into marine sediments (Jenkyns and Clayton, 1997; Wierzbowski, 2004). In general, it appears that times of major, short-lived positive excursions occur during relatively cooler or icehouse climates, which are

also associated with falls in sea level (e.g., Price *et al*., 2000; Price and Mutterlose, 2004). However, it should be noted that positive carbon isotope excursions can also be associated with enhanced volcanism that increases the carbon dioxide in the atmosphere and leads to enhanced weathering, nutrient supply to oceans and warming (van de Schootbrugge *et al*., 2000). Positive carbon-isotope excursions can be associated with warming or cooling depending on the cause of the excursion. It is important also to obtain a palaeotemperature proxy, i.e., oxygen-isotope ratios, whenever possible.

Carbon isotope excursions can also be used in stratigraphy for regional or global correlation of marine carbonate strata (see Saltzman and Thomas, 2012 and Gröcke, 2020 for a comprehensive review on the applications of carbon isotope stratigraphy). Belemnites have been used extensively to identify carbon-isotope excursions and stratigraphic correlation for Jurassic and Cretaceous sequences (e.g., O'Dogherty *et al.,* 2006, 2018; Korte and Hesselbo, 2011).

The isotopic composition of carbon in carbonates depends on several factors as outlined by Faure and Mensing (2005, p.764-765):

1) isotope fractionation between CO_2 gas in the atmosphere and biogenic/abiogenic $CaCO_3$.

2) Isotope fractionation among the *aqueous* carbonate species ($CO_{2(aq)}$, H_2CO_3, HCO_3^-, and CO_3^{2-}) and pH-dependent species.

3) Temperature of the water at the time of secretion.

4) The mineral composition of the $CaCO_3$ – calcite or aragonite as well as elemental impurities.

5) Introduction of non-atmospheric CO_2 formed by oxidisation of organic matter.

6) Vital effects related to metabolic processes of organisms.

7) Alteration of $CaCO_3$ during diagenesis (and in extreme example metamorphism) and the deposition of secondary $CaCO_3$ in fractures/cavities from groundwater/subsurface brines.

The potential of diagenesis to alter primary $\delta^{13}C$ values must be evaluated on a case-by-case basis (Marshall, 1992). Meteoric water diagenesis generally also results in lowered $\delta^{18}O$ values. Therefore, a positive correlation between $\delta^{13}C$ and $\delta^{18}O$ values is expected (Banner and Hanson, 1990; Knauth and

Kennedy, 2009; Fujioka *et al*., 2019). The depth of formation within the water column would also have affected the $\delta^{13}C$ values of biogenic calcite. Shackleton and Kennet (1975) demonstrated that pelagic foraminifera ('forams') are enriched in $\delta^{13}C$ relative to benthic forams due to the preferential removal of ^{12}C in organic matter from the surface layer by photosynthetic organisms. The subsequent decay of organics at the ocean floor enriches deeper waters in ^{12}C and thus causes benthic species to be depleted in ^{13}C compared to pelagic forms. Several studies (e.g., Podlaha *et al*., 1998) have shown $\delta^{13}C$ depletion in bivalves and enrichment in belemnites, a result that is consistent with foram data presented in Shackleton and Kennet (1975). Short term isotopic fluctuations may be caused by changes in water mass rather that changes in temperatures. Carbon isotope ratios change dramatically within the thermocline, a depth at which the temperature of a body of water rapidly changes over a short distance (Hilting *et al*., 2008; Figure 1.5)

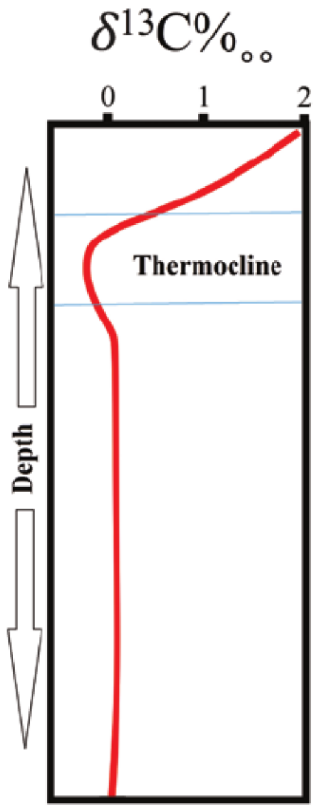

Figure 1.5: $\delta^{13}C$ gradient at different water depths depending on C fractionation in surface waters and subsequent remineralization on the way to the seafloor. From Wilkin (2018).

1.4 Pitfalls in Belemnite Geochemistry for Palaeoenvironmental Reconstruction.

1.4.1 Scatter in Geochemical Proxies

Carbonate skeletons of marine fossil organisms are widely used to reconstruct palaeoceanographic parameters. Notably, the geochemistry of Jurassic and Cretaceous belemnite rostra are interpreted to represent near shelf seafloor properties (i.e., used as 'geochemical proxies'). A number of authors (e.g., Podlaha *et al*., 1998; McArthur *et al*., 2000; Bailey *et al*., 2003; Wierzbowski and Joachimski, 2009; Ullmann *et al*., 2013a, 2015; Price *et al*., 2018) have reported significant scatter in geochemical data (e.g., $\delta^{18}O$, $\delta^{13}C$, element/Ca ratios) when comparing rostra from the same stratigraphic level, or within a single belemnite rostrum. The reasons for the geochemical scatter in the rostra are summarised by Ullmann *et al*. (2015):

> *"The causes for this heterogeneity are not very well constrained but are of much importance for better understanding past environments. Besides diagenesis, environmental parameters such as seawater composition and temperature, metabolic and taxon-specific effects, as well as calcite precipitation rate, might play variably important roles in determining how each geochemical proxy is represented within rostra."*

Spaeth *et al.* (1971) reported variations of up to 5‰ in $\delta^{18}O$ and 14‰ in $\delta^{13}C$ and concluded that accurate temperature records could not be distinguished from diagenetically altered records. Subsequent studies (e.g., Veizer, 1974; Dutton *et al.,* 2007; Li *et al.*, 2012, 2013; Ullmann *et al*., 2015 and many more), however, have successfully used belemnite $\delta^{18}O$ proxies to reconstruct past climates and instead suggest that the data collected by Spaeth *et al.* (1971) was influenced by diagenesis and methods used to help identify diagenetically altered material had not then been developed. Calculated palaeotemperatures reported from epicontinental seas, from which belemnites are known (e.g., Jenkyns and Clayton, 1997; Mutterlose *et al*., 2009, 2010; Harazim *et al*., 2013), can be affected by evaporation, freshwater riverine input, or a combination of the two (Grossman, 2012a). If evaporation played a

significant role in the $^{18}O/^{16}O$ ratio in the ocean water, then the overall $\delta^{18}O$ signal of local seawater would be shifted positively due to preferential evaporative removal of the lighter ^{16}O and results in a calculated palaeotemperature lower than the actual palaeotemperature. Conversely, river input results in a negative $\delta^{18}O$ shift, producing a higher apparent temperature.

1.4.2 Salinity

It has been hypothesized by numerous authors (e.g., Veizer, 1974, Li *et al.*, 2012 and more) that salinity plays a role in the elemental and isotopic heterogeneity of the belemnite rostra. Due to the isotopic fractionation of the hydrological cycle, the $\delta^{18}O$ values of seawater is proportional to salinity (see Anderson and Arthur 1983; Railsback *et al*. 1989). Multiple studies have been conducted on belemnites to assess the effects of salinity on $\delta^{18}O$ values. For example, salinity was not considered to have been the dominate control on $\delta^{18}O$ values reported by Railsback *et al*. (1989) because large variations in salinity would be required to produce the ranges of palaeotemperatures observed from the Oxford Clay Formation. In contrast, Saelen *et al.* (1996) argued that salinity strongly influenced stable isotope ratios from certain parts of the Lower Jurassic Whitby Mudstone Formation, suggesting that lower salinity surface waters. For example, Wierzbowski and Joachimski (2007) concluded that palaeotemperature estimates taken from ammonite $\delta^{18}O$ might have been overestimated due to a lower than normal marine surface water salinity at the Bajocian–Bathonian boundary from the Częstochowa Clay Formation in central Poland.

Saelen *et al.* (1996) also argued that belemnites from the Whitby Mudstone Formation might have recorded a mixture of surface and deeper water temperatures either from vertical movement through the water column or horizontal migration in and out of upwelling waters. If this is the case, then the recorded temperatures would have been cooler than that of the sea surface temperature (SST). The $\delta^{18}O$ and $\delta^{13}C$ values of analogous cuttlefish also show a similar change in isotope values due to ontogenetic migrations from nearshore nurseries with lower seawater $\delta^{13}C$ and $\delta^{18}O$ values to offshore overwintering habitats with higher seawater $\delta^{13}C$ and $\delta^{18}O$ values (Dance *et al*., 2014).

Hermoso and Lecasble (2018) studied how the isotopic composition of $\delta^{18}O$ and $\delta^{13}C$ in cultured coccolithophores was influenced by salinity changes independently of the isotopic composition of the water. The study concluded that despite significant physiological changes to the coccolithophores, water salinity variations did not alter the biological fractionation of the oxygen isotopes. Therefore, it would not have affected the temperature estimates derived from the coccoliths $CaCO_3$ tests. By contrast, the $\delta^{13}C$ values of the coccoliths, which are also influenced by growth rates (see Saruwatari *et al*., 2016), can be affected by salinity with more optimal conditions, faster growth and more positive $\delta^{13}C$ values. However, as previously stated, belemnites are extinct with no extant descendants, so instead, we must examine their closest living relatives, sepiids, and analyse of how salinity affects their biogeochemistry. It would therefore stand to reason that variations in salinity would also have influenced the $\delta^{13}C$ values in belemnite calcite.

1.4.3 Vital Effects and Fractionation (oxygen)

The term vital effect refers to any deviation from equilibrium through a direct biological cause; vital effects in calcareous species were first identified by Urey *et al*. (1951) and were the subject of the first study on the isotopic composition of fossil calcite. Regarding vital effects, Urey *et al.* (1951, p.40) wrote the following:

> *"Since we have examples of animals and plants laying down isotopes out of equilibrium with their surroundings, as for example the carbon of organic material, we may well ask whether the deposition of calcium carbonate by an animal or a plant occurs so as to leave the oxygen isotopes in equilibrium with the water from which deposition takes place, that is, we may ask whether there is a vital effect. Probably the equilibrium deposition should be closely approximated in many cases, for the calcium carbonate deposited is constantly bathed with water from the surroundings and hence may exchange its oxygen with the surrounding water during the deposition process. However, one could quite readily imagine mechanisms which would involve the deposition of organic oxygen and thus invalidate these assumptions. The whole question could*

be answered only by experiment, so far as we can judge from the present state of our knowledge of the physiology of deposition of such substances."

A key issue is the lack of understanding and consensus regarding belemnite ecology. Belemnites are often assumed to have been fast epipelagic swimmers based primarily on their superficial resemblance to extant teuthids. The variation in guard shapes is likely the result of different ecological niches and possibly water depths (Rexfort and Mutterlose, 2009).

Although belemnites are generally accepted to have been active predators with a swimming habit, some authors (Anderson *et al.,* 1994; Wierzbowski and Joachimiski, 2009; Wilmsen and Niebuhr, 2017) have proposed a nektobenthic mode of life for belemnites not dissimilar to that of modern sepiids based on oxygen isotope thermometry. This is, however, contradicted by the occurrence of belemnites in black shales representing anoxic bottom water. A well-studied example is the Early Jurassic Posidonienschiefer of southern Germany (see Rexfort and Mutterlose, 2009), which suggests that belemnites were nektonic due to the absence of benthic organisms from the Posidonienschiefer (Hess, 1999).

It remains unclear at present, as Rexfort and Mutterlose (2009) also stated, whether isotopic data from belemnites reflect a surface or deeper ocean water signal as it is currently unknown if the belemnite mode of life changed during ontogeny. Li *et al*. (2012) concluded that belemnites were mobile, experiencing various environmental conditions throughout their lives. These authors also stated that some belemnite species occupied ecological niches that remained unchanged, if not necessarily location, over a substantial period while others had a more cosmopolitan lifestyle. The belemnite rostrum is an internal skeleton, like those of corals and echinoderms, that are known to secrete these calcium carbonate skeletons out of equilibrium with the ambient seawater (see Kim and O'Neil, 1997; Davis and John, 2019; Linsey *et al*., 2019; Prada *et al.,* 2019). However, *Sepia* cuttlebones are probably buried less deeply in the soft tissues than the belemnite rostrum, and this may explain why it shows no evidence of vital effects in oxygen isotope values (Rexfort and Mutterlose, 2006, 2009).

Metabolic factors can lead to biofractionation; this is most prominently observed in fast-growing organisms, which means the shell calcite may not have been precipitated in equilibrium with the surrounding seawater (Rexfort and Mutterlose, 2009). Biofractionation of cephalopod calcite was first observed in an actuopalaeontology experiment by Rexfort and Mutterlose (2006; see Richter, 1928 and Schäfer, 1962 for reviews on actuopalaeontology). After rearing five *Sepia officinalis* in known water temperatures and known isotopic composition, the stable isotopes $\delta^{18}O$ and $\delta^{13}C$ were measured from every septum to assess whether ontogenetic and environmental factors influenced isotope signatures. Rexford and Mutterlose (2006) concluded that the carbon isotopes underwent biofractionation, but oxygen remained unaltered – and the research presented in this thesis comes to the same conclusion. Even if the uniformitarian principle ("the present is the key to the past"; Lyell, 1830) is used carefully concerning extinct organisms, it seems that it is nearly indispensable for the reconstruction of the environments that fossil organisms have modern counterparts.

Modern biogenic carbonates have taxon-specific fractionation (Marshall, 1992). As is the case for oxygen isotopes, because belemnites left no living descendants, we cannot judge the degree to which observed temporal variation and scatter in the carbon isotope composition can be attributed to disequilibrium fractionation. It is known that extant cephalopods secrete oxygen isotopes in isotopic equilibrium with the ambient seawater (see Taylor and Ward, 1983). At present, published studies have not found evidence of significant taxonomic differences in the oxygen isotope composition of belemnites from the same levels. Rosales *et al.* (2004b) proposed that oxygen isotope scatter may result from subtle diagenetic alteration undetected using diagenetic screening.

There is no significant depletion in $\delta^{18}O$ values when comparing $\delta^{18}O$ values of belemnites to other coeval fossils, as would be expected from vital effects, (e.g., Anderson *et al.,* 1994; Wierzbowski and Joachimiski, 2007; Lukeneder, 2015). So, there is no clear evidence of vital effects dominating in belemnite $\delta^{18}O$ records.

Chapter 2: Geological Settings

2.1 Cabo Mondego

2.1.1 Sedimentology and Palaeoenvironments

During the Middle Jurassic, the South Iberian palaeomargin was located between the Central Atlantic Ocean and the Western Tethys Ocean (O'Dogherty *et al*., 2018). The west-central part of the Portuguese mainland and the adjacent continental shelf is one of a family of Atlantic margin rift-basins formed as a response to Mesozoic extension and subsequent opening of the North Atlantic Ocean (Rasmussen *et al*., 1998). The Lusitanian Basin resulted from the initial extension of Pangaea continental crust. The Paleozoic basement evolution and the Mesozoic extension created a complex succession of events and sedimentary infill. The Upper Jurassic sediments from the Cabo Mondego section represent the Lusitanian Basin second rifting episode (Rocha *et al*., 2014).

The cliffs at Cabo Mondego contain a near-complete stratigraphic succession from the Upper Toarcian to Tithonian (Rocha *et al*., 2014). The Jurassic at Cabo Mondego preserves a diverse range of marginal depositional facies, including lagoon, delta, and estuarine deposits (Rocha *et al*., 2014). The lithology of the Middle Jurassic consists of alternating muddy limestones and marlstones (Trincão *et al*., 2018). Most of the limestone beds are under 50 cm thick with marly intervals under 70 cm thick (Fernández-López and Henriques, 2002). The strata studied here were deposited in an open ocean environment on the distal end of a carbonate ramp below the wave base (Fernández-López *et al*., 2006). The Middle Jurassic records in this, the Figueira da Foz, region correspond to the Cabo Mondego Formation. Here, eustatic, climatic and bathymetric conditions allowed calm and relatively monotonous sedimentation typical of offshore marine environments.

Jurassic sediments show strong cyclicity is observed in sedimentary microrhythms typically as alternating limestones and marls, carbonate-rich and carbonate-poor facies, or as siltier and more clay/organic-rich laminae. Some successions, such as at Cabo Mondego, represent continuous or near-

continuous sedimentation over long periods. The periodicity of these microrhythms is consistent with Milankovitch (or orbital) cycles. Milankovitch cycles can be used to astronomically calibrate timescales (Pieńkowski *et al*., 2008; Figure 2.1). To date, over 70% of the Jurassic is covered by a floating astronomical timescale based on Milankovitch cycles (Gradstein et al., 2004; Coe and Weedon, 2006; Pieńkowski *et al*., 2008; Huang, 2018). Occasionally, these sequences are disturbed by synsedimentary deformation and gravitational resedimentation, evidenced by the presence of calciturbidites and debris flows (Watkinson, 1989; Azerêdo, 1998).

It is the period spanning the time of the Bajocian-Bathonian boundary that is of importance for this study. Upper Bajocian and Lower Bathonian deposits exhibit similar litho- and biofacies in the region of Cabo Mondego. They have been informally referred to the Brenha facies (Watkinson, 1989; Azerêdo *et al*., 2002; Azerêdo and Wright, 2004; Azerêdo and Duarte, 2017), and formally included in the Cabo Mondego Formation (Soares *et al.* 1993; Azerêdo *et al*. 2003).

2.1.2 Stratigraphic Significance

Today, Cabo Mondego is well-known to geoscientists for its stratigraphical significance as both the Global Boundary Stratotype Section and Point (GSSP) for the base of the Bajocian Stage (Pavia and Enay, 1997; criteria for becoming a GSSP are discussed in 2.2.2) and the Auxiliary Stratotype Section and Point (ASSP) for the base of the Bathonian Stage (Fernández-López *et al*., 2009; Figure 2.2). The Bajocian Stage was named by d'Orbigny (1842–1851, 1852) after the town of Bayeux in Normandy (Bajoce in Latin). The Bajocian boundary is defined in the base of bed AB11 (Henriques *et al*., 1994; Pavia and Enay, 1997; Trincão *et al*., 2018), by the First Appearance Datum (FAD) of the ammonite *Hyperlioceras* (Pavia and Enay, 1997) and the latest occurrence of *Graphoceras* and *Haplopleuroceras* (Henriques *et al*., 1994). The top of the Bajocian, the period covered by this study, is part of the *parkinsoni* Zone.

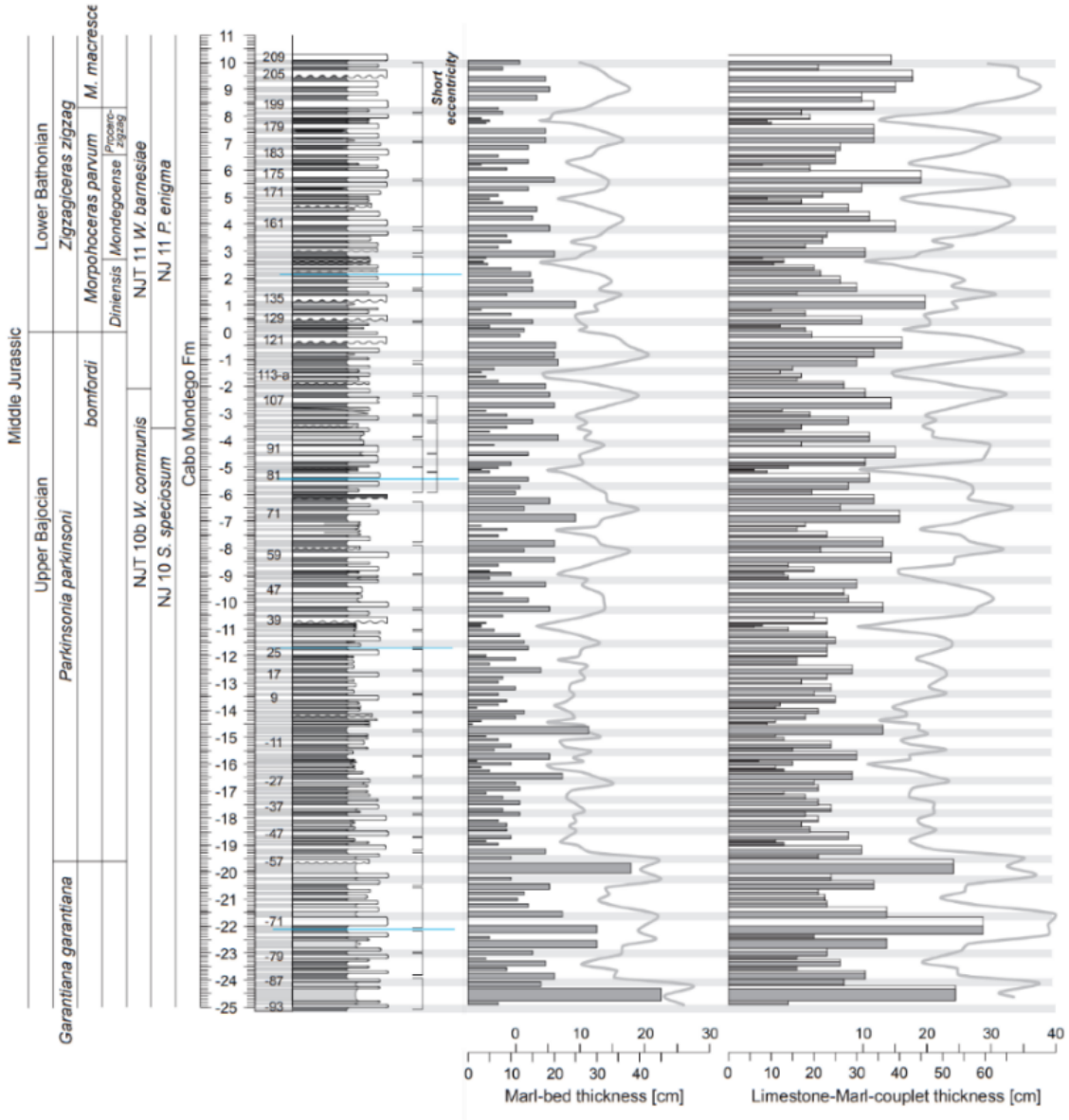

Figure 2.1: The stratigraphy of the Cabo Mondego Formation. Unpublished graphic by Micha Ruhl, Trinity College Dublin.

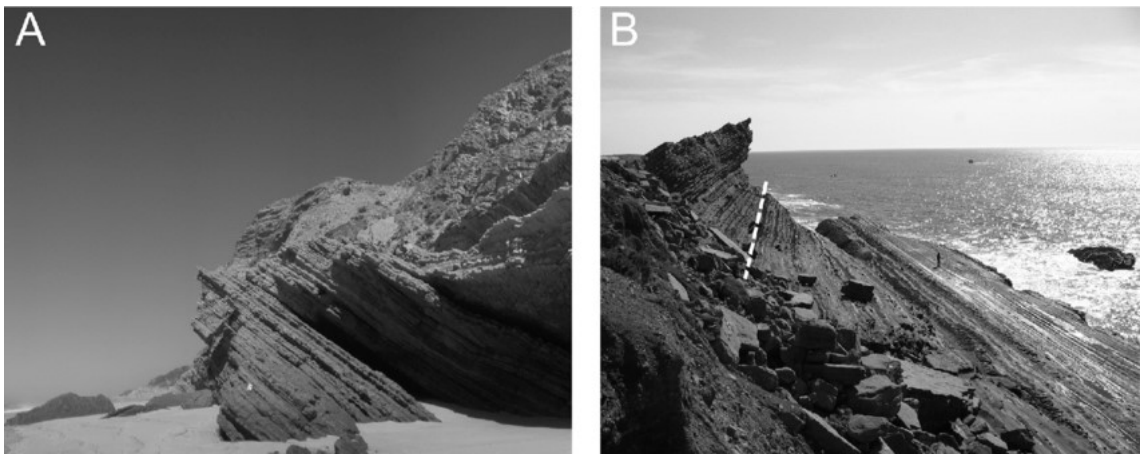

Figure 2.2: (A) the Aalenian-Bajocian GSSP and (B) the Bajocian-Bathonian ASSP. Photograph by Maria Helena Henriques. From Rocha *et al*. (2014).

The occurrence of a particularly rich and diversified ammonite fossil record, the occurrence of calcareous nannofossils, the continuity of the stratigraphic record and the magnetostratigraphic polarity-reversal across the Aalenian–Bajocian boundary supported the proposal of the establishment of the Bajocian Global Stratotype Section and Point (GSSP) at Cabo Mondego in the Murtinheira section (Rocha *et al*., 1990, 2014; Henriques *et al*., 1994).

Cabo Mondego was first proposed as a GSSP for the Bajocian in 1970 and further supported by Rocha *et al*. (1990). Fossil assemblages of ammonites and other fossil groups (calcareous nannoplankton, benthic foraminifers and brachiopods) have been studied in detail across the GSSP and results from these studies have been used to correlate the Aalenian–Bajocian boundary at Cabo Mondego to other sites around the world (Canales and Henriques, 2008, 2013; Neto *et al*., 2011).

Cabo Mondego was established as the Auxiliary Stratotype Section and Point (ASSP) for the base of the Bathonian in 2008 (Fernández-López *et al*., 2009). The Bathonian ASSP is defined at Cabo Mondego (‘section 2’), approximately 7 km north of Figueira da Foz. This section has highly diverse microfossil and macrofossil assemblages, particularly ammonites and foraminifera, whose biostratigraphy and palaeoenvironmental significance are outlined in Fenández-López *et al.* (2006a, b), and Henriques *et al*. (2014). The base of the Bathonian is defined by the FAD of the ammonite species *Morphoceras parvum* and *Gonolkites convergens.* The GSSP for the base of the Bathonian Stage is defined at the base of limestone bed RB071 in the Ravin du Bès Section, southern Subalpine Chains, south-eastern France (Fernández-López *et al*., 2009).

2.1.3 Palaeontology

The rocks at Cabo Mondego are highly fossiliferous, contain abundant Middle Jurassic marine fossils, including ammonites, brachiopods, benthic foraminifera (Canales and Henriques, 2008), calcareous nannofossils, radiolarians, and corals, echinoderms, brachiopods, belemnites, crinoids and ichnofossils which includes dinosaur footprints (Henriques, 2008). Apart from the footprints, these fossil-rich deposits were formed in an open sea, on a distal and

outer environment of a carbonate ramp, below the wave base (Fernández-López, 2006a).

Ammonites are scarce in the Upper Bajocian but common in Lower Bathonian deposits at Cabo Mondego. The ammonite assemblages from the lower Bathonian of Portugal and Spain are composed of Submediterranean taxa (Fernández-López, 2000; Fernández-López and Henriques, 2002; Fernández-López *et al*., 2006a). The section consists of the *parkinsoni* Zone in the uppermost zone of the Bajocian and the *zigzag* Zone of the lowermost zone of the Bathonian. Both zones belong to the Northwest European Province (see Westermann and Callomon, 1988; Callomon and Cope 1995) and the Mediterranean Province (see Sandoval 1983, 1990). Although the *zigzag* Zone can be recognized and characterized as composed of two subunits, the *parvum* and *macrescens* Subzones, the *parkinsoni* Zone cannot be further subdivided due to the scarcity of well-preserved ammonites (Fernández-López *et al*., 2007).

2.1.4 Previous Geochemical Work

Previous stable isotope work on the Lusitanian Basin has been conducted on fossil wood and marine carbonate of the lower Toarcian (Hesselbo *et al.,* 2007). Total organic carbon (TOC) analysis was undertaken by Silva *et al*. (2013) for three sites, including Cabo Mondego, traversing the Middle-Late Jurassic transition in the central-northern Lusitanian basin. However, Silva *et al.* (2013) did not include the Bajocian-Bathonian boundary but instead focused on the Callovian-Oxfordian boundary. No geochemical analysis has been published on the macrofossils at the Bajocian-Bathonian boundary of this region.

2.2 Albstadt-Pfeffingen

2.2.1 Sedimentology and Palaeoenvironment

Albstadt-Pfeffingen records a series of marine mudstones and thin limestone beds dating from the latest Bathonian to the earliest Callovian [approx. 166 Ma]. The section was dated based on the complete and continuous succession of ammonite zones and subzones, ranging from the *zigzag* Zone to the base of the *koenigi* Zone base (Callomon and Dietl, 1990, 2000). Two

lithostratigraphic units represent the Upper Bathonian and Lower Callovian of Southern Germany: the Orbisoolith and the Macrocephalenoolith members of the Dentalienton and Ornatenton formations, respectively, based on Callomon and Dietl (1990, 2000; Figure 2.3).

Both members are composed of nodular oolitic limestones with typical facies containing of berthierine and limonitic ooids, usually ~1 mm in diameter. The limestone beds of both the Orbisoolith and the Macrocephalenoolith are separated by thin marl beds (Mönnig and Dietl, 2017). Each bench or layer is locally restricted and wedges off after a few hundred metres. Together, both members are rarely thicker than 2 m (Mönnig and Dietl, 2017). The first appearance datum (FAD) of the Sub-Boreal ammonite *Kepplerites keppleri* is used to define the Callovian Stage (Callomon *et al*., 1988; Callomon and Dietl, 1990, 2000; Mönnig and Dietl, 2017). This assignment is also supported at Albstadt-Pfeffingen by assemblages of foraminifera (Franz and Knott, 2012) and ostracods (Beher *et al*., 2010).

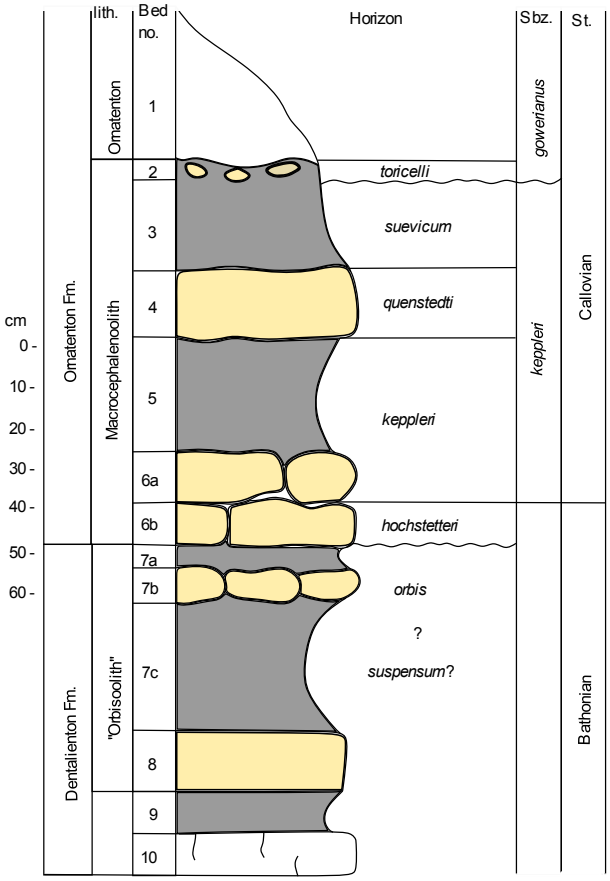

Figure 2.3: Lithology of Albstadt-Pfeffingen. Redrawn from Callomon and Dietl (1990).

2.2.2 Global Boundary Stratotype Section and Points

Within the Phanerozoic, the current internationally agreed method for defining chronostratigraphic boundaries is selecting a Global Boundary Stratotype Section and Point (GSSP) as a physical reference for a particular and optimally correlatable geological time boundary. A stage is defined by the *International Stratigraphy Guide* as "*the smallest unit in the standard chronostratigraphic hierarchy that can be recognized at a global scale*" (Salvador, 1994, p. 78). The International Commission on Stratigraphy has ratified approximately two-thirds of the GSSPs of Phanerozoic stages (71 of 102 in May 2020). Of the four stages in the Middle Jurassic, only the Callovian lacks a ratified GSSP (Cohen *et al*., 2020; see also Cohen *et al*., 2013), hence the motivation for this research. Most Phanerozoic GSSPs are mainly based on biostratigraphy. The process of deciding on a GSSP is a complex one that requires several criteria be met which are outlined by Remane *et al*. (1996), Remane (2003), and summarised by Gradstein and Ogg (2012; Table 2), Smith *et al.* (2014), and Lucas, (2018).

The proposed GSSP should represent continuous sedimentation where there are no gaps or condensation (cf. Föllmi, 2016) at or near the boundary level. Moreover, an absence of metamorphism or strong diagenetic alteration of the sediments and fossils at the section is beneficial to ensure that geochemical and magnetostratigraphic data have not been altered or destroyed. Well preserved geochemical data can be used in chemostratigraphy. GSSP candidates should also yield an abundant and diverse range of fossils; ideally, those that can be used for correlation and those from open marine environments are the most useful (Gradstein and Ogg, 2012).

Table 2: Requirements for establishing a GSSP revised from Remane *et al*. (1996) according to the International Commission on Stratigraphy (ICS) procedures. Adapted from Gradstein and Ogg (2012).

1.	Name and stratigraphic rank of the boundary. Including concise statement of GSSP definition.
2. **GSSP geology.**	Geographic location. Geologic setting (e.g., lithostratigraphy, sedimentology, post-depositional tectonics, biostratigraphic correlation, etc.). Precise location and stratigraphic position of GSSP level. Stratigraphic completeness across the succession. Adequate thickness and stratigraphic extent of section above and below. Accessibility. Provisions for conservation.
3. **Primary and secondary markers.**	Principal correlation event (usually a faunal horizon) at GSSP level. Other primary and secondary markers – e.g., biostratigraphy, magnetostratigraphy, chemostratigraphy, sequence stratigraphy, cyclostratigraphy, etc. Correlation potential between marine and terrestrial deposits. Potential age dating from volcanic ashes (radiometric dating) and orbital tuning. Demonstration of regional and global correlation.
4. **Summary of selection procedure.**	Relation of the GSSP to historical usage; references to historical background and adjacent (stage) units; selected publications. Other potential candidates and reasons for rejection; summary of votes and received comments at the International Commission on Stratigraphy meeting. Useful reference sections.
5. **Official publication**	Summary in IUGS journals *Episodes* or *Newsletters on Stratigraphy.* Full publication in an appropriate journal.

2.2.3 Stratigraphic Significance

In the Swabian Alb, the Bathonian-Callovian boundary is marked by the oolitic limestones of the Macrocephalenoolith Member of the Ornatenton Formation (*Orbis* Zone; Pieńkowski *et al*., 2008 - cf. Dietl *et al*., 1979; Geyer and Gwinner, 1984). Albstadt-Pfeffingen was declared a GSSP candidate for the Callovian in 1990 by the Callovian Stage Research Group (Callomon, 1991). Although alternative GSSPs for the base of the Callovian have been suggested, such as within the Kamennomostskaja Formation of the Northern Caucasus, southwest Russia (Dzyuba *et al.,* 2016), none are currently sufficiently developed to be formally proposed.

The Callovian Working Group in 1990 (Callomon and Dietl, 1991, 2007) concluded that Albstadt-Pfeffingen was a good candidate for the base of the Callovian based on ammonite biostratigraphy, the correlation potential to other localities in the Swabian Alb (see Mönnig and Dietl, 2017), and lack of alternatives with comparable correlation potential, although concerning the stratigraphic completeness of the site have previously been raised (Callomon and Dietl, 2007).

The overall complete and continuous ammonite biostratigraphy (Callomon and Dietl, 2000) has been supported more recently by ostracod data (Beher *et al*., 2010). However, the succession is strongly condensed, and the preservation of individual fossil assemblages is geographically patchy (Callomon and Dietl, 2000; Mönnig, 2014). Prior pilot studies for strontium isotope stratigraphy, magnetostratigraphy, and palynology have yielded ambiguous results (Callomon and Dietl, 1990, 2000; Dietl, 1990). No detailed studies on the Bathonian and Lower Callovian geochemistry of this section have been published. The survey of the geochemistry of belemnite rostra across the Bathonian-Callovian boundary at Albstadt-Pfeffingen reported in this thesis has implications for the potential GSSP status which is discussed in 6.2 based on strontium isotope stratigraphy.

2.3.4 Palaeontology

Macrofossils, specifically ammonites and belemnites, are well persevered three-dimensionally in this section (Mönnig and Dietl, 2017; Figure 2.4). These taphonomic characteristics make this locality a prime candidate for isotopic analysis. An overview of the ammonite fauna is provided by Mönnig and Dietl (2017). Microfossils from Albstadt-Pfeffingen include ostracods (see Beher *et al*., 2010) and foraminifera (see Franz and Knott, 2012),

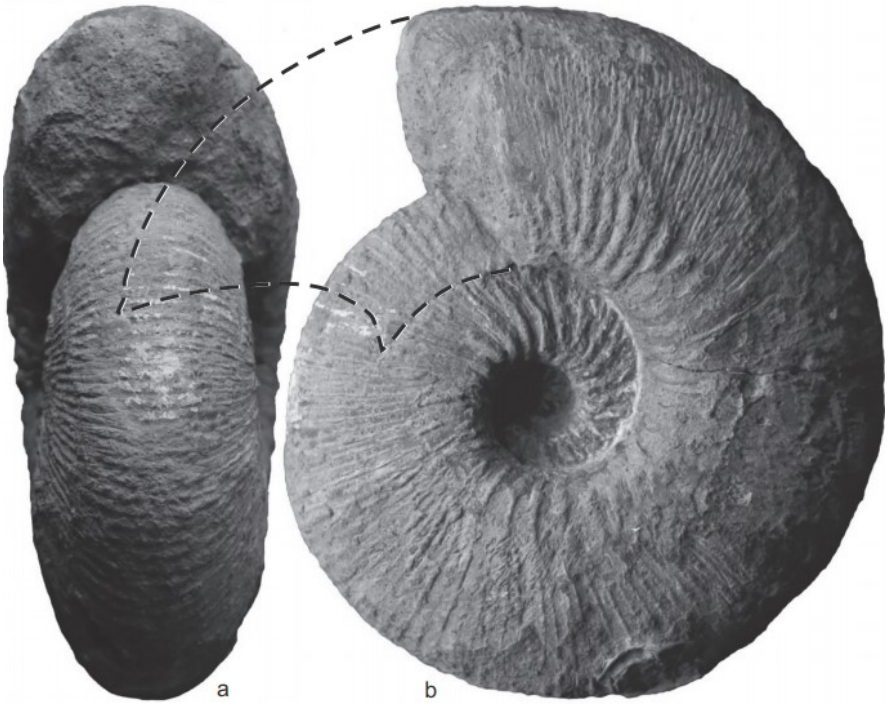

Figure 2.4: The ammonite *Kepplerites* (*Kepplerites*) *aigii* (specimen SMNS-70349(; a) ventral view; b) lateral view, from Albstadt-Lautlingen, a site closely associated with Albstadt-Pfeffingen. From Mönnig and Dietl (2017).

Chapter 3: Methodology

3.1 Rationale

The methods commonly employed in palaeoceanographical research have their origins in biological, chemical, and physical sciences. Palaeoceanography, and all palaeosciences, are, therefore, genuinely cross-disciplinary fields of study. Thus, a wide range of scientific techniques derived from multiple fields must be used to obtain data from palaeoclimate/palaeoceanographic proxies. Such proxy records provide qualitative measurements of key climatic and environment variables, surface water temperatures being one of the most important.

Although two localities of different age (the Bajocian-Bathonian of Portugal and the Bathonian-Callovian of Germany) were chosen as part of this study, the sample preparation is the same. To avoid repetition, the laboratory techniques sections for both localities are combined in this chapter.

For this study, three separate analytical procedures were conducted: firstly to measure the stable isotopes ($\delta^{13}C$ and $\delta^{18}O$); secondly to measure trace elements (Ca, Fe, Mg, Mn, P, S, and Sr), and; thirdly to measure $87Sr/^{86}Sr$ values. Three specimens from Albstadt-Pfeffingen were also selected for CL imaging.

3.2 Sample Collection

3.2.1 Sample Collection (Cabo Mondego)

90 belemnite specimens of undetermined species were collected from the alternating limestones and marls at Cabo Mondego (Central Portugal), which form the so-called Cabo Mondego Formation of the Late Bajocian-Bathonian stages of the Middle Jurassic. The samples come from the Cabo Mondego (section 2; Figure 3.1), approximately 7 km north of Figueira da Foz which is also used to define the Bathonian ASSP. The studied area is biostratigraphically well-

dated based on ammonite fauna and comprises the entire stratigraphic interval between the Upper Bajocian (*garantiana Zone*) and the lower Bathonian (*zigzag* Zone; for detailed stratigraphy, see Henriques et al., 1994; Fernández-López et al., 2007). The total thickness of the studied section is 36 m.

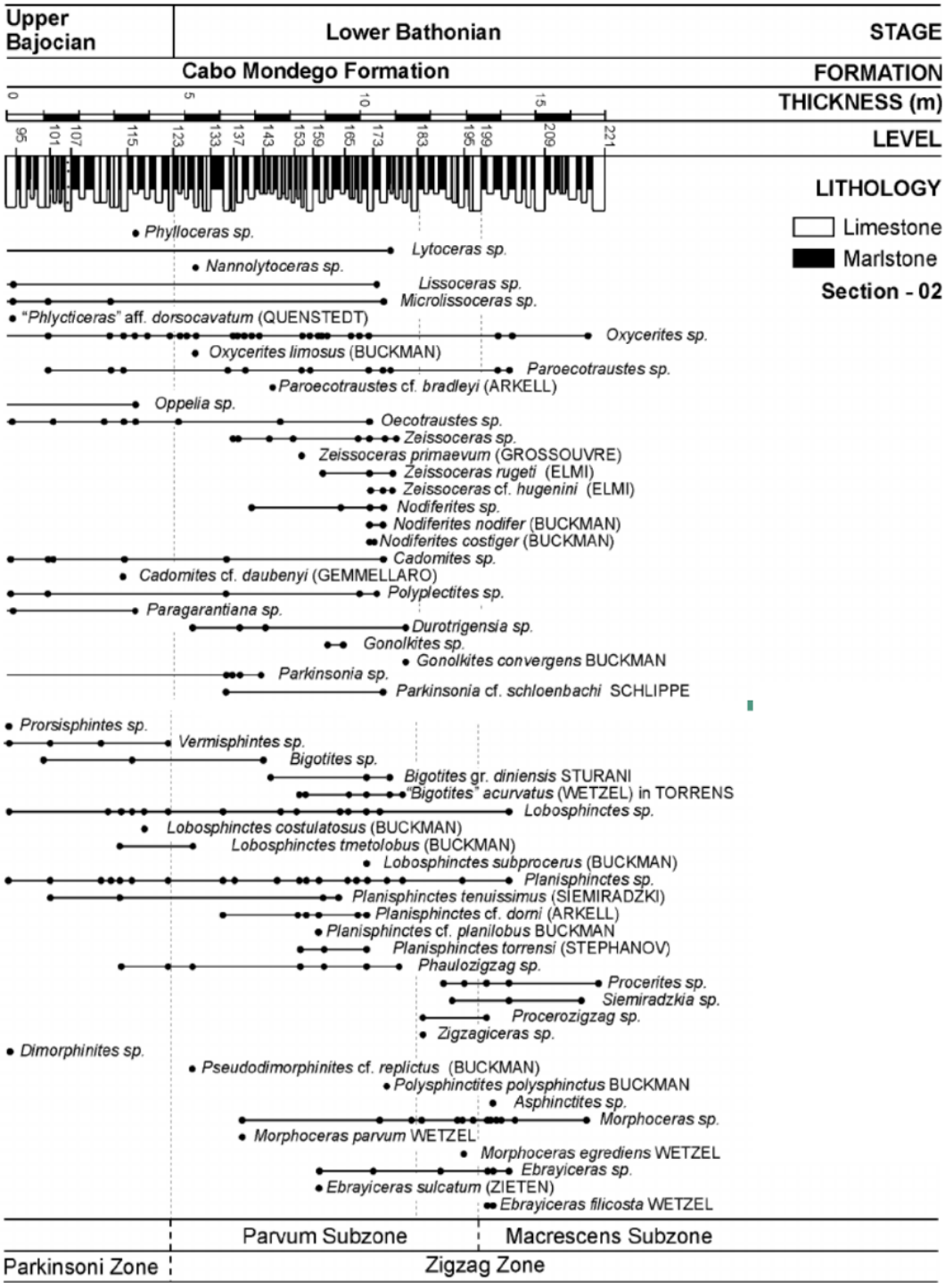

Figure 3.1: Ammonite biostratigraphy from Cabo Mondego (Section 2). Taken from Fernández-López *et al*. (2006a).

3.2.2 Sample Collection (Albstadt-Pfeffiengen)

Belemnites up to 1.5 cm in cross sectional diameter were extracted from 50 cm of strata downward from the top of the *Keppleri* Horizon. as defined in Callomon and Dietl (2000). Samples were collected at Albstadt-Pfeffingen, 1 km west of the town of Pfeffingen (Figure 3.2). There are no natural exposures of the Macrocephalenoolith in southern Germany (Callomon and Dietl, 2000). As a conservation measure, previously excavated sections are kept unexposed except when the material is required for bona fide research.

A new section was excavated by Stuttgart Museum staff and a University of Copenhagen team in 2014 at a site in a Nature Reserve in which geological collecting is generally not permitted. The excavation was carried out with permission from the relevant authorities in Germany. All of the samples for the present study were collected during this 2014 excavation. A rough sedimentary log containing the ammonite horizons was made from the 2014 excavation (Figure 3.3). Key horizons, most notably the *hochstetteri* Horizon, were identified in Callomon and Dietl (2000) and the new section making it possible to correlate the two sections (Figure 3.4). At the request of the landowner and to preserve the site for future research, the exact coordinates of the 2014 excavation cannot be disclosed in this work. The precise coordinates of the 2014 site are lodged at the Stuttgart Museum.

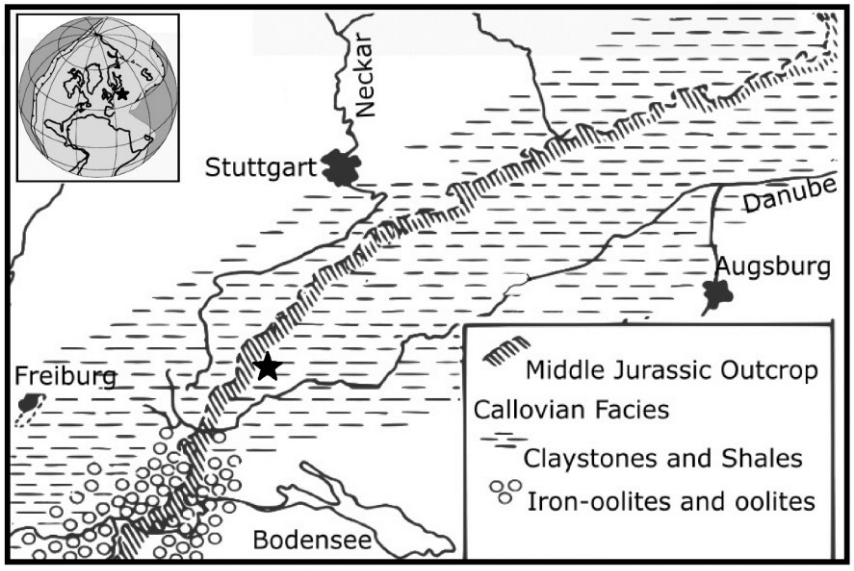

Figure 3.2: Middle Jurassic geology of southern Germany. A star indicates the location of the studied section. Redrawn from Dimter and Smelror (1990). Insert shows global palaeogeography of the Middle Jurassic modified from Ullmann *et al.* (2013a

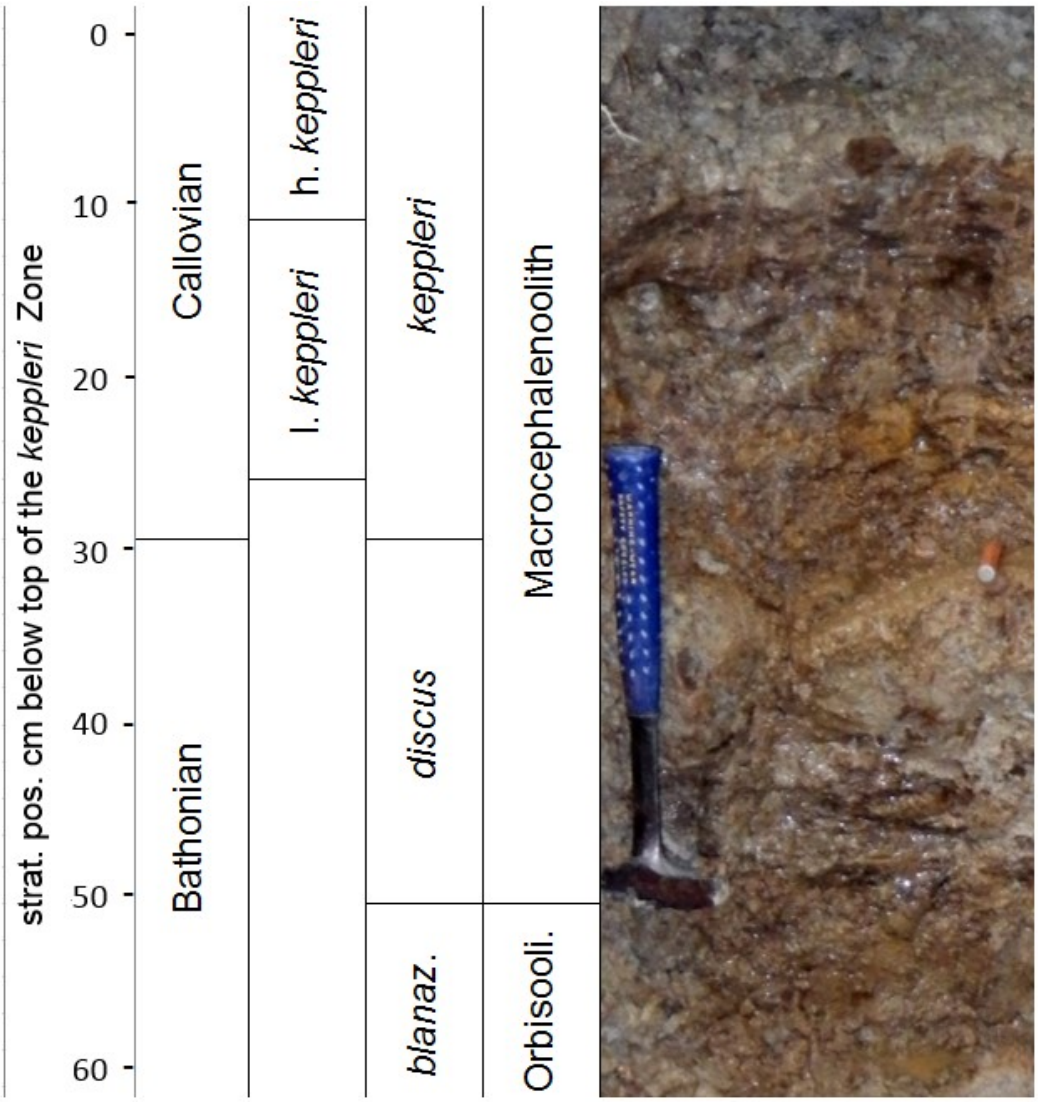

Figure 3.3: Field photograph showing the collection area matched to lithostratigraphy from field notes provided by Christoph Korte. The *keppleri* Horizon is subdivided into the higher (h.) and lower (l.) *keppleri.*

The chemostratigraphic study was carried out on isolated low-Mg calcite marine components (belemnite rostra). The analysis includes major and trace element contents and carbon-, oxygen- and strontium-isotope ratios of belemnite calcite. Belemnite specimens were collected from a relatively short stratigraphic interval (*Orbis* to *Gowerianus* Zones, ~1 million years; Callomon and Dietl, 2000; cf. Wierzbowski *et al*., 2017).

Thirty belemnite specimens were extracted from this section, partially with multiple specimens from the same horizon, allowing for a dataset of sufficient resolution to test for stratigraphic completeness using belemnite $^{87}Sr/^{86}Sr$. It is worth noting that the locality excavated by Callomon and Dietl (2000) and

recorded in subsequent publications (e.g., Beher *et al*., 2010; Mönning and Dietl, 2017) is not the same section reported on in this study. The belemnites, although well preserved, are fragmentary, making taxonomic diagnosis difficult.

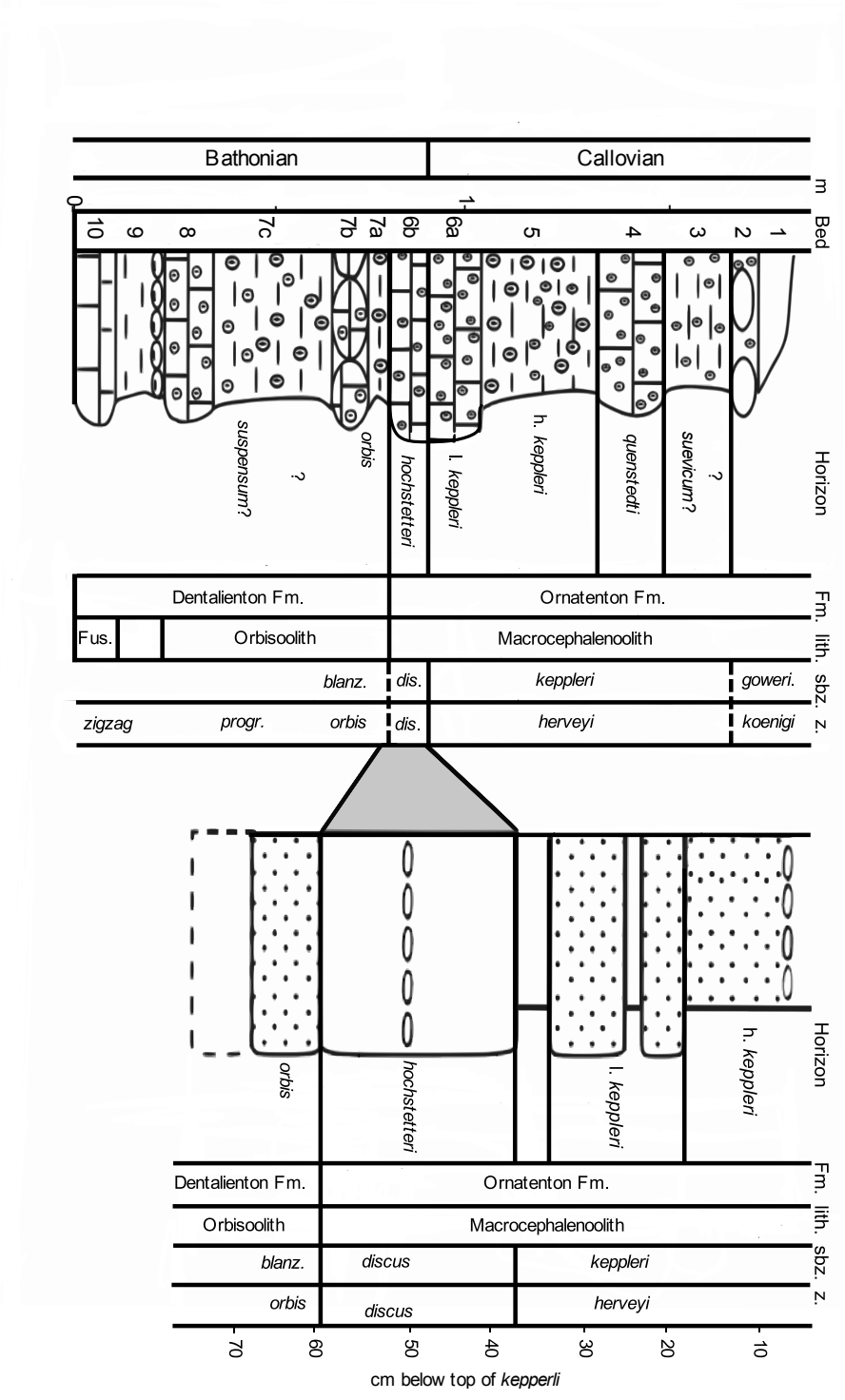

Figure 3.4: The lithology of the studied section used in this paper (right) compared to the original Albstadt-Pfeffingen beds (left) redrawn from Callomon and Dietl (2000) and Beher *et al*. (2010).

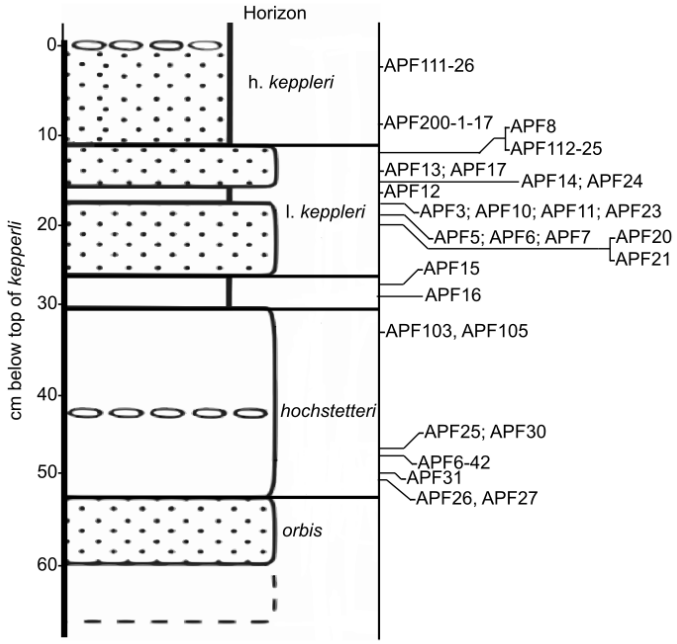

Figure 3.5: Stratigraphic positions of belemnites that were analysed at the University of Exeter Penryn Campus for minor elements and stable isotopes.

3.3 Laboratory Techniques

3.3.1 Sample Preparation

Calcite from the inner and outermost parts of the rostra was avoided as these areas are most susceptible to diagenetic alteration due to proximity to the sediment and diagenetic fluids. Such locations include the rostrum exterior, apical region, alveolus, and noticeable cracks/fractures (Koleva-Rekalova, 2003; McArthur et al., 2007a; Ullmann and Korte, 2015; Ullmann et al., 2015; Benito et al., 2016; Price et al., 2018). To avoid altered material, sample extraction focussed on the intermediate growth increments (e.g., Ullmann and Korte, 2015).

Calcite was extracted using a hand-held automatic drill with a 0.5 mm diamond-coated steel drill head at the Camborne School of Mines (University of Exeter). To prevent cross-contamination between samples, the drill head was wiped down after every sample was taken. *Ca.* 1-2 milligrams of calcite powder were taken and subsequently split into aliquots for isotope and element analysis. The calcite powder was weighed using a microbalance. Multiple samples were

taken from the same rostrum in some of the specimens to determine variations over the lifetime of individuals.

3.3.2 Cathodoluminescence and Petrography

The preservation of selected belemnite rostra from Albstadt-Pfeffingen was assessed using cathodoluminescence (CL) using a Cold Cathodoluminescence microscope (CITL CCL 8200 MK3) with attached JVC digital camera at a spatial resolution of 1.5 µm per pixel and with a 4 second exposure time at the Camborne School of Mines. Three specimens from Albstadt-Pfeffingen (A-PF 105, A-PF 108, and A-PF 118) were chosen for microscopy and CL. These specimens were chosen because they were the largest specimens in cross section. Both thin sections (30 µm) and thick sections (50 µm) were made for each of the specimens, with the thick section used for CL.

3.3.3 Elemental Analyses

Samples amounting to 356 to 750 µg (average = 490 µg) from Cabo Mondego, and 189 to 800 µg (average = 530 µg) from Albstadt-Pfeffingen were weighed into 15 mL centrifuge tubes using a Micro Balance with precision of 1µg. The centrifuge tubes were then weighed to a precision of 10 µg using a microbalance. 2% concentrated HNO_3 was added from an FEP wash bottle to the centrifuge tubes to dissolve the fossil calcite. The amount HNO_3 was calculated using the following equation: acid needed (ml) = weight sample (µg) * 0.4 * 0.93 / 25 (µg/ml) resulting in a dilution to 25 µg /g Ca. The minimum amount of acid needed for analysis was 4.5 ml, so specimens whose powder weights were low and did not meet the 4.5 ml threshold had to be topped up. After dilution, the tubes were again weighed using the semi-microbalance to calculate precise dilution factors.

The element/Ca ratios were quantified using an Agilent 5110 VDV Inductively Coupled Optical Emission Spectrometer (ICP-OES) with Seaspray U-series glass nebuliser and double pass cyclonic spray chamber in the wet chemistry laboratory in the Camborne School of Mines. Sample and the standard transfer were done automatically by an Agilent SPS4 autosampler.

Analysis using the ICP-OES was performed in batches of 120 samples subdivided into blocks of 30 samples bracketed by calibrations and subdivided into sets of 10 samples by quality control solutions (BCQC & BCQ2) and international reference materials (JLs-1 limestone; UN AK carbonate; Table 3). This protocol resulted in 5 calibrations, 12 analyses of JLs-1, 8 analyses of UN AK, and 4 analyses of BCQC or BCQ2 per batch of 120 samples to ensure the geochemical data from Cabo Mondego and Albstadt-Pfeffingen were accurate.

3.3.4 Oxygen and Carbon Isotopes

Carbon and oxygen isotope ratios were measured using a Sercon 20-22 Gas Source Isotope Ratio Mass Spectrometer (GS-IRMS) in continuous flow mode at the Environment and Sustainability Institute (University of Exeter). The analytical procedures used in this study were the same as those outlined in Ullmann *et al*. (2020), with some modifications.

Samples are analysed in batches of 80 together with 22 vials of the in-house standard CAR (Carrara Marble, $\delta^{13}C$ = +2.10 ‰ V-PDB; $\delta^{18}O$ = -2.03‰ V-PDB and 8 of the in-house reference NCA (Namibia Carbonatite, $\delta^{13}C$ = -5.63 ‰ V-PDB; $\delta^{18}O$ = -21.90 ‰ V-PDB). Both standards have been previously calibrated against the international standards NBS-18, CO-8 and LSVEC. The in-house materials used on the Penryn Campus are also calibrated with those used at the University of Copenhagen (LEO, Carrara Marble).

Between 433 to 574 µg (average = 506 µg) of fossil calcite weighed to a precision of 1 µg in a randomised order using a micro balance. The samples were then transferred into a 4.5 ml round-bottom vial (borosilicate Labco Exetainers). All samples were held at 70 °C and flushed with He for 80 seconds before manual injection of 100 µL of anhydrous phosphoric acid (H_3PO_4). Isotope ratios are expressed in per mil (‰) relative to the ratios of international reference standards ($R_{standard}$), which is the Vienna PeeDee Belemnite (VPDB).

For a more detailed explanation of the Penryn Campus methodology for geochemical analysis, both element/Ca and stable isotopes, readers are directed towards the supplementary material for Ullmann *et al.* (2020).

Table 3: Standards used for elemental analysis.

Standards								
		Mg/Ca mmol/mol	Sr/Ca mmol/mol	Mn/Ca mmol/mol	Fe/Ca mmol/mol	S/Ca mmol/mol	P/Ca mmol/mol	Li/Ca mmol/mol
JLs-1	1	15.195	0.3417	0.0315	0.139	0.57	0.57	0.04
JLs-1	2	15.204	0.3437	0.0323	0.141	0.32	0.46	0.03
JLs-1	3	15.198	0.3428	0.0326	0.139	0.39	0.49	0.02
JLs-1	4	15.232	0.3425	0.0322	0.140	0.28	0.43	0.04
JLs-1	5	15.218	0.3427	0.0324	0.140	0.32	0.44	0.05
JLs-1	6	15.206	0.3427	0.0322	0.140	0.36	0.34	0.11
JLs-1	7	15.200	0.3437	0.0321	0.136	0.49	0.29	0.06
JLs-1	8	15.174	0.3429	0.0321	0.140	0.62	0.43	0.04
JLs-1	9	15.192	0.3426	0.0323	0.138	0.34	0.45	0.04
JLs-1	10	15.243	0.3429	0.0314	0.134	0.45	0.37	0.02
JLs-1	11	15.240	0.3428	0.0310	0.137	0.38	0.45	0.03
JLs-1	12	15.227	0.3430	0.0311	0.136	0.39	0.51	0.03
	average	**15.211**	**0.3428**	**0.0319**	**0.138**	**0.409**	**0.435**	**0.041**
	2sd	**0.043**	**0.0010**	**0.0010**	**0.004**	**0.211**	**0.151**	**0.050**
	2rsd	**0.28**	**0.30**	**3.3**	**3.1**	**52**	**35**	**121**
AK	1	2.533	3.0373	0.0447	1.348	1.93	0.45	0.05
AK	2	2.531	3.0483	0.0449	1.351	1.74	0.38	0.06
AK	3	2.535	3.0527	0.0452	1.349	1.65	0.40	0.07
AK	4	2.535	3.0428	0.0448	1.351	1.93	0.37	0.06
AK	5	2.532	3.0433	0.0450	1.349	1.89	0.35	0.06
AK	6	2.536	3.0389	0.0451	1.350	1.69	0.29	0.07
AK	7	2.540	3.0509	0.0438	1.351	2.00	0.38	0.05
AK	8	2.539	3.0538	0.0436	1.351	1.92	0.30	0.06
	average	**2.535**	**3.046**	**0.045**	**1.350**	**1.845**	**0.365**	**0.060**
	2sd	**0.006**	**0.013**	**0.001**	**0.002**	**0.263**	**0.102**	**0.015**
	2rsd	**0.24**	**0.41**	**2.8**	**0.18**	**14**	**28**	**24**
BCQC	1	13.254	0.9281	0.7294	1.442	2.58	2.61	1.13
BCQC	2	13.275	0.9277	0.7304	1.443	2.69	2.66	1.14
BCQC	3	13.238	0.9259	0.7301	1.442	2.61	2.77	1.13
BCQC	4	13.249	0.9269	0.7294	1.436	2.54	2.60	1.13
	average	**13.254**	**0.927**	**0.730**	**1.441**	**2.604**	**2.660**	**1.131**
	2sd	**0.031**	**0.002**	**0.001**	**0.006**	**0.123**	**0.162**	**0.013**
	2rsd	**0.24**	**0.21**	**0.14**	**0.44**	**4.7**	**6.1**	**1.19**

Bias (BCQC)							
	Mg/Ca mmol/mol	Sr/Ca mmol/mol	Mn/Ca mmol/mol	Fe/Ca mmol/mol	S/Ca mmol/mol	P/Ca mmol/mol	Li/Ca mmol/mol
should	13.28	0.923	0.730	1.445	2.518	2.613	1.161
is	13.25	0.927	0.730	1.441	2.604	2.660	1.131
deviation	-0.03	0.004	-0.001	-0.005	0.086	0.047	-0.030
Bias %	**-0.20**	**0.41**	**-0.07**	**-0.34**	**3.41**	**1.81**	**-2.59**

3.3.5 $^{87}Sr/^{86}Sr$ Ratios

Seventeen belemnite specimens from Albstadt-Pfeffingen were analysed for $^{87}Sr/^{86}Sr$ ratios at the University of Copenhagen using the same methodology as Ullmann *et al*. (2013a). The calcite powder was dissolved in 0.5 M HCl and then, after drying on a hotplate at 80°C, re-dissolved in ~0.2 ml of 3 M nitric acid. The Sr was then purified using Sr-spec resin. The samples were then diluted using de-ionised water, had 25µl of 0.1 M H_3PO_4 added before subsequent drying on 80°C hotplates and finally the material was transferred on to single rhenium filaments in 5 µl of Ta_2O_5–H_3PO_4–HF matrix.

The $^{87}Sr/^{86}Sr$ ratios were measured on a Sector VG 54 TIMS with 8 Faraday cups in dynamic multi-collection mode at 1250 to 1400 °C. The international standard used was NISTSRM-987. Signal intensities for the atomic masses 84, 85, 86, 87, and 88 were recorded. Due to havingthe same mass as ^{87}Sr, interference from ^{87}Rb was monitored by ^{85}Rb signal intensities and, whenever necessary, corrected for by the $^{87}Rb/^{85}Rb$ ratio of 0.3857.

Chapter 4: Results

4.1 Cabo Mondego

4.1.1 Carbon and Oxygen Isotopes

The $\delta^{18}O$ and $\delta^{13}C$ values of belemnite rostra from the entire study interval show a significant scatter (Table 4). Associated brachiopod data, analysed by Maria Paulsen, shows not such shift in $\delta^{13}C$ values (Figure 4.1). The $\delta^{13}C$ values range from -1.9 to 1.2 ‰ (V-PDB). The belemnite $\delta^{13}C$ record from Cabo Mondego is characterised by a distinct positive carbon-isotope shift within the upper *parkinsoni* Zone (bed 101; 3 m below the Bajocian-Bathonian boundary). The $\delta^{13}C$ values before the shift range from -1.6 to +0.4 V-PDB‰ with an average of -0.7 V-PDB‰ and post-shift range from -1.9 to +1.2 V-PDB‰ with an average of 0.1 V-PDB‰. However, some specimens exhibit $\delta^{13}C$ values different from this trend; one example being low $\delta^{13}C$ values of a single rostrum from the Lower Bathonian (bed 191; -1.91).

The $\delta^{18}O$ record from Cabo Mondego displays only modest variability ranging from -3.8 to -0.0 ‰ (V-PDB). The greatest variability in the $\delta^{18}O$ values comes from specimens below bed 75. This implies that the specimens below bed 75 were more likely to have been diagenetically altered than the specimens above bed 75.

Also, no correlation of $\delta^{18}O$ and $\delta^{13}C$ values can be observed for the belemnite samples when taken from the complete data set. However, when $\delta^{18}O$ and $\delta^{13}C$ values are split into pre-carbon-shift (beds 1 to 101) and post-carbon-shift (beds 108 to 200), a weak negative correlation can be observed in the post-shift $\delta^{18}O$ and $\delta^{13}C$ values (figure 4.2).

Table 4: Stable isotope data from Cabo Mondego.

Sample name	bed number	$\delta^{13}C$ ‰ VPDB	$\delta^{18}O$ ‰ VPDB	Sample name	bed number	$\delta^{13}C$ ‰ VPDB	$\delta^{18}O$ ‰ VPDB
JW_CM_001	1	-0.35	-1.66	JW_CM_060	93	-0.81	-0.88
JW_CM_002	2	-0.36	-1.85	JW_CM_061	94	-0.64	-0.53
JW_CM_003	5	-1.32	-0.72	JW_CM_062	95	-0.67	-0.38
JW_CM_004	6	-0.92	-0.38	JW_CM_063	95	-0.44	-0.28
JW_CM_005	7	-0.94	-0.63	JW_CM_064	96	-0.36	-0.17
JW_CM_006	10	-0.35	-2.75	JW_CM_065	99	-1.55	-0.69
JW_CM_007a	10	-1.42	-0.68	JW_CM_066	101	-0.31	-0.68
JW_CM_007b	10	-1.55	-0.45	JW_CM_067	108	0.44	-0.2
JW_CM_008	11	-0.06	-2.62	JW_CM_068	111	0.51	-0.66
JW_CM_009	16	-1.39	-0.6	JW_CM_069	112	0.22	-0.42
JW_CM_010	17	-0.47	-0.69	JW_CM_070	113	-0.14	-0.56
JW_CM_011	20	0.35	-2.02	JW_CM_072	116	1.1	-0.58
JW_CM_012	21	-0.3	-0.57	JW_CM_074	120	-0.11	-0.72
JW_CM_013	22	-0.21	-0.81	JW_CM_076	122	0.19	-0.5
JW_CM_014a	24	-0.5	-3.04	JW_CM_077	127	1.2	-0.53
JW_CM_014b	24	-1.13	-1.81	JW_CM_078	129	-0.07	-0.51
JW_CM_015	24	-0.81	-0.49	JW_CM_079	131	-0.44	-0.37
JW_CM_016	28	-0.48	-0.83	JW_CM_080	132	-0.12	-0.82
JW_CM_017	30	-0.61	-0.76	JW_CM_081	134	1.11	-0.19
JW_CM_018	30	-0.21	-2.71	JW_CM_083	136	0	-0.81
JW_CM_020	33	-1.61	-1.09	JW_CM_085	144	-0.78	-0.43
JW_CM_023	36	-1.12	-0.83	JW_CM_086	150	-0.17	-0.51
JW_CM_024	38	-1.14	-0.35	JW_CM_087	152	-0.17	-1.04
JW_CM_026	41	-1.07	-1.8	JW_CM_089	156	-0.11	-1.12
JW_CM_027	45	-0.09	-0.84	JW_CM_090	156	0.22	-0.37
JW_CM_028	47	-0.41	-0.78	JW_CM_092	158	1.13	-3.84
JW_CM_029	47	-0.96	-0.55	JW_CM_093	158	-0.48	-0.71
JW_CM_030	48	-0.79	-0.52	JW_CM_094	159	0.2	-0.73
JW_CM_031	50	-0.19	-0.63	JW_CM_097	164	-0.2	-0.31
JW_CM_033	52	-0.64	-0.39	JW_CM_099	166	0.14	-0.57
JW_CM_035	53	-0.65	-0.7	JW_CM_100	167	0.65	-0.58
JW_CM_038	58	-0.55	-0.55	JW_CM_101	167	0.06	-0.4
JW_CM_040	62	-0.3	-0.9	JW_CM_102	169	0.22	-0.63
JW_CM_041	62	-0.67	-2.2	JW_CM_103	170	1.12	-0.F04

Table 4 continued

Sample name	bed number	$\delta^{13}C$ ‰ VPDB	$\delta^{18}O$ ‰ VPDB	Sample name	bed number	$\delta^{13}C$ ‰ VPDB	$\delta^{18}O$ ‰ VPDB
JW_CM_043	65	-0.09	-2.93	JW_CM_104	171	0.17	-0.93
JW_CM_044	65	-0.81	-0.81	JW_CM_105	172	0.14	-0.49
JW_CM_046	69	-0.16	-0.6	JW_CM_106	172	0.33	-0.48
JW_CM_050	69	-0.18	-0.62	JW_CM_109	179	-0.04	-0.4
JW_CM_051	70	-0.88	-0.6	JW_CM_110	180	-0.77	-0.6
JW_CM_052	70	-0.49	-0.23	JW_CM_111	181	-0.18	-0.83
JW_CM_053	78	-0.87	-1.71	JW_CM_113	182	-0.09	-1.21
JW_CM_054	78	-0.31	-0.1	JW_CM_114	183	0.08	-0.94
JW_CM_055	79	-1.53	-0.64	JW_CM_116	187	-0.6	-0.78
JW_CM_057	82	-1.21	-0.94	JW_CM_117	191	-1.91	-0.47
JW_CM_058	90	-0.39	-0.68	JW_CM_118	200	0.27	-0.31

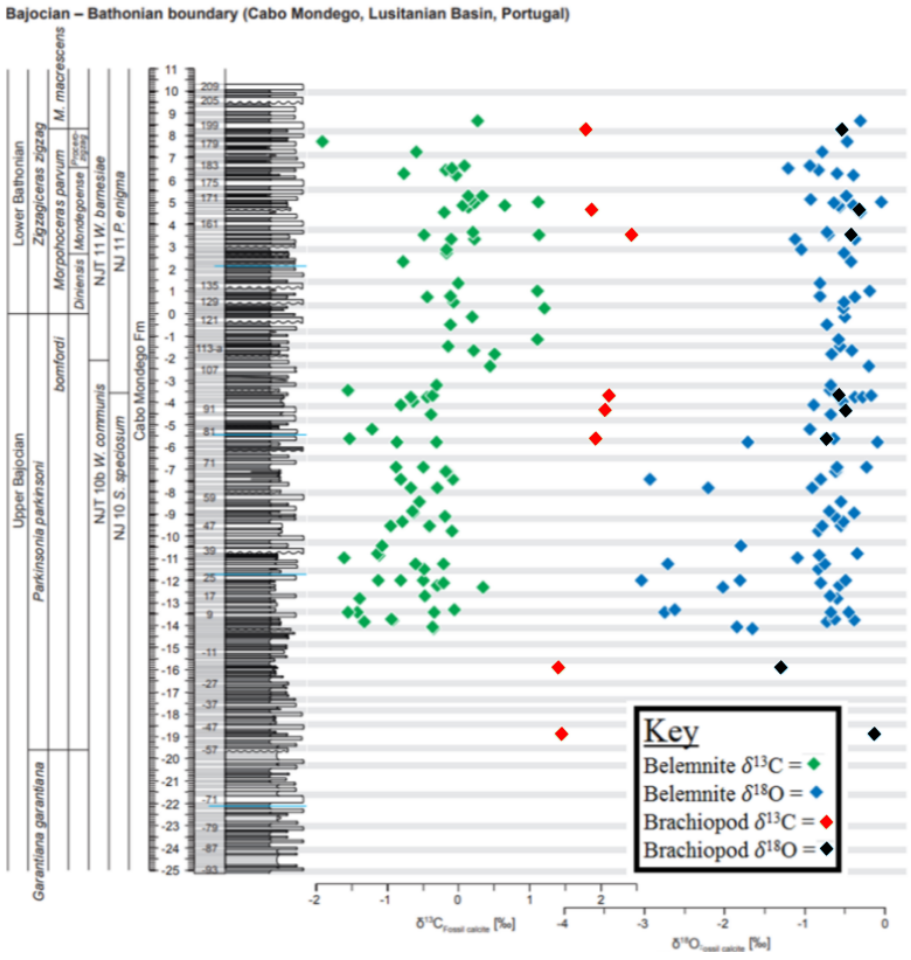

Figure 4.1: Stable isotope data from belemnite calcite, Cabo Mondego, Portugal showing positive $\delta^{13}C$ shift in belemnite data, but no such carbon isotope

excursion can be observed in the coeval brachiopod data. Lithographical succession based on Fernández-López *et al*. (2006a). Unpublished graphic provided by Dr Micha Ruhl.

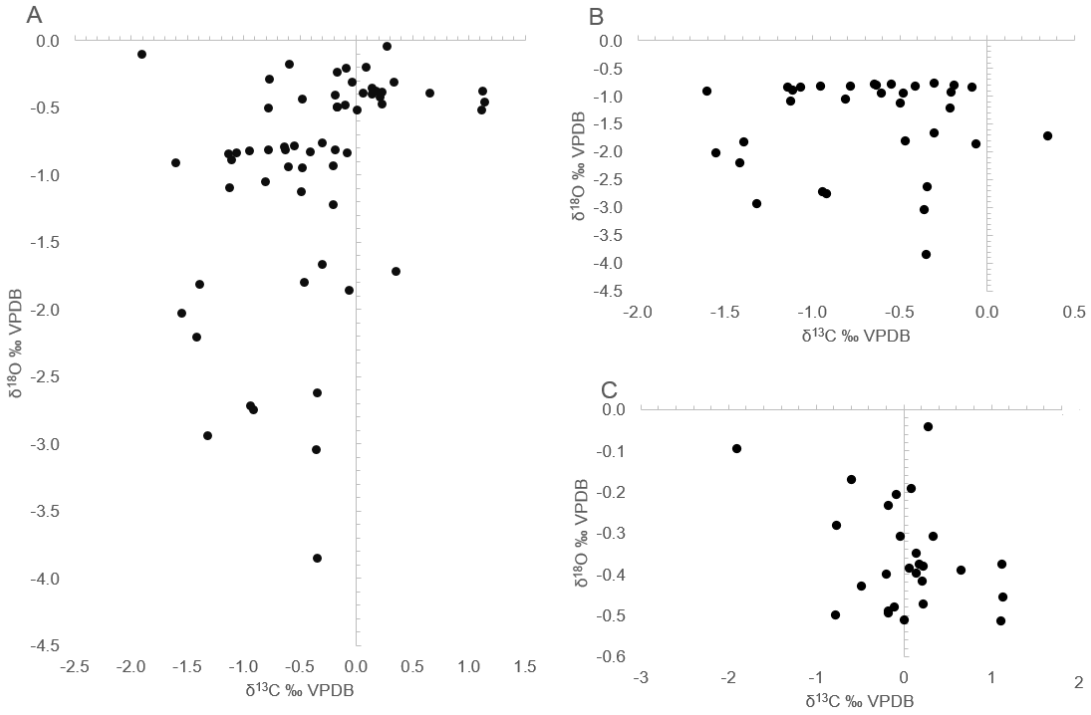

Figure 4.2 Correlations between $\delta^{13}C$ and $\delta^{18}O$ from Cabo Mondego. Y-axis = $\delta^{13}C$; X-axis = $\delta^{18}O$. A) entire section; B) pre-carbon isotope excursion (beds 1 to 101; correlative coefficient = 0.04); C) post-carbon isotope excursion showing a weak negative correlation (beds 108 to 200; correlative coefficient = -0.35).

4.1.2 El/Ca Ratios

The determined elemental/Ca ratios from the calcite samples were as follows: Fe/Ca 0-13.6 mmol/mol, mean 0.9 mmol/mol; Mn/Ca 0.01-1.4, mean 0.1 mmol/mol; Mg/Ca 8.2-27.4 mmol/mol, mean 16.5 mmol/mol; Sr/Ca 0.4- 1.5 mmol/mol mean 1.2 mmol/mol. Low Mn/Ca (<1.5) and average Fe/Ca values were low (<1). Relatively low Mn and Fe can be assumed to reflect well preserved shell material, since that is what is observed in modern molluscs (e.g., Pirrie and Marshall, 1990; Podlaha *et al*., 1998; Price and Mutterlose, 2004). Results from Fe and Mn will be discussed in 5.1.2. Trace element data is shown in Table 5 and gas source IRMS standards are shown in Table 6.

Table 5: Minor element data from Cabo Mondego.

Sample name	bed number	Mg/Ca mmol/mol	Mn/Ca mmol/mol	Sr/Ca mmol/mol	Fe/Ca mmol/mol
JW_CM_001	1	16.3	0.07	1.35	0.3
JW_CM_002	2	19.5	0.05	1.31	0.5
JW_CM_003	5	17.4	0.24	1.23	13.6
JW_CM_004	6	13.4	0.14	1.23	0.6
JW_CM_005	7	12.7	0.37	0.66	3.9
JW_CM_006	10	14.2	0.84	0.9	5.3
JW_CM_007a	10	16.2	0.05	1.36	0.3
JW_CM_007b	10	18.7	0.06	1.33	0.6
JW_CM_008	11	12.4	0.38	0.69	3.4
JW_CM_009	16	18.8	0.08	1.27	1.4
JW_CM_010	17	19.6	0.35	1.11	3.1
JW_CM_011	20	13.9	0.47	0.92	1.3
JW_CM_012	21	12.9	0.06	1.25	0.4
JW_CM_013	22	19.2	0.36	1.42	0.2
JW_CM_014a	24	21.3	0.33	0.93	2.6
JW_CM_014b	24	20.8	0.09	1.2	0.8
JW_CM_015	24	16.6	0.16	1.29	2.1
JW_CM_016	28	16.9	0.16	1.21	4.6
JW_CM_017	30	13.5	0.04	1.16	0.3
JW_CM_018	30	8.2	0.26	0.43	2.5
JW_CM_020	33	23.8	0.01	1.41	0.3
JW_CM_023	36	19.3	0.02	1.37	0.2
JW_CM_024	38	11.6	0.02	1.23	0.2
JW_CM_026	41	23.2	0.05	1.34	0.6
JW_CM_027	45	15	0.21	1.31	0.6
JW_CM_028	47	14.5	0.01	1.23	0.1
JW_CM_029	47	19.7	0.02	1.35	0.3
JW_CM_030	48	14.7	0.04	1.25	0.3
JW_CM_031	50	11.1	0.05	1.04	0.6
JW_CM_033	52	13.9	0.04	1.43	0.5
JW_CM_035	53	20.7	0.05	1.31	0.4
JW_CM_038	58	15.4	0.02	1.31	0.1
JW_CM_040	62	18.1	0.09	1.27	1.5
JW_CM_041	62	25	0.86	1.51	1.5
JW_CM_043	65	25.3	1.45	1.42	3.7
JW_CM_044	65	25	0.04	1.47	0.6
JW_CM_046	69	16.9	0.04	1.22	0.4
JW_CM_050	69	20.2	0.11	1.3	1.2
JW_CM_051	70	24.4	0.06	1.38	0.7
JW_CM_052	70	18	0.05	1.33	0.5
JW_CM_053	78	14.6	0.24	0.81	1.9
JW_CM_054	78	10.9	0.07	1.19	1.1
JW_CM_055	79	27.4	0.04	1.46	0.5
JW_CM_057	82	20.7	0.01	1.41	0.1

Table 5 continued

Sample name	bed number	Mg/Ca mmol/mol	Mn/Ca mmol/mol	Sr/Ca mmol/mol	Fe/Ca mmol/mol
JW_CM_058	90	16.4	0.01	1.27	0.1
JW_CM_060	93	21.6	0.01	1.39	0.1
JW_CM_061	94	14.6	0.01	1.25	0.1
JW_CM_062	95	12.8	0.02	1.4	0.3
JW_CM_063	95	18.7	0.01	1.26	0.3
JW_CM_064	96	20.1	0.04	1.36	0.1
JW_CM_065	99	23.7	0.01	1.43	0
JW_CM_066	101	15.9	0.03	1.35	0.5
JW_CM_067	108	11.3	0.02	1.21	0.3
JW_CM_068	111	12.2	0.03	1.23	0.1
JW_CM_069	112	13.8	0.02	1.23	0.2
JW_CM_070	113	13.1	0.04	1.27	0.4
JW_CM_072	116	18	0.1	1.26	1.4
JW_CM_074	120	17.3	0.02	1.23	0.2
JW_CM_076	122	12.4	0.03	1.19	0.3
JW_CM_077	127	21.3	0.02	1.29	0.2
JW_CM_078	129	14.1	0.06	1.22	6.7
JW_CM_079	131	11.1	0.03	1.26	0.2
JW_CM_080	132	13.3	0.05	1.14	0.5
JW_CM_081	134	16.9	0.01	1.53	0.2
JW_CM_083	136	19.3	0.01	1.52	0.1
JW_CM_085	144	10.4	0.11	0.77	1.7
JW_CM_086	150	14.6	0.01	1.45	0.1
JW_CM_087	152	19.3	0.02	1.41	0.3
JW_CM_089	156	8.9	0.06	0.69	0.7
JW_CM_090	156	20.2	0.02	1.33	0.2
JW_CM_092	158	12.3	0.24	0.83	0.8
JW_CM_093	158	25	0.03	1.35	0.1
JW_CM_094	159	14.6	0.01	1.26	0.1
JW_CM_097	164	15.2	0.02	1.29	0.1
JW_CM_099	166	12.4	0.01	1.29	0.1
JW_CM_100	167	10.8	0.05	1.2	0.4
JW_CM_101	167	12.9	0.07	1.21	2
JW_CM_102	169	12.2	0.05	1.3	0.4
JW_CM_103	170	11.8	0.01	1.3	0.1
JW_CM_104	171	16.5	0.14	1.23	0.9
JW_CM_105	172	12.9	0.03	1.25	0.2
JW_CM_106	172	15.3	0.02	1.46	0.2
JW_CM_109	179	13.9	0.02	1.23	0.4
JW_CM_110	180	14.2	0.02	1.34	0.3
JW_CM_111	181	24.9	0.15	1.54	0.7
JW_CM_113	182	14.8	0.04	1.32	0.5
JW_CM_114	183	16.6	0.02	1.27	0.2
JW_CM_116	187	13.5	0.01	1.34	0.2

Table 5 continued

Sample name	bed number	Mg/Ca mmol/mol	Mn/Ca mmol/mol	Sr/Ca mmol/mol	Fe/Ca mmol/mol
JW_CM_117	191	23.7	0.02	1.33	0.2
JW_CM_118	200	15.9	0.01	1.25	0

Table 6: Gas source IRMS standards for Cabo Mondego. Abbreviations: *CAR = Carrara Marble; NCA = Namibia Carbonatite.*

Name	$\delta^{13}C$ ‰ VPDB	$\delta^{18}O$ ‰ VPDB		$CaCO_3$ %	$\delta^{13}C$ ‰ VPDB	$\delta^{18}O$ ‰ VPDB
	2.1	**-2.03**		**97.2**	**-5.63**	**-21.9**
	0.07	**0.19**		**1.1**	**0.07**	**0.52**
	36	**36**		**16**	**16**	**16**
CAR	2.16	-2.1	NCA	97.1	-5.61	-22.31
CAR	2.04	-1.93	NCA	96.9	-5.6	-21.99
CAR	2.12	-2.07	NCA	97.7	-5.63	-21.86
CAR	2.07	-2.11	NCA	98.2	-5.68	-22.01
CAR	2.19	-1.94	NCA	97.9	-5.64	-21.73
CAR	2.06	-1.99	NCA	96.2	-5.61	-21.72
CAR	2.12	-2.02	NCA	97.7	-5.65	-22.04
CAR	2.06	-2.02	NCA	97.7	-5.6	-21.54
CAR	2.09	-2.26	NCA	96.8	-5.66	-22.31
CAR	2.08	-1.99	NCA	97.1	-5.63	-22.13
CAR	2.11	-2.05	NCA	97.1	-5.66	-22.08
CAR	2.14	-1.86	NCA	97.3	-5.68	-22.08
CAR	2.08	-2.12	NCA	96.4	-5.59	-21.91
CAR	2.09	-1.97	NCA	97.3	-5.58	-21.54
CAR	2.08	-1.98	NCA	96.6	-5.65	-21.57
CAR	2.12	-2.1	NCA	97.2	-5.58	-21.58
CAR	2.11	-2.04				
CAR	2.09	-2.01				
CAR	2.12	-2.04				
CAR	2.07	-2.03				
CAR	2.1	-2.02				
CAR	2.13	-1.98				
CAR	2.09	-2.06				
CAR	2.08	-2.14				
CAR	2.08	-2.04				
CAR	2.13	-1.86				
CAR	2.09	-2.07				
CAR	2.08	-2.06				
CAR	2.17	-2.06				
CAR	2.11	-2.06				
CAR	2	-2				
CAR	2.12	-1.95				
CAR	2.1	-2.27				
CAR	2.13	-1.88				
CAR	2.12	-1.86				
CAR	2.08	-2.18				

4.1.3 Belemnite Rostrum Cross-section Measurements (Cabo Mondego)

As a basic tool to differentiate taxa difference between heights and widths was calculated (height/width) to calculate how circular the samples were, where 1 is perfectly circular (Table 7). The “circularity” of the belemnite rostra ranged from 0.6 to 1.0. The most elliptical belemnites were found above the carbon shift (Figure 4.3). Rostrum cross-sections that were rounder tended to have lower $\delta^{13}C$ values (Figure 4.4). A strong correlation can also be identified between roundness and higher $\delta^{18}O$ values (Figure 4.5).

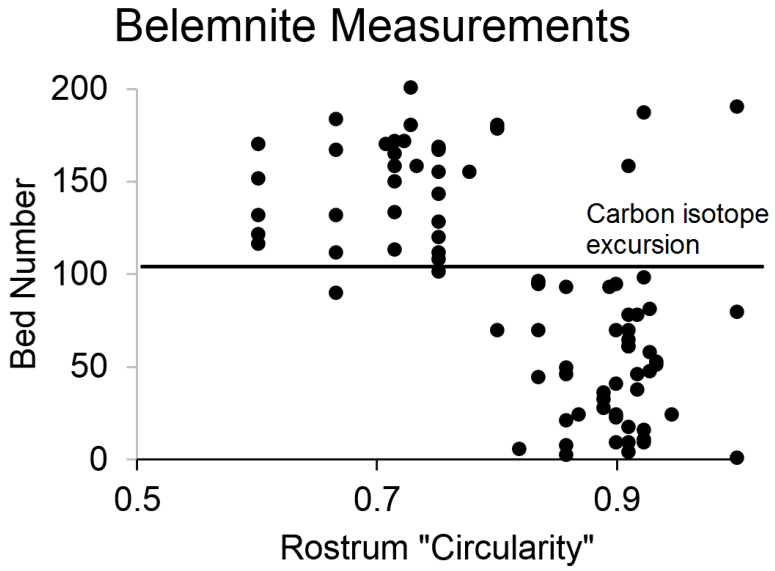

Figure 4.3: Cross plot showing belemnite rostrum “circularity” throughout the studied section. The rostrum become more oval after the carbon isotope excursion (cf. Figure 4.1).

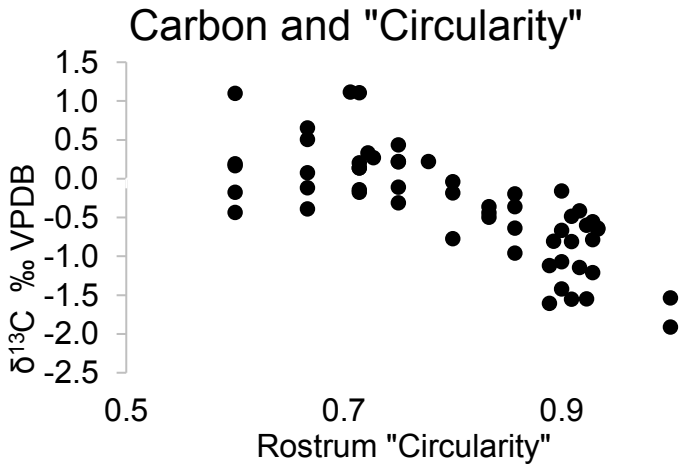

Figure 4.4: Cross plot of $\delta^{18}O$ values and circularity index Belemnites with higher $\delta^{13}C$ values have less circular rostrum cross sections. Correlation coefficient = -0.75.

Table 7: Belemnite "circularity". The closer to 1 the specimen's cross-section than the more circular the rostrum cross section.

Sample name	height mm	width mm	" Circularity "	Sample name	height mm	width mm	" Circularity"
JW_CM_001	3	3	1	JW_CM_060	5	5.6	0.89
JW_CM_002	3	3.5	0.86	JW_CM_061	6	7	0.86
JW_CM_003	5	5.5	0.91	JW_CM_062	4.5	5	0.9
JW_CM_004	4.5	5.5	0.82	JW_CM_063	5	6	0.83
JW_CM_005	6	7	0.86	JW_CM_064	2.5	3	0.83
JW_CM_006	6	6.5	0.92	JW_CM_065	6	6.5	0.92
JW_CM_007a	4.5	5	0.9	JW_CM_066	6	8	0.75
JW_CM_007b	5	5.5	0.91	JW_CM_067	3	4	0.75
JW_CM_008	6	6.5	0.92	JW_CM_068	2	3	0.67
JW_CM_009	6	6.5	0.92	JW_CM_069	3	4	0.75
JW_CM_010	5	5.5	0.91	JW_CM_070	5	7	0.71
JW_CM_011	-	-	-	JW_CM_072	3	5	0.6
JW_CM_012	3	3.5	0.86	JW_CM_074	6	8	0.75
JW_CM_013	4.5	5	0.9	JW_CM_076	3	5	0.6
JW_CM_014a	6.5	7.5	0.87	JW_CM_077	-	-	-
JW_CM_014b	8.5	9	0.94	JW_CM_078	3	4	0.75
JW_CM_015	4.5	5	0.9	JW_CM_079	3	5	0.6
JW_CM_016	4	4.5	0.89	JW_CM_080	4	6	0.67
JW_CM_017	-	-	-	JW_CM_081	5	7	0.71
JW_CM_018	-	-	-	JW_CM_083	-	-	-
JW_CM_020	8	9	0.89	JW_CM_085	6	8	0.75
JW_CM_023	8	9	0.89	JW_CM_086	5	7	0.71
JW_CM_024	5.5	6	0.92	JW_CM_087	3	5	0.6
JW_CM_026	4.5	5	0.9	JW_CM_089	6	8	0.75
JW_CM_027	5	6	0.83	JW_CM_090	7	9	0.78
JW_CM_028	5.5	6	0.92	JW_CM_092	5.5	7.5	0.73
JW_CM_029	6	7	0.86	JW_CM_093	5	5.5	0.91
JW_CM_030	6.5	7	0.93	JW_CM_094	2.5	3.5	0.71
JW_CM_031	6	7	0.86	JW_CM_097	-	-	-
JW_CM_033	7	7.5	0.93	JW_CM_099	5	7	0.71
JW_CM_035	7	7.5	0.93	JW_CM_100	3	4.5	0.67
JW_CM_038	6.5	7	0.93	JW_CM_101	4.5	6	0.75
JW_CM_040	5	5.5	0.91	JW_CM_102	3	4	0.75
JW_CM_041	5	5.5	0.91	JW_CM_103	6	8.5	0.71
JW_CM_043	-	-	-	JW_CM_104	3	5	0.6
JW_CM_044	5	5.5	0.91	JW_CM_105	5	7	0.71
JW_CM_046	4.5	5	0.9	JW_CM_106	6.5	9	0.72
JW_CM_050	4	5	0.8	JW_CM_109	4	5	0.8
JW_CM_051	5	5.5	0.91	JW_CM_110	6	7.5	0.8
JW_CM_052	5	6	0.83	JW_CM_111	4	5.5	0.73
JW_CM_053	5	5.5	0.91	JW_CM_113	-	-	-
JW_CM_054	5.5	6	0.92	JW_CM_114	3	4.5	0.67
JW_CM_055	4	4	1	JW_CM_116	6	6.5	0.92
JW_CM_057	6.5	7	0.93	JW_CM_117	4	4	1
JW_CM_058	4	6	0.67	JW_CM_118	4	5.5	0.73

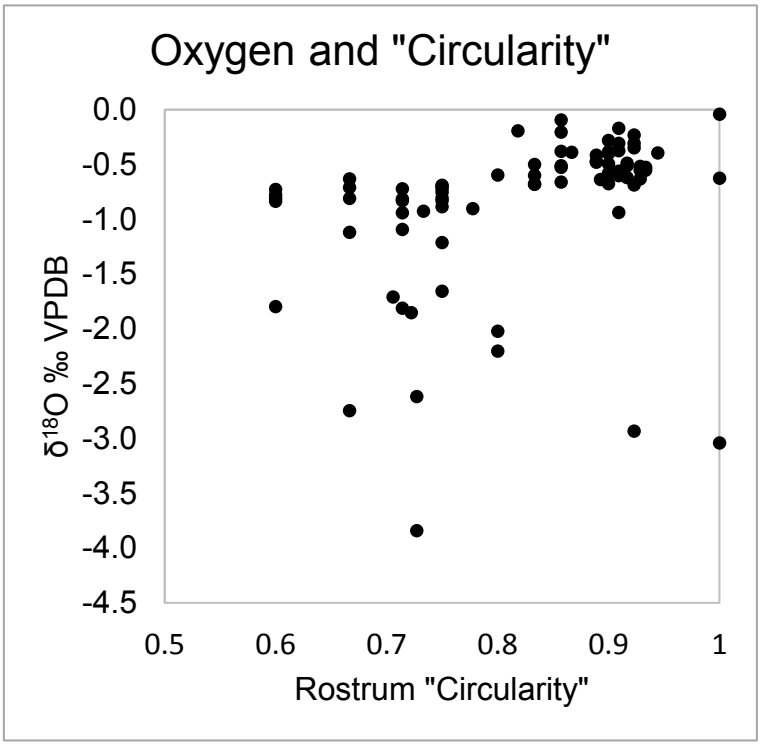

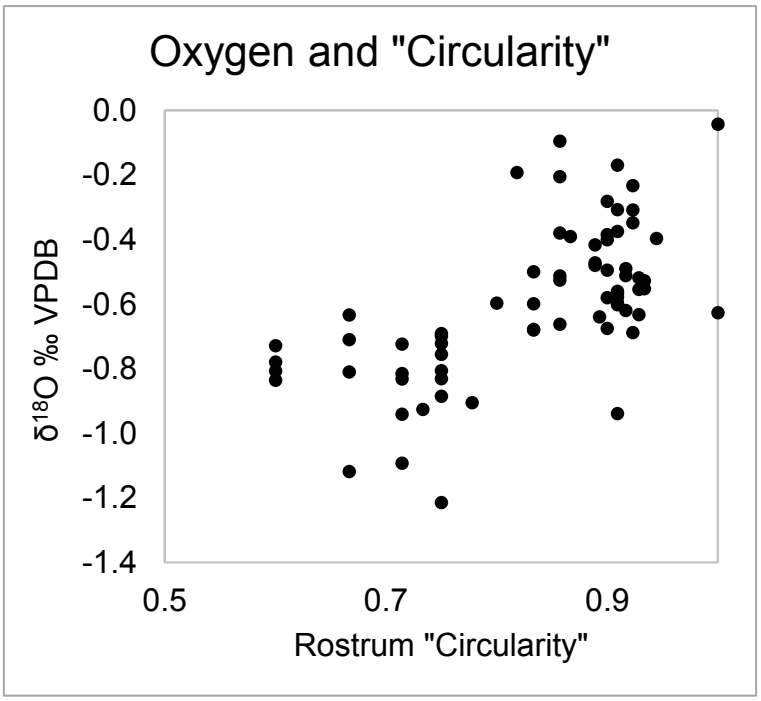

Figure 4.5: Cross plot of $\delta^{18}O$ values and circularity index. (Top) there is very weak correlation between $\delta^{18}O$ values and the rostrum “circularity (correlation coefficient = 0.33). (Bottom) when low $\delta^{18}O$ values, those <-1.5, the correlation coefficient increases to 0.63.

4.2 Albstadt-Pfeffingen

4.2.1 Carbon and oxygen isotopes

The late Bathonian – early Callovian geochemical data based on the belemnite calcite from Albstadt-Pfeffingen are shown in Figure 4.6, and the individual geochemical values are listed in Table 8 and gas source standards are shown in table 9. There are gaps in the carbon and oxygen records between 3-9 cm, 21-28 cm, and 33.5-46 cm. The $\delta^{13}C$ values range from -0.4 to +2.1 ‰ (V-PDB). A slight decrease in $\delta^{18}O$ values has also been observed. However, $\delta^{13}C$ shows little variation with no significant shift through the studied section. The $\delta^{18}O$ record from belemnites from Albstadt-Pfeffingen displays only modest variability ranging from -1.1 to +0.9 ‰ (V-PDB;). Minimum $\delta^{18}O$ ratios are observed from the base of the Macrocephalenoolith in the late Bathonian. Throughout the studied succession, there is a slight decrease in $\delta^{18}O$ values. A weak positive correlation exists between $\delta^{13}C$ and $\delta^{18}O$ in the studied population (Figure 4.7).

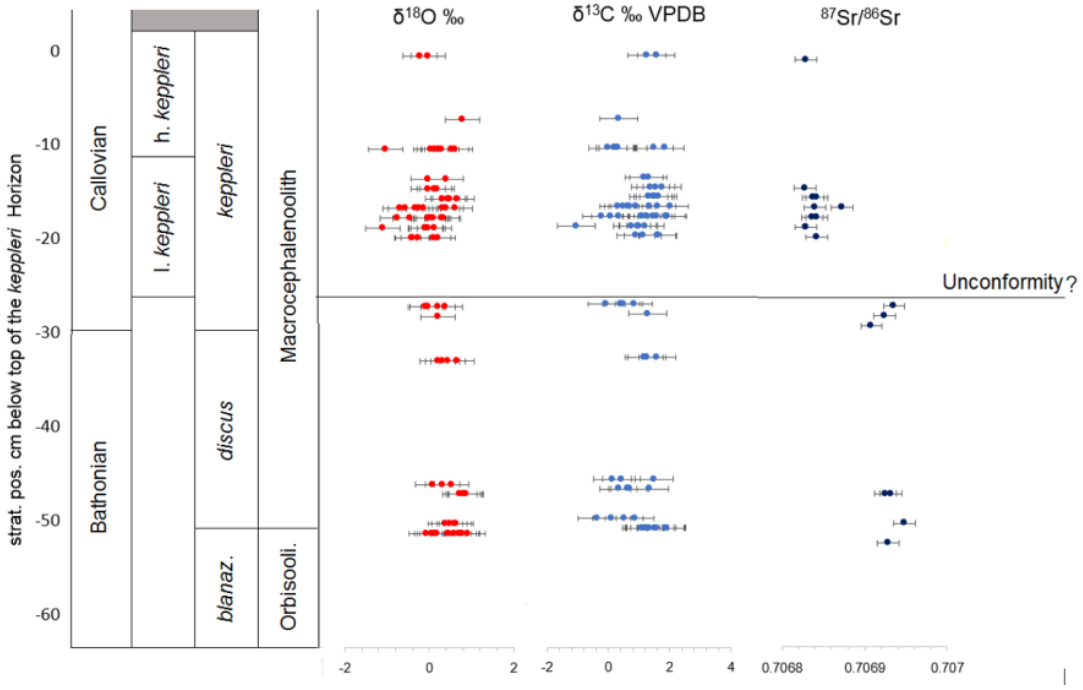

Figure 4.6: Profile of the studied section across the Bathonian-Callovian boundary showing $\delta^{18}O$, $\delta^{13}C$ and $^{87}Sr/^{86}Sr$ ratios. $^{87}Sr/^{86}Sr$ ratios show a noticeable decrease at the bottom of the *l. keppleri* Horizon, which may represent a possible unconformity, while $\delta^{13}C$ values show little variation, a gradual trend of decreasing $\delta^{18}O$ values can also be observed.

Table 8: Stable isotope data ($\delta^{13}C$ and $\delta^{18}O$) from Albstadt-Pfeffingen. Top of *kep.* refers to the *keppleri* Horizon.

name	Distance from top of *kep.* (cm)	$\delta^{13}C$ ‰VPDB	$\delta^{18}O$ ‰VPDB	name	Distance from top of *kep.* (cm)	$\delta^{13}C$ ‰VPDB	$\delta^{18}O$ ‰VPDB
APF111-26A	2.5	1.57	-0.03	APF21B	20	0.77	0.13
APF111-26B	2.5	1.26	-0.22	APF21G	20	1.21	-0.1
APF200-1-17B	9	0.34	0.79	APF20A	20	0.95	-0.09
APF8B	12	0.3	-1.03	APF20B	20	0.99	-0.08
APF8D	12	0.23	0.13	APF15C	28	0.5	0.37
APF8C	12	0	0.22	APF15A	28	-0.06	-0.09
APF8E	12	0.21	0.04	APF15B	28	0.41	0.2
APF8A	12	0.32	0.28	APF15D	28	0.83	-0.04
APF8F	12	0.31	0.2	APF16	29	1.29	0.2
APF112-25A	12	69.44	66.23	APF103	33.5	1.26	0.66
APF112-25B	12	1.86	0.61	APF105A	33.5	1.59	0.2
APF17A	15	1.31	0.4	APF105B	33.5	1.17	0.32
APF13	15	1.16	-0.02	APF105C	33.5	1.26	0.44
APF14	16	1.76	-0.04	APF25A	46	0.44	0.08
APF24B	16	1.55	0.18	APF25B	46	0.14	0.31
APF24A	16	1.37	0.12	APF30	46	1.49	0.53
APF12B	17	1.32	0.32	APF6-42A	47	1.34	0.8
APF12A	17	1.46	0.49	APF6-42D	47	0.69	0.85
APF12C	17	1.63	0.45	APF6-42B	47	0.33	0.71
APF12D	17	1.52	0.66	APF6-42C	47	0.64	0.87
APF3A	18	1.6	0.39	APF31C	50	-0.36	0.38
APF3B	18	2.01	0.32	APF31B	50	0.53	0.64
APF10	18	1.34	0.62	APF31A	50	0.11	0.47
APF11C	18	0.49	-0.25	APF31D	50	0.87	0.6
APF11A	18	0.63	-0.13	APF26G	51	1.22	0.43
APF11B	18	0.33	-0.57	APF26H	51	1.86	0.76
APF23A	18	0.9	-0.32	APF26A	51	1.53	0.19
APF23B	18	0.7	-0.69	APF26B	51	1.91	0.59
APF5C	19	1.1	0	APF26C	51	1.34	-0.08
APF5D	19	1.07	-0.03	APF26E	51	1.87	0.47
APF5A	19	1.27	0.05	APF26D	51	1.22	0.06
APF5E	19	1.46	0.05	APF26F	51	1.59	0.12
APF5B	19	1.26	0.09	APF27B	51	1.07	0.71
APF6B	19	1.87	0.34	APF27C	51	1.18	0.92
APF6A	19	1.94	0.29	APF27A	51	1.15	0.79
APF7A	19	0.34	-0.46	APF117A	21	1.57	-0.26
APF7B	19	-0.23	-0.75	APF117C	21	0.91	-0.4
APF7C	19	0.07	-0.76	APF117B	21	1.13	-0.41
APF21A	20	-1.05	-1.09	APF117D	21	1.63	0.1
APF21D	20	0.99	-0.02	APF117E	21	1.6	0.2

Table 9: Gas source standards from Albstadt-Pfeffingen. Abbreviations: *CAR = Carrara Marble; NCA = Namibia Carbonatite.*

name	$\delta^{13}C$ ‰ VPDB	$\delta^{18}O$ ‰ VPDB
CAR	2.07	-2.15
CAR	2.14	-1.86
CAR	2.08	-1.99
CAR	2.08	-2.18
CAR	2.13	-1.95
CAR	2.10	-2.04
CAR	2.04	-2.12
CAR	2.19	-1.81
CAR	2.00	-2.13
CAR	2.12	-2.11
CAR	2.18	-1.99
CAR	2.06	-2.10
CAR	2.10	-1.89
CAR	2.12	-1.99
CAR	2.07	-2.05
CAR	2.11	-2.12
CAR	2.09	-2.05
CAR	2.11	-1.99

name	% CaCO3	$\delta^{13}C$ ‰ VPDB	$\delta^{18}O$ ‰ VPDB
NCA	97.1	-5.58	-22.06
NCA	96.5	-5.71	-22.13
NCA	97.5	-5.63	-21.98
NCA	94.6	-5.64	-21.96
NCA	97.6	-5.59	-21.87
NCA	98.5	-5.70	-21.79
NCA	97.6	-5.57	-21.51

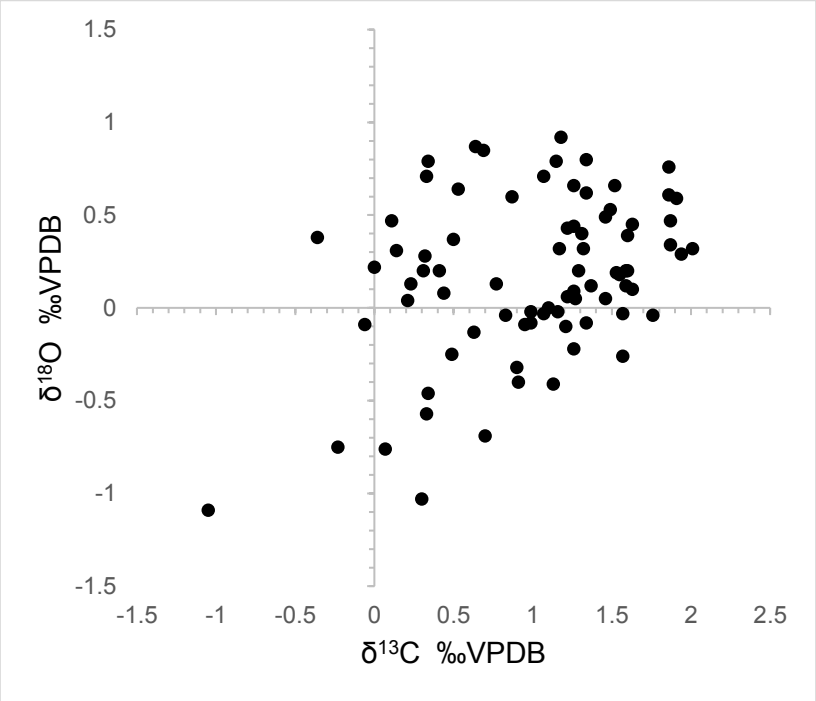

Figure 4.7: Cross plot of $\delta^{18}O$, and $\delta^{13}C$ values showing possible, though weak, positive correlation which may be caused by fractionation due to water depth. Correlation coefficient = 0.37.

5.2.2 El/Ca Ratios

Elemental/Ca ratios from Albstadt-Pfeffingen were as follows: Fe/Ca 0.05-7.7 mmol/mol, mean 0.9 mmol/mol; Mn/Ca 0.01-1.4, mean 0.1 mmol/mol; Mg/Ca 9.6-25.5 mmol/mol, mean 14.5 mmol/mol; S/Ca 2.4-8.5 mmol/mol, mean 3.9 mmol/mol; Sr/Ca 1-1.8 mmol/mol mean 1.4 mmol/mol; P/Ca 0.5-2.3 mmol/mol, mean 1 mmol/mol. Minor element data is presented in Table 10.

Table 10: Minor element data from Albstadt-Pfeffingen. Top of *kep.* refers to the *keppleri* Horizon.

Specimen name	Distance from top of *kep.* (cm)	Mg/Ca mmol/mol	Sr/Ca mmol/mol	Mn/Ca mmol/mol	Fe/Ca mmol/mol	S/Ca mmol/mol	P/Ca mmol/mol
APF111-26A	2.5	12.03	1.372	0.164	0.5	4.76	0.88
APF111-26B	2.5	12.1	1.362	0.124	0.67	4.55	1.01
APF200-1-17B	9	13.76	1.625	0.062	0.4	4.83	0.83
APF8B	12	17.34	1.509	0.339	1.59	5.22	1.59
APF8D	12	13.35	1.422	0.516	2.99	3.3	1.23
APF8C	12	13.55	1.491	0.13	0.72	4.06	1.07
APF8E	12	12.78	1.373	0.114	0.64	3.78	1.04
APF8A	12	12.34	1.388	0.162	1.24	4.34	1.09
APF8F	12	13.59	1.526	0.036	0.25	3.97	1.17
APF112-25A	12	11.24	1.444	0.1	4.49	4.05	0.83
APF112-25B	12	11.47	1.441	0.14	7.79	2.75	0.61
APF17A	15	14.07	1.355	0.057	0.24	5.03	0.76
APF13	15	13.03	1.323	0.06	0.52	3.07	0.64
APF14	16	11.04	1.25	0.435	2.16	4.56	0.76
APF24B	16	12.33	1.402	0.012	0.05	3.52	0.92
APF24A	16	11.51	1.533	0.174	1.77	2.95	0.85
APF12B	17	10.05	1.2	0.05	0.26	3.69	0.66
APF12A	17	9.87	1.08	0.079	0.33	3.81	0.62
APF12C	17	10.1	1.213	0.053	0.23	3.56	0.54
APF12D	17	10.22	1.17	0.02	0.05	3.68	0.63
APF3A	18	18.42	1.626	0.403	0.83	5.34	1.12
APF3B	18	14.35	1.669	0.018	0.07	2.41	0.81
APF10	18	15.51	1.266	1.476	7.78	4.02	0.75
APF11C	18	17.3	1.711	0.414	1.18	4.72	1.14
APF11A	18	13.68	1.563	0.044	0.21	4.05	0.7
APF11B	18	15.65	1.64	0.22	0.59	4.48	0.89
APF23A	18	12.4	1.513	0.038	0.13	4.18	0.83
APF23B	18	13.66	1.524	0.045	0.22	4.4	0.71
APF5C	19	11.03	1.225	0.1	0.41	2.45	0.54
APF5D	19	10.83	1.277	0.048	0.16	2.5	0.67
APF5A	19	12.95	1.395	0.092	0.6	3.89	1
APF5E	19	12.71	1.34	0.065	0.3	3.22	0.98

Table 10 continued

Specimen name	Distance from top of *kep.* (cm)	Mg/Ca mmol/mol	Sr/Ca mmol/mol	Mn/Ca mmol/mol	Fe/Ca mmol/mol	S/Ca mmol/mol	P/Ca mmol/mol
APF6B	19	16.78	1.562	0.258	0.48	4.54	1.13
APF6A	19	12.59	1.521	0.086	0.35	3.05	0.82
APF7A	19	12.66	1.439	0.356	0.38	3.49	0.66
APF7B	19	16.51	1.523	0.46	0.45	4.18	1.1
APF7C	19	16.32	1.438	0.429	0.43	4.24	1.08
APF20A	20	12	1.387	0.111	1.35	3	0.74
APF20B	20	15.39	1.527	0.171	1.06	4.22	1
APF21A	20	25.56	1.402	0.167	0.69	5.04	2.13
APF21D	20	14.76	1.348	0.096	0.36	4.38	1.43
APF21B	20	14.48	1.308	0.1	0.34	4.17	1.31
APF21C	20	14.83	1.25	0.13	0.57	4.1	1.47
APF117A	21	13.55	1.452	0.395	2.85	3.12	0.93
APF117C	21	21.42	1.837	0.065	0.37	2.79	1.37
APF117B	21	21.92	1.741	0.065	0.19	3.08	1.38
APF117D	21	15.58	1.741	0.049	0.19	3.76	1.35
APF117E	21	15.2	1.499	0.035	0.28	3.12	1.24
APF15C	28	18.94	1.456	0.044	0.21	4.29	1.13
APF15A	28	18.62	1.647	0.038	1.62	3.64	1.25
APF15B	28	15.15	1.585	0.032	0.23	3.11	1.08
APF15D	28	12.85	1.448	0.14	4.57	3.14	0.96
APF16	29	13.49	1.426	0.114	0.64	4.23	0.94
APF103	33.5	13.62	1.592	0.249	2.23	4.5	1.62
APF105A	33.5	12.3	1.493	0.219	1.01	4.96	1.08
APF105B	33.5	9.75	1.222	0.07	0.31	3.37	0.78
APF105C	33.5	10.5	1.226	0.092	0.38	2.88	0.92
APF25A	46	18.16	1.368	0.192	0.59	5.64	1.21
APF25B	46	17.27	1.482	0.134	0.96	4.32	1.36
APF30	46	14.67	1.678	0.145	0.6	4.87	1.2
APF6-42A	47	17.64	1.552	0.151	0.46	8.54	1.15
APF6-42D	47	23.17	1.792	0.042	0.1	5.93	1.95
APF6-42B	47	20.42	1.762	0.018	0.13	4.55	1.67
APF6-42C	47	19.52	1.549	0.035	0.09	3.63	1.64
APF31C	50	23.46	1.64	0.867	3.68	4.33	2.34
APF31B	50	21.02	1.631	0.083	0.53	3.76	1.9
APF31A	50	18.11	1.675	0.091	0.42	3.3	1.47
APF31D	50	19.49	1.677	0.151	0.94	4.69	2.06
APF26G	51	14.07	1.27	0.056	0.2	3.35	1.01
APF26H	51	10.56	1.292	0.066	0.22	2.9	0.88
APF26A	51	10.65	1.336	0.043	0.29	2.86	0.73
APF26B	51	9.59	1.253	0.064	0.26	2.96	0.87
APF26C	51	12.74	1.45	0.126	0.75	4.5	0.99
APF26E	51	9.68	1.239	0.062	0.72	3.17	0.84

Table 10 continued

Specimen name	Distance from top of *kep.* (cm)	Mg/Ca mmol/mol	Sr/Ca mmol/mol	Mn/Ca mmol/mol	Fe/Ca mmol/mol	S/Ca mmol/mol	P/Ca mmol/mol
APF26D	51	11.99	1.407	0.086	0.55	3.85	0.93
APF26F	51	11.34	1.313	0.078	0.41	3.95	0.97
APF27B	51	14.74	1.375	0.035	0.13	4.53	0.83
APF27C	51	16.03	1.562	0.051	0.22	3.74	1.11
APF27A	51	17.28	1.37	0.038	0.24	4.69	1.8

4.2.3 Cathodoluminescence and Petrography

Possible diagenetic alterations of the studied belemnites have been evaluated using petrographic and geochemical techniques. In general, petrographic observations of most of the studied belemnites indicate good microstructural preservation.

The third method commonly used to identify diagenesis is cathodoluminescence; a specialist laboratory technique which is used to provide textual and geochemical analysis of rocks and fossils. Cathodoluminescence works by bombarding samples with high energy electrons. Different minerals and elements then emit photons at different intensities. The process and applications of cathodoluminescence are summarized by Boggs and Krinsley (2006).

The intensity of cathodoluminescence in calcite is usually grouped into three categories defined by Savard *et al*. (1995): non-luminescent characterised by black and dull colours that show no diagenetic alterations and material with a high level of diagenetic alteration (e.g., those with high amounts of Mn) appear as orange-red (e.g. Sælen, 1989; Podlaha *et al*., 1998; Wierzbowski and Joachimski, 2009; Ullmann and Korte, 2015; Stevens *et al*., 2020). In pure calcite or calcite with minor traces of substituting elements shows a faint blue colour under CL caused by crystal imperfection (Sipple and Glover, 1965; Mason, 1987; Habermann *et al*., 1998), while the orange-red CL is already induced by very low Mn contents (< 1 ppm) in the calcite crystal-lattice (e.g., Habermann *et al*., 1998).

Orange to red luminescence, indicative of alteration, is observed in the section perpendicular to the apical line, in concentric bands (strongest in the first thicker band around the apical zone) and along fracture lines which can be seen in both light microscopy and under CL (Figure 4.8). The apical line and growth bands are often diagenetically overprinted (e.g., McArthur *et al.,* 2000, 2007a; Bailey *et al.,* 2003, Benito and Reolid, 2012, 2020; Li *et al*., 2012; Ullmann., 2013a, 2015), so this result was expected.

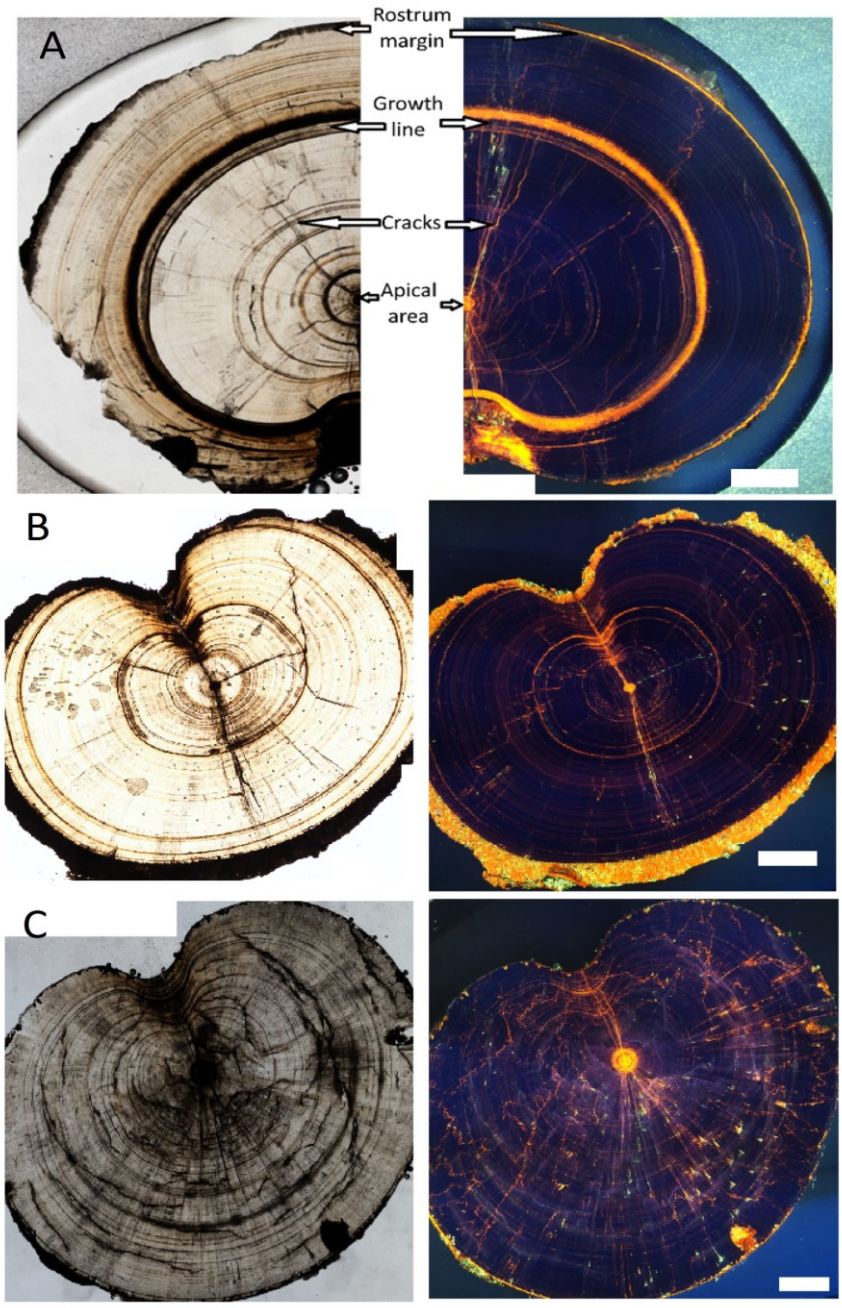

Figure 4.8: Light microscope (left) and cathodoluminescence (right) photographs of three belemnite rostra (A. APF-105; B. APF-108; C. APF-118) from Albstadt-Pfeffingen. Areas with the most diagenetic alternation, shown in yellows and oranges, are found along the margins, apical region, and prominent cracks and growth bands. Scale bar = 1mm.

4.2.4 $^{87}Sr/^{86}Sr$ Ratios

$^{87}Sr/^{86}Sr$ ratios from the belemnite calcite at Albstadt-Pfeffingen vary from 0.706828 to 0.706948 and are shown in Table 11. Such values are within the expected range for the Middle Jurassic (Jones *et al*., 1994; Howarth and McArthur, 1997; McArthur *et al*., 2000, 2012; Jenkyns *et al*., 2002; Wierzbowski *et al*., 2012, 2017; Ullmann *et al*., 2013a). The $^{87}Sr/^{86}Sr$ show a decrease from an average of 0.70693 to 0.70684 at 29 cm below the top of the *Keppleri* Horizon, which corresponds to the bottom of the l*. keppleri* Subzone (cf. Figure 4.6). The average $^{87}Sr/^{86}Sr$ value from 47 cm below (214 and 217; mean 0.706928), 30-28 cm below (211, 212 and 213; mean 0.706923) and 21-20 cm below (209 and 210; mean 0.706836) were also plotted on the LOWESS 5 Fit.

Table 11: Strontium isotope data and associated minor elements from belemnite calcite, Albstadt-Pfeffingen. Analysis performed at the University of Copenhagen.

Sp. name	$^{87}Sr/^{86}Sr$ ratio	Distance below top *keppleri* cm	1 err rel.	2err abs	Mn/Ca mmol/mol	Sr/Ca mmol/mol	Mg/Ca mmol/mol	Fe/Ca mmol/mol
201	0.706829	-3	6	-36	0.06	1.25	10.4	0.15
202	0.706828	-16	5	-160	0.06	1.12	9.7	0.38
203	0.706842	-17	5	-170	0.06	1.17	9.6	0.18
204	0.706838	-17	6	-204	0.01	1.43	15.3	0.13
205	0.706872	-18	6	-216	0.05	1.53	13.4	0.18
206	0.706840	-18	7	-252	0.07	1.45	13	0.32
207	0.706842	-19	5	-190	0.06	1.26	13.2	0.21
208	0.706836	-19	6	-228	0.05	1.38	12.5	0.19
209	0.706829	-20	6	-240	0.08	1.3	9.6	0.28
210	0.706842	-21	5	-210	0.01	1.43	14.8	0.02
211	0.706936	-28	5	-280	0.06	1.4	11.2	0.63
212	0.706924	-29	6	-348	0.04	1.39	12.1	0.23
213	0.706908	-30	7	-420	0.04	1.5	12.1	0.14
214	0.706925	-47	5	-470	0.06	1.4	11.1	0.35
215	0.706932	-47	7	-658	0.03	1.32	16.6	0.23
216	0.706948	-50	5	-500	0.11	1.3	15.3	0.39
217	0.706928	-52	5	-520	0.06	1.22	11.2	0.18

Chapter 5: Sample Preservation

5.1 Elemental Contamination

5.1.1 Alternation Indicators

The elements incorporated into belemnite calcite can be subdivided into two groups: structural and detrital (see Table 12). Elements incorporated during the structural phase can be substituted for Ca in the calcite crystal lattice. The detrital phase are elements that are insoluble and form solid contamination particles that are absorbed in altered areas of the belemnite rostra. Mn and Fe were selected to be diagenetic markers in this study (see 5.1.2 and 5.1.3). Marine invertebrates do contain some Fe as a metabolic element. Concentrations of Fe >30 ppm and Mn >10ppm are toxic in live organisms, so elevated Fe and Mn comes from post-mortem diagenetic fluids. Mn and Fe also reflect different alternation conditions, Mn refers to alteration under Mn-reducing conditions which precede Fe-reduction (Li, 2011).

Table 12: Element incorporation into belemnite calcite. Mn^{2+} and Fe^{2+} can substitute for Ca^{2+} only under post-oxic/anoxic conditions so indicate alternation. Adapted from Li (2011).

Phase	Elements	Compounds
Structural	Ca, Na, Mg, Sr, SO_4^{2+}, Mn^{2+}, Fe^{2+}	Na_2CO_3, $SrCO_3$, $CaMg(CO_3)_2$
Detrital	Mn, Fe, Rb, Y, Ce, Pb, Th, U	FeS_2, MnO_2, RbO_2 , CeO_2
Both	Zn, Ba	$ZnCO_3$, ZnS_2, $BaSO_4$

In modern *Sepia officinalis,* the Fe and Mn values are reported by Milliman (1974) as 32 ppm and 4 ppm respectively (these values are also supported by Miramand and Bentley, 1992). Such studies suggest that relatively low Fe and Mn concenrtractions should be present in well-preserved belemnite rostra. Researchers (Pirrie and Marshall, 1990; Podlaha *et al*., 1998; Price and Mutterlose, 2004) accept that values of <150 ppm Fe and <100 ppm indicate well-preserved belemnite samples.

5.1.2 El/Ca Ratios (Cabo Mondego)

Trace element analysis from Cabo Mondego revealed low Fe (<13.60 mmol/mol; av. 0.98 mmol/mol) and Mn (<1.45 mmol/mol; av. 0.11 mmol/mol) as well as high Sr (>0.43 mmol/mol; av. 1.24 mmol/mol) concentrations in all belemnite rostra which indicates good preservation of these fossils (cf. Price and Sellwood, 1997; Wierzbowski, 2004; Wierzbowski and Joachimski, 2007; Ullmann and Korte, 2015). There is a decrease in Mn/Ca ratios throughout the studied succession (Figure 5.1).

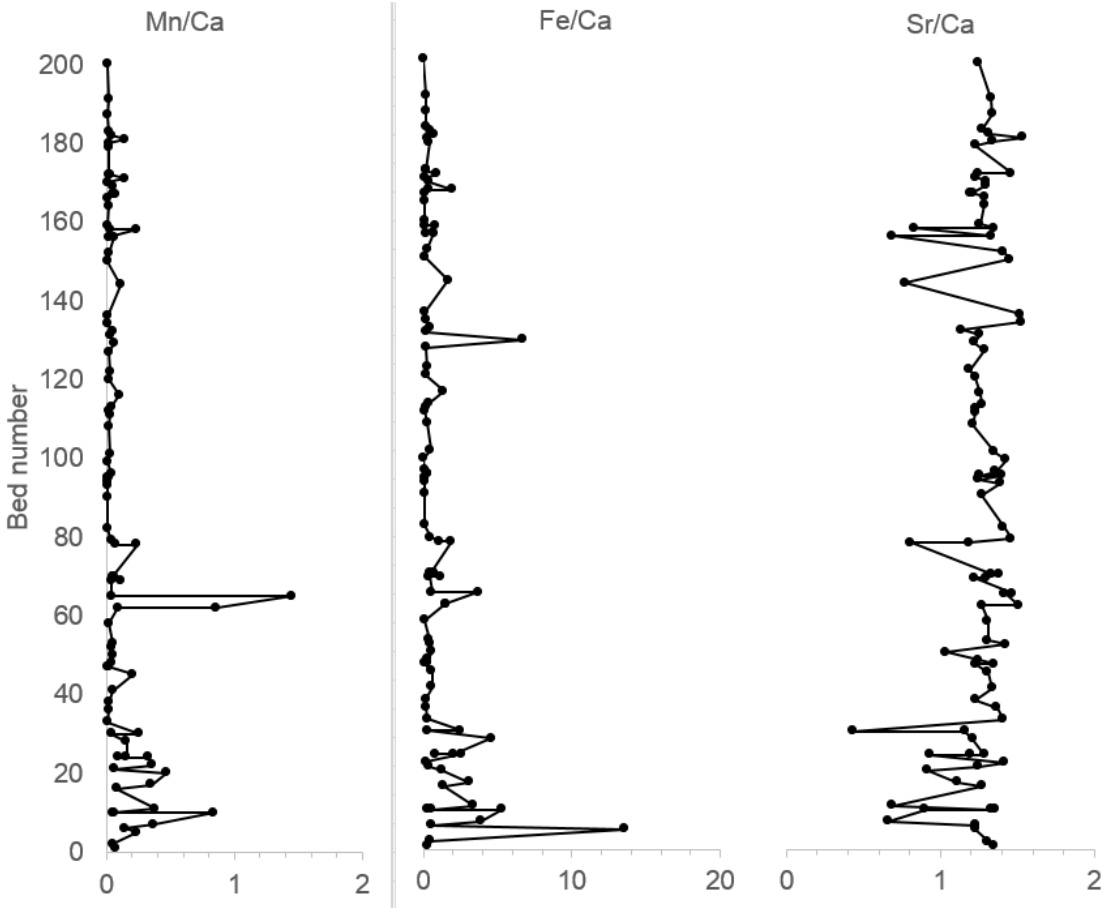

Figure 5.1: Specimens from the lower part of the section are more prone to elevated Mn and Fe ratios but no such trend is observed in Sr/Ca ratios at Cabo Mondego.

No diagenetic trend is observed in Sr/Ca ratios but a decreasing Mn/Ca and Fe/Ca ratios are observed within the studied section. The higher Fe/Ca and Mn/Ca and lower Sr/Ca ratios corresponds with diagenetically altered oxygen isotopes (those with lower $\delta^{18}O$ values). The ratios of Fe/Ca, and Mn/Ca and $\delta^{18}O$

values return to more expected “background” levels above bed 75. One of the causes for this might be that the lower beds (those below bed 75) are more susceptible to diagenetic alteration. This would explain why the change to a more expected background level co-occurs when the lower $\delta^{18}O$ values become less prevalent.

The rock type may explain the decrease in diagenesis. The lower Cabo Mondego Formation contains more prominent marls while limestone becomes more dominant as the formation progresses. Marlstone is a sedimentary rock consisting of calcium carbonate and clay (Meyer and Martínez-Casasnovas, 1999). Marlstones friable are more than the limestone beds. The higher friability would make marlstone more porous than limestones would have resulted in more interactions between shell material and pore fluids resulting in a higher degree of diagenetic alteration. Because the change in the Mn/Ca and Fe/Ca ratios occurred before the carbon isotope shift, the positive $\delta^{13}C$ excursion could not have been caused by diagenesis.

The Mn/Ca is the most widely employed alteration marker because Mn levels in primary shell material are usually very low, while diagenesis leads to Mn enrichment (Veizer, 1974, Brand and Veizer, 1980, Ullmann *et al*., 2014). For this study, samples with Mn/Ca >0.2 mmol/mol were excluded from subsequent palaeotemperature analysis. It is imperative that highly altered samples, those with elevated Mn/Ca ratios, should be excluded as these samples exhibit lower $\delta^{18}O$ values of diagenetic origin. An Mn/Ca threshold of >0.2 mmol/mol used here falls in the lower end of applied limits (see Table 1 in Ullmann and Korte, 2015; Figure 5.2). This Mn limit was chosen as it corresponds with the Mn/Ca ratios of the lowest, and therefore most diagenetically altered, $\delta^{18}O$ ratios. This Mn/Ca ratio is thus adopted for the maximum acceptable degree of alteration. The enrichment of altered macrofossil calcite depends on Mn availability and solubility within the diagenetic environment. Mn becomes incorporated in calcite from Mn-bearing phases in the sediments, and the Mn/Ca ratio can be highly variable, even within individual rostra, as is observed at Cabo Mondego.

Belemnite specimens recovered from the clay layers at Cabo Mondego may be less susceptible to diagenetic alteration. Clays are more prevalent in the upper portions of the studied section, explaining the lower Fe/Ca and Mn/Ca

ratios higher in the succession. A study on Eocene planktonic foraminifera by Pearson *et al.* (2001) looked at samples from impermeable clays and coarse-grained deep marine permeable sediments. The authors concluded that the "sealed" forams (i.e., those recovered from the clay layers) retained their original geochemical composition. Simultaneously, those from the coarse-grained sediments had shown evidence of recrystallization and thus resetting their stable isotopes to that of the deep ocean.

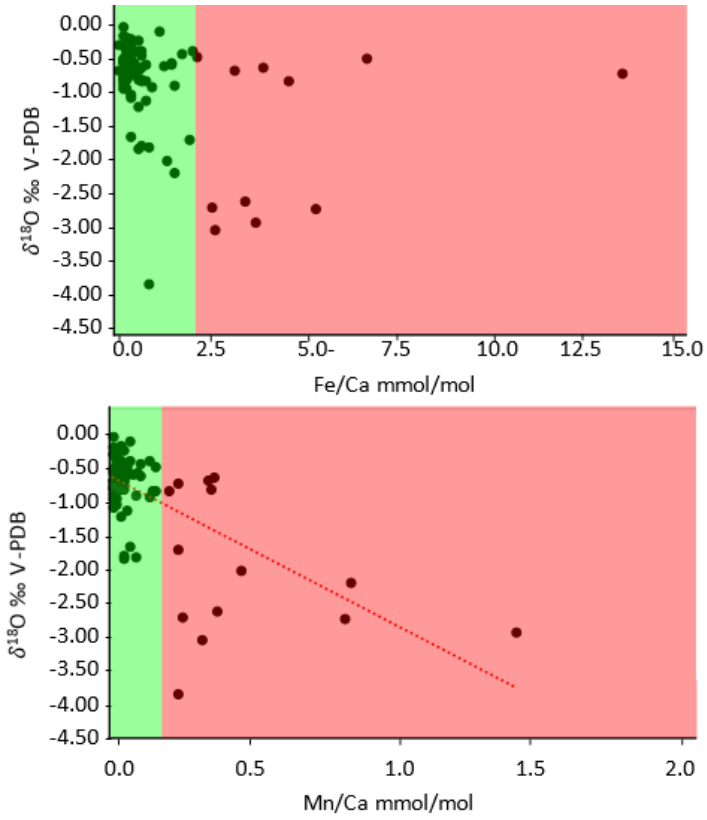

Figure 5.2: Scatterplots of oxygen isotope ratios versus Fe/Ca (correlation coefficient = -0.25) and Mn/Ca ratios (correlation coefficient = -0.63). $\delta^{18}O$ results above the diagenetic cut off point of Mn/Ca >0.2 mmol/mol were excluded from later analysis. A strong negative correlation between Mn/Ca and $\delta^{18}O$ values suggests that both were changing as a response to diagenetic overprinting and is, potentially, more reliable for identifying diagenesis in the studied section. A potential diagenetic trend in Mn/Ca is based on an observation made in Korte and Hesselbo (2011).

5.1.3 El/Ca Ratios (Albstadt-Pfeffingen)

An upper limit of 0.2 Mn/Ca mmol/mol was also chosen (Figure 6.3) for the same reasons stated in 5.1.2. The samples with the highest Mn/Ca ratios were taken from the apical line. During diagenesis, carbon and oxygen isotopes are

usually shifted to lower ratios (e.g., Marshall, 1992; Korte and Hesselbo, 2011). However, these higher Mn/Ca values do not correspond to decreased $\delta^{18}O$ values, as would be expected from secondary diagenesis (Brand and Veizer, 1981).

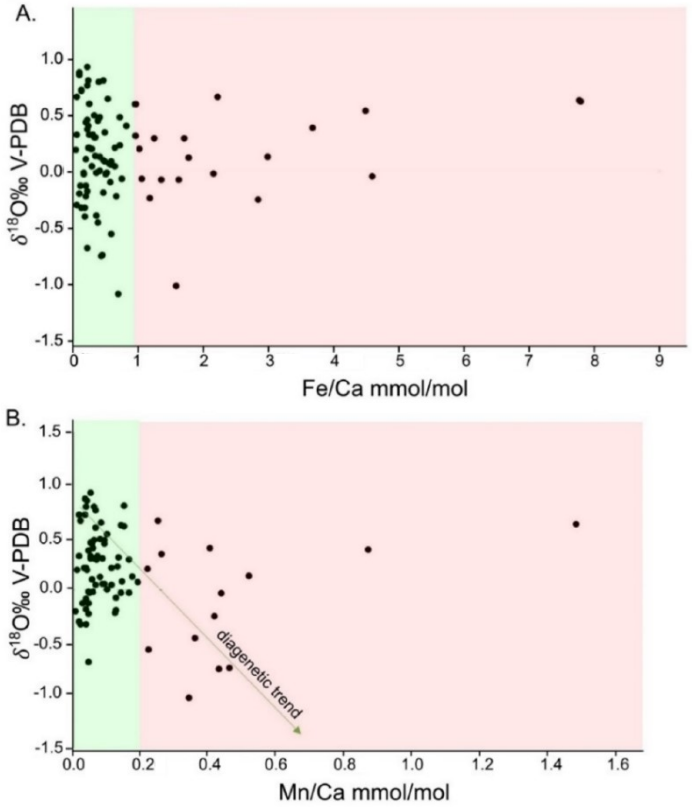

Figure 5.3: (A) Scatterplots of oxygen isotopes versus Fe/Ca concentrations at Albstadt-Pfeffingen (correlation coefficient = 0.29). The diagenetic cut-off point of Fe/Ca for samples was 1.0 mmol/mol. (B) Scatterplots of oxygen isotopes versus Mn/Ca concentrations (correlation coefficient = -0.03). The diagenetic cut-off point of Mn/Ca for samples was 0.2 mmol/mol.

Unlike Cabo Mondego, the Mn/Ca ratios at Albstadt-Pfeffingen shows no correlation with $\delta^{18}O$ (correlation coefficient =-0.03). Thus, Mn appears to be a poor marker for diagenesis as the covariation with $\delta^{18}O$ is non-existent and the power to discriminate between preserved and altered material is minimal as low $\delta^{18}O$ values are still present even with a low Mn/Ca cut-off point.

However, Fe/Ca shows a weak positive correlation with $\delta^{18}O$ (correlation coefficient = 0.29) which is the opposite as would be expected from diagenesis (e.g.). This unexpected result may have been a result of the high iron content of the surrounding matrix and the highest Fe/Ca ratios corresponds with a darker

bed ca. 8-22 cm below the top of the *keppleri* Subzone (Figure 5.4). High iron content was expected from Albstadt-Pfeffingen as the Macrocephalenoolith is an iron-oolite horizon (Beher et al, 2010)

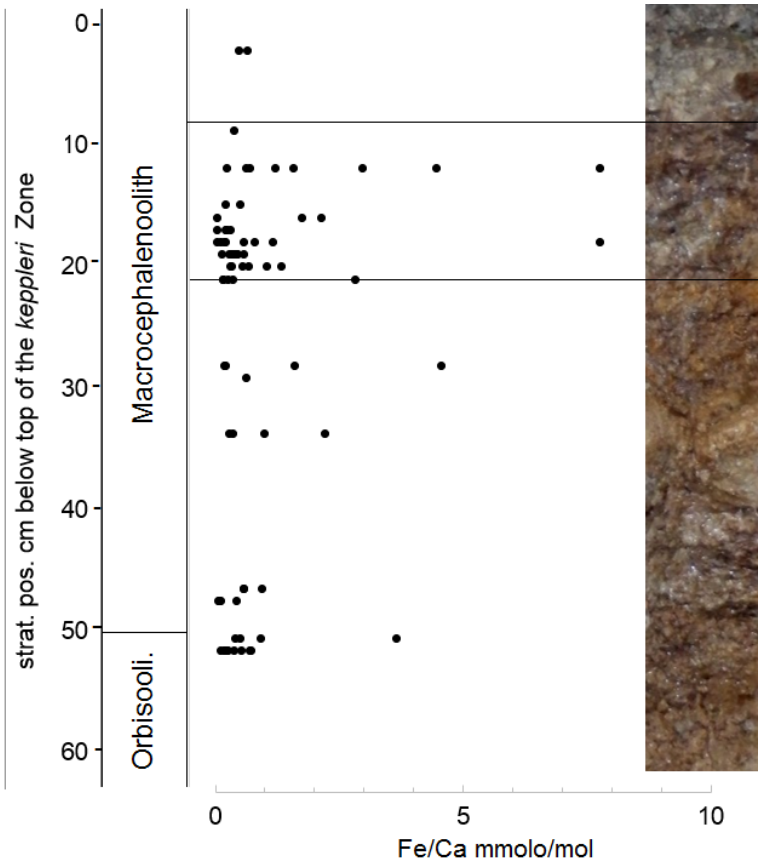

Figure 5.4: Fe/Ca compared to stratigraphy at Albstadt-Pfeffingen. The increase in Fe/Ca between 8-12 cm below the top of the *keppleri* Subzone can likely be explained by an increase in iron content in the sediment.

5.2 Cathodoluminescence and Petrology

Cathodoluminescence was conducted on three specimens from Albstadt-Pfeffingen to identify the belemnite rostrum areas most prone to diagenetic alteration. Still, it was not performed on any specimens from Cabo Mondego due to the 2020 Covid-19 pandemic (though it is hoped that cathodoluminescence imaging can be conducted on the Portuguese material before the publication of a peer-review paper based on this thesis). The results gathered from CL imaging shows that the margins, the region surrounding the apical canals, fractures within the calcite, and prominent growth bands are most susceptible to diagenesis and secondary mineral replacement.

Chapter 6: Discussion

6.1 Carbon Isotope Excursion at Cabo Mondego.

A pronounced positive $\delta^{13}C$ isotopic shift can be seen in the belemnite stable isotope record from the studied section of Cabo Mondego (Figure 4.1). Two potential causes for the excursion may be considered: changes in the carbon cycle and faunal turnover.

6.1.1 Hypothesis 1: Changes in the Carbon Cycle During the Middle Jurassic.

If the marine $\delta^{13}C$ curve based on analysis of marine calcite fossils is considered to represent variation in the global carbon cycle, pronounced positive and negative shifts within the carbon-isotope record may be of some palaeoenvironmental significance. The general trend of the Iberian Peninsula during the Middle Jurassic (Upper Aalenian to Lower Callovian) carbon cycle is summarised by O'Dogherty *et al.* (2006):

(a) *concavum* to *limitatum* Subzones: large excursion to lighter values (δ =0.8‰)

(b) *walkeri* to *romani* Subzones: large positive excursion (δ =1‰),

(c) *humphriesianum* to *blagdeni* Subzones: back to median values and stabilization,

(d) *banski* to *baculata* Subzones: shift to lower values,

(e) *garantiana* Zone to *daubenyi* Subzone: stabilization,

(f) *dimorphus* Subzone to *zigzag* Zones: weak positive shift,

(g) *aurigerus* to *orbis* Zones: weak shift to lower values (Bathonian minimum),

(h) *orbis* to *gracilis* Zones: positive shift (δ =0.7‰).

The shift of interest for this study is the *dimorphus* Subzone to *zigzag* Zone. There was a minor increase in $\delta^{13}C$ values during the *dimorphus* Subzone to the *zigzag* Zone (O'Dogherty *et al.,* 2006, pp. 328). However, because the isotopic shift was of small magnitude, the authors concluded that there was no

significant change in the global carbon cycle during the Late Bajocian to Early Bathonian, a view supported by subsequent authors (Wierzbowski and Joachimiski, 2007). The positive carbon isotope excursion found at Cabo Mondego is far more prominent than those detected elsewhere (Wierzbowski and Joachimiski, 2007; Price *et al*., 2018) even within the same geological setting (O'Dogherty *et al.,* 2006)

The lack of significant changes in the belemnite $\delta^{13}C$ record from southern Spain (O'Dogherty *et al.,* 2006) and central Europe (Wierzbowski and Joachimski, 2007; Price *et al*., 2018) suggests that the Late Bajocian to Early Bathonian was a time characterized by generally stable $\delta^{13}C$ values in marine carbonates. Furthermore, the positive $\delta^{13}C$ excursion from Cabo Mondego cannot be detected in other localities from Europe, including those from bulk rock samples.

6.1.2 Hypothesis 2: Faunal Turnover

Faunal turnovers are defined by Badgley and Gingerich (1988) as "*episodes of synchronous appearance and disappearance of species from a community"*. Such events may be local or, in the most extreme cases, mass extinctions. The turnover may not mean that a taxon has become extinct but may have migrated out of a biome due to factors such as climate change and replacement by a new species.

The faunal turnover hypothesis would explain the lack of a shift in the $\delta^{13}C$ from the associated brachiopod data from Cabo Mondego (cf. Figure 4.1). Suppose the carbon isotope shift reflected changes in $\delta^{13}C$ values of ancient oceanic dissolved inorganic carbon (DIC). In that case, it is expected that brachiopods, being benthic, immobile, and have shells composed of $CaCO_3$, would also detect the positive $\delta^{13}C$ excursion. Biogenic fractionation, or vital effects, of carbon and oxygen isotopes during metabolism is common among marine organisms, with fractionation of carbon isotopes within mollusc shells being well documented (e.g., McConnaughey, 1989a, b; Wefer and Berger, 1991; Wierzbowski and Joachimski, 2007).

The influence of vital effects on the isotopic compositions of fossil brachiopods is well understood with several studies (e.g., Lowenstam, 1961;

Brand, 1989; Grossman *et al*., 1991; Qing and Veizer, 1994; Lee and Wan, 2000) concluding that no such vital effect occurs within brachiopods and that they secreted their shells in isotopic equilibrium with the ambient seawater and would represent the actual ocean $\delta^{13}C$ values (Lowenstam, 1961; Lee and Wan, 2000). However, to be certain we would need to extract the material from certain shell segments of certain brachiopod taxa to be confident in the data. It is, therefore, reasonable to conclude that significant deviations from brachiopod data must be the result of variables not related to changes in the $\delta^{13}C$ of DIC, the most likely being vital effects - the vital fractionation of carbon isotopes within mollusc shells. By extension, the belemnite rostrum is well known and produced by incorporating isotopically light respiratory carbon into shell carbonate (cf. McConnaughey, 1989a, b; McConnaughey *et al.*, 1997).

The Middle Jurassic of Europe is associated with strong ammonite provincialism with three separate palaeobiogeographical realms. Faunal turnovers of ammonites are observed by Fernández-López *et al.* (2007, 2009) at the Ravin du Bès Section, SE France, the GSSP for the base of the Bathonian. O'Dogherty *et al.* (2006) found evidence of an ammonite faunal turnover in fossil assemblages, including just before the Bajocian-Bathonian Boundary in the Betic Cordillera, southern Spain. In total, six faunal turnover events were identified by O'Dogherty *et al* (2006) during the Middle Jurassic,

Disequilibrium fractionation of oxygen isotopes during precipitation of biogenic carbonate skeletons is caused by kinetic isotope fractionation, which relies on discriminating against heavy oxygen and carbon isotopes during hydration hydroxylation of CO_2 (McConnaughey, 1989a, b; McConnaughey *et al*., 1997; Wierzbowski and Joachimski, 2007). Therefore, kinetic isotope fractionation is reflected in a simultaneous depletion in ^{18}O and ^{13}C and a significant linear correlation of $\delta^{18}O$ and $\delta^{13}C$. The general lack of such correlations in the dataset for the present study suggests that belemnite, ammonite, and bivalve shell carbonate was precipitated in oxygen isotopic equilibrium with seawater.

The faunal turnover hypothesis is supported by the cross-section measurements of the belemnite rostra (see Figure 4.3), which shows a shift from more rounded cross-sections before the isotopic excursion to more oblong cross-

sections after the excursion. There also exists a correlation between $\delta^{13}C$ values and the “circularity” of the rostra (Figure 4.4), which suggests that the belemnite taxa that had more “rounded” cross-sections had lower $\delta^{13}C$ values and therefore evidence of carbon fractionation in different belemnite taxa.

The main problem for interpreting the change in carbon isotope values is that the carbon source is unknown, and the high fractionation factors associated with exchange reactions during carbon fixation (Rexfort and Mutterlose, 2006). Metabolic carbon is usually not incorporated into biogenic carbonate by animals with efficient respiratory systems (Weber, 1968). Belemnites are thought to have respiratory systems like extant cephalopods and therefore need to have well-oxygenated water due to their relatively inefficient jet-propulsion-based locomotion (cf. Webber and O’Dor,1986; Klug *et al*., 2016), and cephalopods use the copper-containing protein haemocyanin in their blood cells, which is a less-efficient oxygen transporter than the iron-containing protein haemoglobin (Hoffmann and Stevens, 2020). Kinetic isotope-effects are likely too small to have caused the scale of variation observed at Cabo Mondego (Rexfort and Mutterlose, 2006). It would not explain the carbon isotope shift within the *Zigzag* Zone or the correlation with rostrum size (for more information on mollusc kinetic isotope-effects, see McConnaughey *et al.,* 1997*)*.

Metabolic fractionation of carbon isotopes was reported in recent *Sepia* (Bettencourt and Guerra, 1999; Rexfort and Mutterlose, 2006) and Oxfordian belemnites from central Poland (Wierzbowski, 2002). The latter study revealed a depletion in $\delta^{13}C$ between 2.5 to 3‰ in contemporaneous belemnopsid belemnite with respect to brachiopod data. The data from the lower part of the studied section at Cabo Mondego, before the excursion, shows a depletion in $\delta^{13}C$ averaging 2‰, comparable to Wierzbowski (2002) and Wierzbowski and Joachimski (2007). Modern brachiopods secrete calcite in the second shell layer in either near-isotopic equilibrium with ambient seawater or slight disequilibrium characterized by decreased $\delta^{13}C$ values (Lowenstam, 1961; Lee and Wan, 2000), the lower $\delta^{13}C$ values of the belemnites compared to the brachiopods would have resulted from non-equilibrium fractionation.

6.2 Strontium stratigraphy at Albstadt-Pfeffingen

6.2.1 Strontium Chemostratigraphy

Changes in strontium isotope ($^{87}Sr/^{86}Sr$) composition of seawater through time can be used for stratigraphic correlation and dating, and for deciphering oceanographic change within the geological record. Systematic variations in marine $^{87}Sr/^{S6}Sr$ ratios have been recognized for some time (Wickman, 1948; Gast, 1955; Hedge and Walthall, 1963). The first comprehensive Sr isotope record for the Phanerozoic was developed by Peterman *et al*. (1970). This early Sr isotope curve, however, was not precise enough to be used as a stratigraphic tool (Elderfield, 1986).

Strontium-isotope data can be reported in several different ways. Many authors report it as $^{87}Sr/^{86}Sr$, as this is what is measured by the mass spectrometer. However, some authors convert the $^{87}Sr/^{86}Sr$ data into a $\delta^{87}Sr$, where (McArthur, 1994):

$$\delta^{87}\mathrm{Sr} = \left(\frac{\left(\frac{^{87}\mathrm{Sr}}{^{86}\mathrm{Sr}}\right)_{Sample}}{\left(\frac{^{87}\mathrm{Sr}}{^{86}\mathrm{Sr}}\right)_{standard}} - 1 \right) * 10^{6}$$

Strontium isotopes are an established proxy for the rate of chemical weathering of the continents and seafloor spreading (Asmeron *et al*., 1991; Blum and Erel, 1995). The $^{87}Sr/^{86}Sr$ ratio of seawater is uniform throughout the oceans because of the residence time of strontium which is much longer than the mixing time of seawater (DePaolo and Ingram, 1985; Elderfield, 1986; Veizer, 1989; McArthur, 1994; Jones and Jenkyns, 2001). The seawater $^{87}Sr/^{86}Sr$ can be recorded in well-preserved marine carbonates and phosphates and may be used for dating sedimentary rocks based on previously reconstructed seawater strontium isotope curves for the Jurassic (e.g., Jones *et al*., 1994; Howarth and McArthur, 1997; Jenkyns *et al*., 2002; McArthur, 1994; McArthur *et al*., 2001, 2004, 2012; Wierzbowski *et al*., 2012, 2017). Strontium uniformity makes it possible, in some instances, to date and correlate geographically distant sedimentary sequences without involving biostratigraphic and radioisotopic data (e.g., Kuznetov *et al*., 2018).

Using the full look-up table for the marine Sr-isotope curve for the last 206 million years (Howarth and McArthur, 1997), it is possible to assign a likely age to the Pfeffingen section. The $^{87}Sr/^{86}Sr$ value of the lowermost two samples (216 and 217; mean 0.706938) indicates the latest Bathonian to early Callovian age of between 165.85 – 166.05 Ma for the stratigraphic position 50-52 cm below the top of the *keppleri* Horizon.

However, it is worth stating that $^{87}Sr/^{86}Sr$ is not an absolute dating technique but instead relies on detailed knowledge about the strontium-isotope ratios in the ambient seawater at any given point in time. The quality of the data derived by strontium-isotope from well-preserved samples depends on three factors outlined by McArthur (1994):

1. the slope of the curve of $^{87}Sr/^{87}Sr$ against numeric age;
2. the accuracy of the age model used to calibrate the isotope curve;
3. the analytical quality of the data, and how well inter-laboratory bias can be quantified.

To get such a look-up chart that lists $^{87}Sr/^{86}Sr$ values throughout geological time, strontium-isotope measurements must be taken from a large sample base of well-preserved fossils of known age. One such data set, and the one used in this study, is the LOWESS 5 Fit provided by Prof. John McArthur.

Inaccuracies of up to 4 million years can occur due to uncertainties in biostratigraphically based age models used to calibrate Cenozoic isotope curves (Miller *et al*., 1991). Such inaccuracies generally increase with age (McArthur, 1994).

One way to test the reliability of $^{87}Sr/^{86}Sr$ samples is to test the different specimens from the same stratigraphic level. If the material yields similar $^{87}Sr/^{86}Sr$ values, then the data can be considered reliable (Jones *et al*., 1994; McArthur, 1994).

6.2.2 $^{87}Sr/^{86}Sr$ Values During the Middle Jurassic

The evolution of seawater $^{87}Sr/^{86}Sr$ ratio during the Late Bajocian–Callovian is summarised by Jones *et al.* (1994) and Jenkyns *et al.* (2002). A broad and deep trough characterises the Jurassic strontium isotope curve at the Middle-Late Jurassic transition with $^{87}Sr/^{86}Sr$ ratios decreasing throughout the Middle Jurassic due hypothetically to enhanced hydrothermal activity of the seafloor, which resulted in the influx of isotopically light strontium into the oceans (Jones *et al*., 1994; Jenkyns *et al*., 2002; Wierzbowski *et al*., 2012, 2017; Ullmann *et al*., 2013a; Rosales *et al*., 2021), so a decrease in strontium isotope ratios is to be expected at Albstadt-Pfeffingen. Wierzbowski *et al*. (2017) reported a reduction of seawater $^{87}Sr/^{86}Sr$ from *ca.* 0.70730 to *ca*. 0.70683 from the Middle Aalenian to the Early Oxfordian.

The $^{87}Sr/^{86}Sr$ ratios from the Bathonian-Callovian boundary are widely studied, with Middle-Late Jurassic strontium-isotope trends based on well-preserved belemnite rostra and oyster shells presented by several authors (Jenkyns *et al*., 2002; McArthur *et al.,* 2012; Wierzbowski *et al*., 2017). The Bathonian-Callovian boundary saw one of the steepest falls in the strontium isotope ratio during the Phanerozoic of 0.00009 per 1 Ma. The enhanced hydrothermal (non-radiogenic) strontium input to Middle Jurassic seawater was likely a consequence of the rapid acceleration in seafloor spreading rates (see Wierzbowski *et al*., 2017). This acceleration in the rate of seafloor spreading during the Middle Jurassic has been confirmed by geophysical and palaeomagnetic data from the oceanic crust (e.g., Labails *et al*., 2010). The results collected from Albstadt-Pfeffingen are consistent with the published literature, with Wierzbowski *et al*. (2017) reporting $^{87}Sr/^{86}Sr$ ratios of ca. 0.706950 at the Bathonian–Callovian boundary (Figure 6.1).

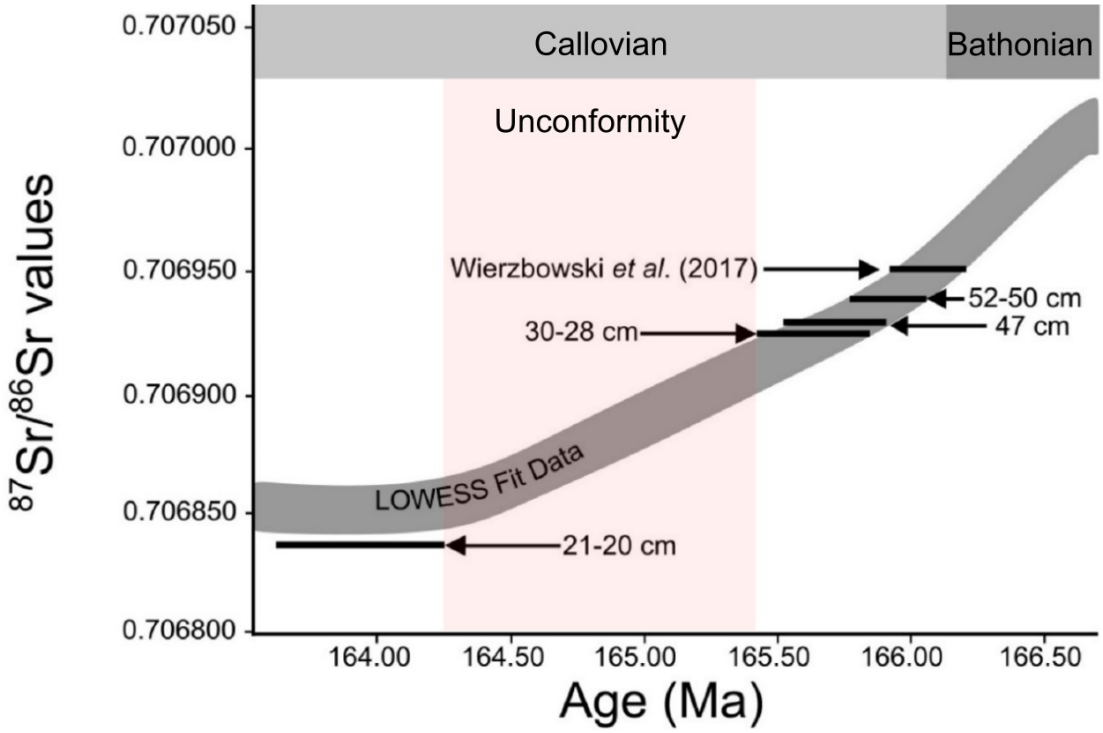

Figure 6.1: Matching results of belemnite $^{87}Sr/^{86}Sr$ ratios from Albstadt-Pfeffingen and Wierzbowski *et al*. (2017) with LOWESS Fit 5 data for Jurassic strontium-isotope data. The significant step-change in $^{87}Sr/^{86}Sr$ values between 28 and 21 cm below the top of *kepperli* Zone may indicate an unconformity.

6.2.3 Step Change in Strontium Data

The $^{87}Sr/^{86}Sr$ data from 52 to 28 cm below the top of the *keppleri* Horizon $^{87}Sr/^{86}Sr$ values of 6.25e-7 (0.000000625) per cm of strata. The difference in $^{87}Sr/^{86}Sr$ values between 30-28 cm below the top of the *keppleri* Horizon to 21-20 cm below the top of the *keppleri* Horizon was 0.0000869, which equates to a change of 0.000012 per cm of strata, a rate approximately 2000 times faster than values reported for 52-28 cm. Even though the Bathonian-Callovian transition was one of the steepest falls in the $^{87}Sr/^{86}Sr$ ratio during the Phanerozoic (Wierzbowski *et al*. 2017; McArthur *et al*., 2012; Figure 6.2), it would not have been enough to account for the rate of change observed at Albstadt-Pfeffingen.

One possible reason for this shift in $^{87}Sr/^{86}Sr$ is an unconformity. Unconformities are physical surfaces dividing strata of different ages represented by missing sediments caused by erosion or periods of no deposition. Changes in $^{87}Sr/^{86}Sr$ values have been used to identify unconformities in previous studies (e.g., Jenkyns et al., 2002; Mabrouk *et al*., 2006; Lever, 2007).

The rate of change in $^{87}Sr/^{86}Sr$ values can be estimated through the Bathonian-Callovian transition, with the absolute rate of change calculated by Wierzbowski *et al*. (2017) to have been approximately 0.00009 per 1 Ma. Thus, it is possible to approximate the amount of time missing from the stratigraphic record at the studied section using the LOWESS 5 Fit as a reference (Figure 6.3). The specimens at 30-28 cm below the top of the *kepperli* Zone range from 165.50 to 165.85 Ma and post-unconformity specimens range from 163.70 to 164.50 Ma. Therefore, using this method, the hiatus at Albstadt-Pfeffingen might be between 1.0-1.8 million years long. However, there are uncertainties in the LOWESS Fit curve (cf. Howarth and McArthur, 1997), so the age estimates and the estimated duration of the unconformity are not exact and the time estimation of the duration of the unconformity is unprecise.

An alternative estimate is based on the rate of change in $^{87}Sr/^{86}Sr$ values calculated by Wierzbowski *et al*. (2017). Using the average $^{87}Sr/^{86}Sr$ ratios before (0.706929) and after (0.706840), the unconformity gives a difference of 0.000089, which implies the unconformity present at Albstadt-Pfeffingen represents a gap of *ca.*1 million years.

The acceleration in seafloor spreading during the Bathonian-Callovian hypothetically resulted in global sea-level rise at the Middle-Jurassic (see Norris and Hallam, 1995; Hallam, 2001; Wierzbowski *et al*., 2009, 2017). The tectonically induced sea-level rise led to widespread gaps in the sedimentary record throughout the Middle Jurassic (Gygi and Persoz, 1986; Rais *et al*., 2007; Wierzbowski *et al*., 2009, 2017). Therefore, it is highly probable that the unconformity present at Albstadt-Pfeffingen was formed due to erosion and non-deposition of sediments during sea-level rise at regional extent.

The $^{87}Sr/^{86}Sr$ ratios from Albstadt-Pfeffingen show that the site does not represent a continuous depositional sequence in the excavated section. Albstadt-Pfeffingen does not meet the requirements set by the International Stratigraphic Commission (Remane *et al*., 1996). As Ager (1981, p. 77) wrote, a potential GSSP *"should be chosen in a section where sedimentation seems to have been nearly as continuous as is ever possible, where there are no marked lithological changes and where there are unbroken records of several different groups of fossils."* Therefore, Albstadt-Pfeffingen, following the criteria laid out by numerous

authors (e.g., Ager, 1981; Cowie *et al*., 1986; Cowie, 1986; Salvador, 1994; Remane *et al*., 1996; Smith *et al.,* 2014; Lucas, 2018), should be considered as a poor GSSP candidate for the Bathonian-Callovian boundary.

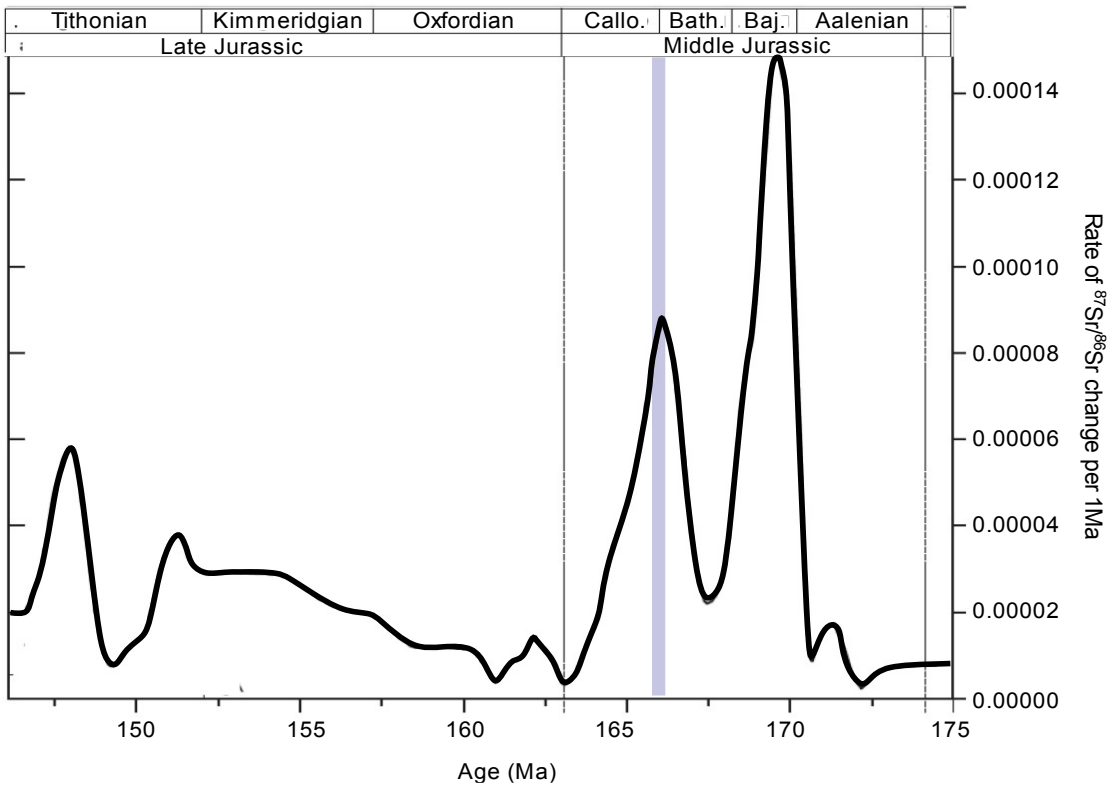

Figure 6.2: Rate of change in seawater $^{87}Sr/^{86}Sr$ ratio per 1 Ma during the Middle-Late Jurassic. Redrawn from Wierzbowski *et al.* (2017).

6.2.4 Disparity with Previous Work

Previous analysis on strontium-isotope ratios around the Bathonian-Callovian boundary, but not performed at Albstadt-Pfeffingen, have so far contributed little to the definition of the Bathonian-Callovian boundary and, unlike in this work, did not show any step-changes within the succession despite the geochemical data coming from belemnite calcite (Callomon and Dietl, 2000). Callomon and Dietl (2000, p. 50) commented, *"… the ratio of marine Sr(87): Sr(86) changes only slowly in the region of the Bathonian-Callovian boundary"*, which contrasts the abrupt change to strontium ratios observed in this study.

This disparity in results cited by Callomon and Dietl (2000; Figure 6.3) and this paper cannot be explained by diagenetic alteration as any of the $^{87}Sr/^{86}Sr$ ratios from Albstadt-Pfeffingen had an Mn/Ca ratio above the 0.2 Mn/Ca

mmol/mol cut-off point, it must, however, be pointed out that Mn/Ca ratios is not a failsafe diagenetic proxy.

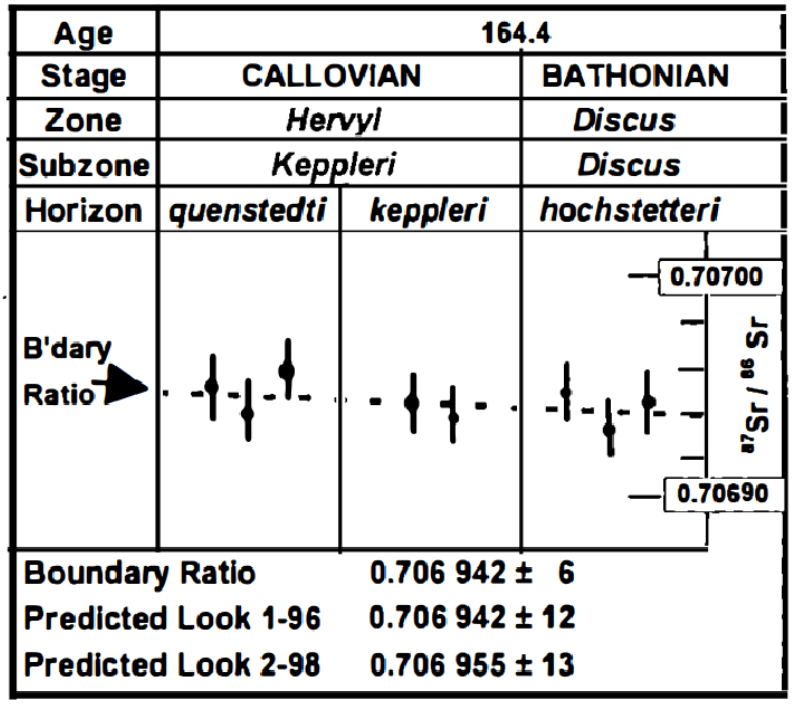

Figure 6.3: Measured $^{87}Sr/^{86}Sr$ ratios from Albstadt-Pfeffingen in belemnites around the Bathonian-Callovian boundary. From Callomon and Dietl (2000).

Figure 6.4 (redrawn from Mönnig and Dietl, 2017- cf. Buck *et al*., 1966; Terzidis, 1966; Dietl, 1981; 1990) shows that geographically close sections from the Pfeffingen area can have vastly different profiles with some, even if separated by mere metres, omitting entire faunal horizons. On this interpretation, the $^{87}Sr/^{86}Sr$ data shown in Callomon and Dietl (2000) may still be reliable for the time frame around the Bathonian-Callovian boundary as similar results have been recorded by other authors (Howarth and McArthur, 1997) and the existing strontium ratios for the boundary (0.706942±6) is also consistent with data from the studied section. Because the section examined by Callomon and Dietl (2000) and the section presented in this study are different, a disparity in strontium-isotope data would be expected as the sections are highly condensed and patchy (Mönning, 2014). It would be reasonable for an unconformity to be present in one section but not in one nearby. Similar results are known from other localities such as the Middle Jurassic Inferior Oolite Group in southern and eastern England (e.g., Callomon and Cope, 1995).

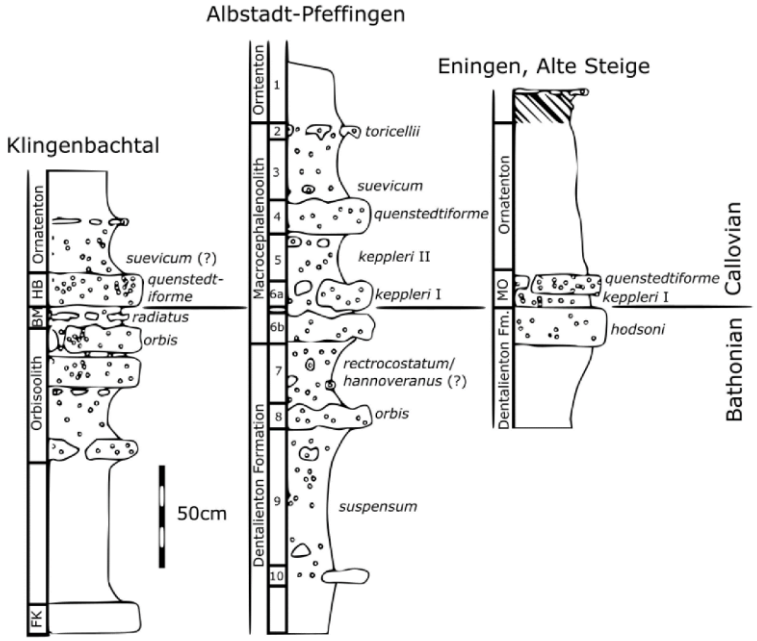

Figure 6.4: Sections of Upper Bathonian and Lower Callovian beds in southern Germany; Klingenbachtal near Bisingen-Thanhein, Zollernalb, modified after Dietl (1981), Albstadt-Pfeffingen, village centre, construction pit 1986, modified after Dietl (1990), Achalm near Eningen, Alte Steige, modified after Terzidis (1966) and Buck *et al*. (1966). Abbreviations: *FK: Fuscus Bank (Lower Bathonian); MO: Macrocephalenoolith; BM: Basis-Mergellage* (Upper Bathonian). Redrawn from Mönnig and Dietl (2017).

6.3 Mg/Ca and Sr/Ca as Palaeothermometers

Seawater chemistry has varied with changes in the global climate throughout geological time, making past seawater cation ratios such as Mg/Ca and Sr/Ca potential proxies for various palaeoceanographic parameters (Cohen *et al*., 2002; Coggon *et al*., 2010). Both Mg/Ca and Sr/Ca ratios have been considered by some authors (e.g., Rosales *et al*., 2004a; McArthur *et al*., 2007; Wierzbowski and Rogov, 2010 and others) as potential palaeothermometers. If this were to be the case for Middle Jurassic belemnites collected from Cabo Mondego and Albstadt-Pfeffingen, one would expect a correlation between elemental proxies with $\delta^{18}O$ values.

Since the 1960s, some Russian authors (e.g., Berlin *et al.,* 1967; Naydin and Teys, 1976) proposed that the Mg/Ca ratios in belemnite calcite may be used as a palaeothermometer, but published data comparing Mg/Ca to $\delta^{18}O$ has thus far yielded mixed results. The use of Mg/Ca as a palaeothermometer is based on two assumptions: 1) that $\delta^{18}O$ of belemnite calcite reflects calcification

temperature and the isotopic composition of the ambient seawater (Urey *et al*., 1951, Saelen *et al*., 1996, Podlaha *et al*., 1998 and in this work); and 2) the Mg/Ca, and possibly Sr/Ca, of belemnite calcite thought by some researchers to be dependent on temperature (Berlin *et al*., 1967; McArthur *et al*., 2000, 2007a, b; Bailey *et al*., 2003; Rosales *et al*., 2004a). This second point has some credibility as some studies shown in figure 6.5 (cf. McArthur *et al*., 2000; Bailey *et al*., 2003; Rosales *et al*., 2004a) show an inverse covariance between $\delta^{18}O$, and Sr/Ca and Mg/Ca in belemnite calcite. These studies may suggest that belemnite El/Ca ratios are a feasible palaeotemperature proxy, at least for the Early Jurassic. However, the influences of factors other than temperature on both El/Ca ratios and $\delta^{18}O$ must also be considered.

Mg/Ca and Sr/Ca is used as palaeotemperature a proxy in other $CaCO_3$ fossil groups such as foraminifera. Some authors prefer to use Mg/Ca and Sr/Ca ratios over oxygen-isotopes as the elemental data are not as sensitive to fluctuations in salinity. Some researchers observed correlations between Mg/Ca and $\delta^{18}O$ in bulk belemnite samples and thereby proposed a temperature control on Mg/Ca (e.g., Rosales *et al*., 2004a; McArthur *et al*., 2007a; Armendáriz *et al*., 2012). However, some studies (e.g. Wierzbowski and Joachimski, 2009, Li *et al*., 2013, Sørensen *et al.,* 2015, Ullmann *et al*., 2015) found no such correlation between Mg/Ca and $\delta^{18}O$ in ontogenetic records from individual rostra. By analogy with other calcifying organisms, such as foraminifera, the response of these presumed palaeo-proxies in belemnites may have been species-dependent, so interpreting undifferentiated belemnites, at genus or family level, as is the case here, would inevitably lead to misinterpretation of the results. Because belemnites are extinct, their response to Mg/Ca to variations in water temperature cannot be tested experimentally. Furthermore, the skeletons of modern cephalopods are predominantly aragonitic (Wilbur, 1972) rather than calcite as in belemnites (Ullmann *et al*., 2015), which uptake trace and minor elements differently, and the aragonitic phragmocone of belemnites is seldom preserved (Hoffmann and Stevens, 2020).

No correlation between oxygen-isotopes and Mg/Ca was observed in Jurassic–Cretaceous belemnites by Wierzbowski and Rogov (2010), Li *et al*. (2012), or Benito and Reolid (2012). Previous studies of Mg/Ca, Sr/Ca, and

Na/Ca in belemnite species or genera noted intra-rostral variations, often interpreted as diagenetic signals, and inter-species/genus differences (e.g., McArthur *et al*., 2007b, Wierzbowski and Joachimski, 2009, Wierzbowski and Rogov, 2010, Li *et al*., 2012;).

On the other hand, fossil calcite is a promising substrate for reconstructing past seawater Sr/Ca ratios, as Sr/Ca variability within a given shell is comparatively low, e.g., ~20% in modern oysters (Almeida *et al*., 1998), and small sample sizes (< 1 mg) are sufficient for analysis allowing for the generation of large data sets and precise average values with very little material (Ullmann *et al*., 2013b). A downward trend in fossil Sr/Ca ratios is observed through the Early and Middle Jurassic. The Sr flux from increased Mid Ocean Ridge activity in the Early Jurassic is thought to have outbalanced the input of riverine Sr, leading to the gradual lowing of seawater $^{87}Sr/^{86}Sr$ parallel and a substantial decrease in seawater Sr/Ca ratios (Ullmann *et al*., 2013a).

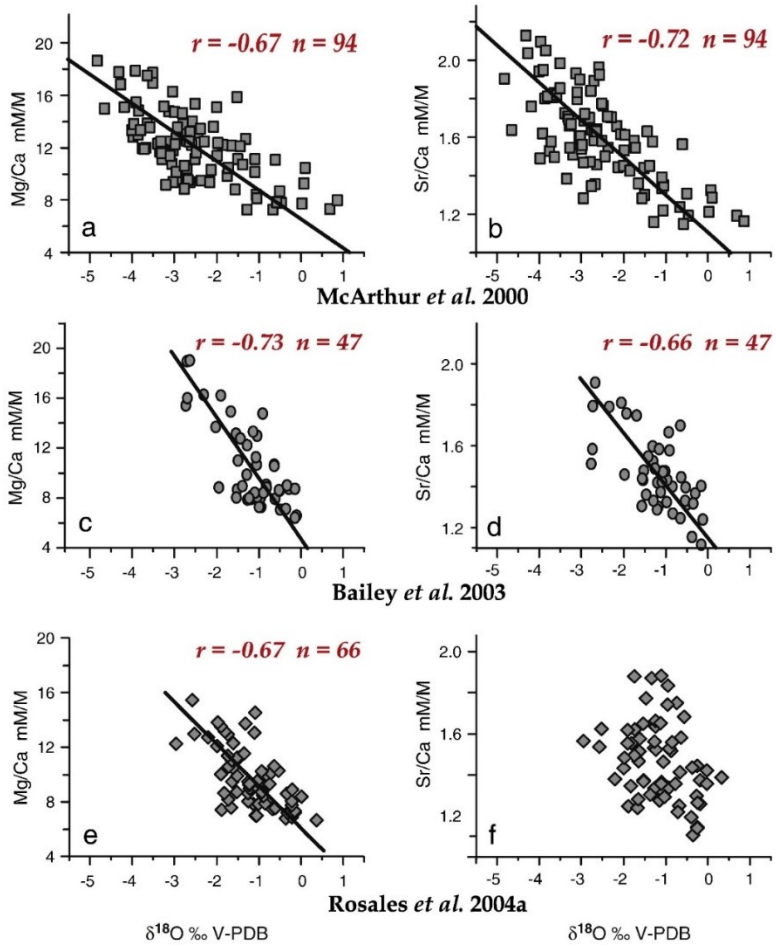

Figure 6.5: Cross-plots of Mg/Ca and Sr/Ca against and $\delta^{18}O$ for Pliensbachian–Toarcian belemnites from Yorkshire of the UK (data of McArthur *et al*., 2000), southern Germany (data from Bailey *et al*., 2003) and northern Spain (data from Rosales *et al*., 2004a). From Li (2011).

The most critical factors influencing Sr/Ca ratios in shell material are presented by Ullmann *et* al. (2013a):

> *(I) the composition of the liquid from which they are precipitated, (II) the calcium carbonate polymorph, (III) the species specific fractionation of the Sr/Ca ratio, (IV) metabolic controls on this fractionation factor and (V) water temperature.*

Negative correlations between $\delta^{18}O$ and Sr/Ca ratios (e.g., McArthur *et al*., 2000; Bailey *et al*., 2003; Rosales *et al*., 2004a) imply that incorporating Sr/Ca into shell carbonate may have been, at least partially, temperature dependent. These empirical relationships contrast with the positive relationship between $\delta^{18}O$ and Sr/Ca predicted by theoretical and experimental work by Tang *et al*. (2008) and DePaolo (2011), but temperature-induced changes in growth rate may be a plausible explanation for negative correlations (e.g., Stoll and Schrag, 2001; Tang *et al*., 2008; Ullmann *et al*., 2013a).

Sr/Ca ratios are more challenging to interpret than Mg/Ca ratios, reflecting a combination of calcification temperature, calcification rate, carbonate chemistry, seawater Sr/Ca, and salinity, and may also be an indicator for diagenesis (Baker *et al*., 1982). The Sr concentration in biogenic low-magnesium calcite, such as belemnite rostra, is often higher than Sr levels in thermodynamic equilibrium from in abiogenic calcite, resulting in Sr-depletion in calcite fossils during diagenesis (Ullmann and Korte, 2015; cf. Carpenter and Lohmann, 1992; Tang *et al.,* 2008; DePaolo, 2011*)* One can therefore use Sr/Ca as a diagenetic proxy in calcite shells (e.g., Bruckschen and Veizer, 1997; Korte *et al*., 2003; Ullmann and Korte, 2015).

Using the lower suggested limits of Sr/Ca as an alternation marker is problematic for a few reasons. Perhaps the most important concern is the primary Sr/Ca ratios present in the animals when they are still alive. This is because the rate of Sr incorporation in different taxonomic groups is related to vital effects with animals with high metabolic rates incorporating more Sr (Purton *et al*., 1999). These probably led belemnites to have a much higher rate of Sr incorporation than osteroids (Veizer, 1974; Korte and Hesselbo, 2011) and brachiopods (Voigt

et al., 2003) due to belemnites having faster metabolisms and a more active lifestyle (Korte and Hesselbo, 2011).

Another issue that arises when using Sr is secular changes in seawater Sr/Ca ratios through the Phanerozoic, possibly spanning a large range between 2 and 14 mmol/mol (Steuber and Veizer, 2002; Ullmann and Korte, 2015). Generally, Sr/Ca ratios in low-Mg calcite are expected to be higher during predicted Calcite Sea intervals and lower in Aragonite Sea intervals because Sr is more readily incorporated in aragonite than in calcite (Steuber and Veizer, 2002; Ries, 2010; Ullmann *et al*., 2013a, b; Ullmann and Korte, 2015).

The belemnites from Cabo Mondego and Albstadt-Pfeffingen presented in this study do not show any correlation between $\delta^{18}O$ values with Mg/Ca and Sr/Ca ratios (Figure 6.6). The absence of a correlation between Mg/Ca and $\delta^{18}O$ in belemnite samples from both Cabo Mondego and Albstadt-Pfeffingen questions the assumption that Mg/Ca in belemnite calcite reflects mainly calcification temperature (e.g., Berlin *et al*., 1967; Bailey *et al*., 2003; McArthur *et al*., 2007a) and suggests that Mg/Ca is an unreliable palaeotemperature indicator for upper Bajocian - lower Callovian belemnites.

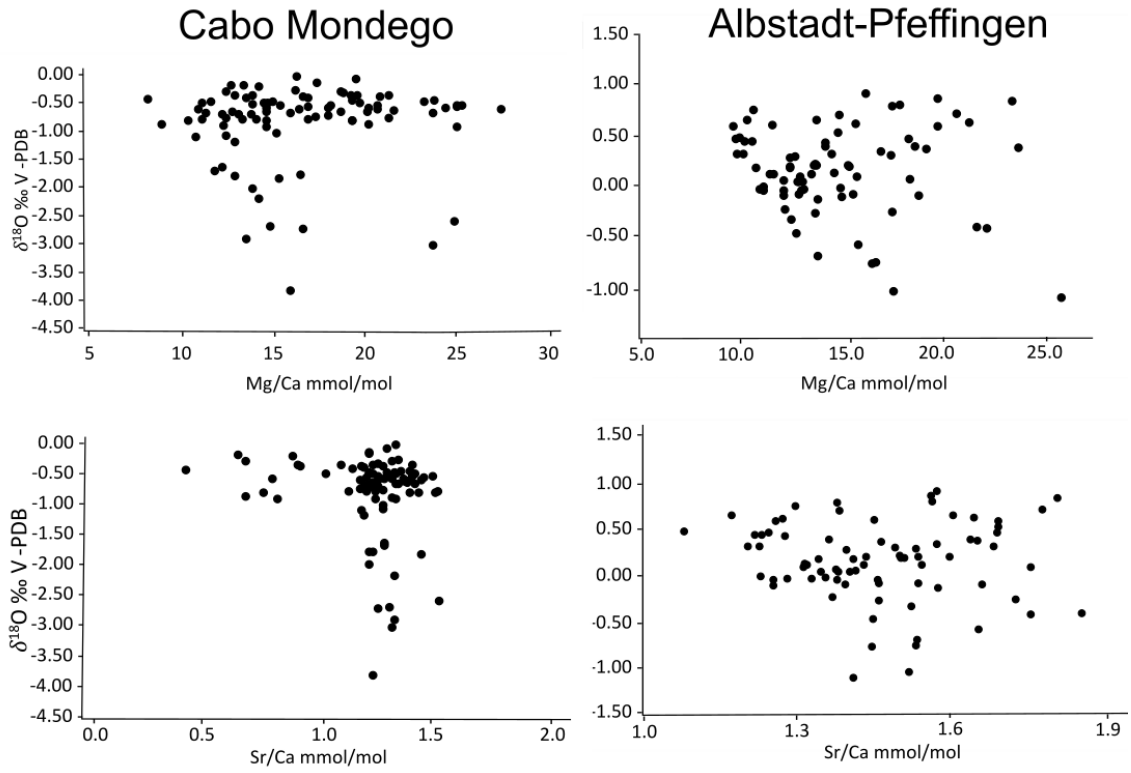

Figure 6.6: Cross plots of Sr/Ca and Mg/Ca versus $\delta^{18}O$ values from Cabo Mondego and Albstadt-Pfeffingen

The absence of the correlation of El/Ca ratios with $\delta^{18}O$ values was also found by Wierzbowski and Rogov (2010) in each of the three Callovian-Oxfordian belemnite genera from the Russian Platform. However, when the belemnite data are combined, a negative correlation can be inferred even though no such correlation is present within any of the genera (Figure 6.7). This suggests that correlations in Mg/Ca, and Sr/Ca ratios with $\delta^{18}O$ values in undifferentiated belemnites represent false correlations, a view also supported by Li (2011, p. 182):

> *"…species difference in composition may be the reason for the observed correlation between El/Ca with $\delta^{18}O$, and that El/Ca ratios in belemnites are influenced by the bio-fractionation effects besides temperature and show no correlation with $\delta^{18}O$ at species level."*

The challenge in applying belemnite elemental ratios (e.g., Mg/Ca and Sr/Ca) as an independent palaeotemperature proxy is the poorly quantified temperature dependence and species-specific fractionation of these elements during belemnite calcification which is exacerbated by the lack of living descendants. Unless the effects of temperature and species-specific fractionation on belemnite El/Ca ratios can be separately quantified, El/Ca ratios of belemnites are of little use as palaeotemperature proxies.

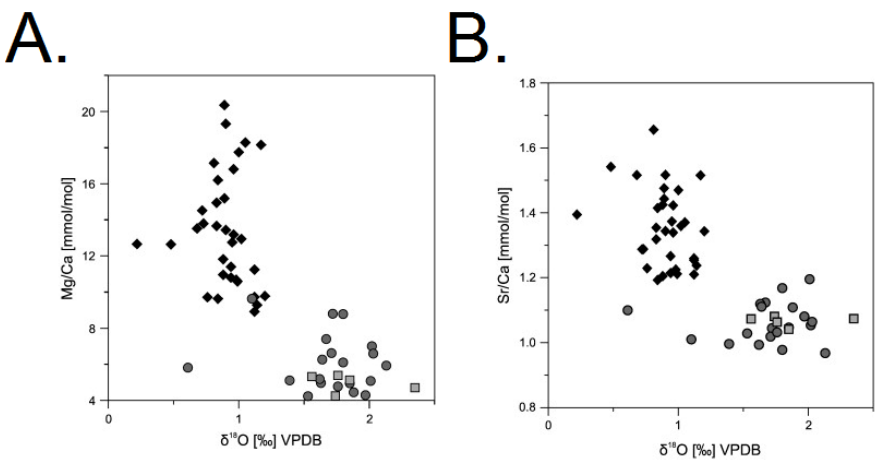

Figure 6.7: A). Mg/Ca ratios versus $\delta^{18}O$ values of well-preserved belemnite rostra shows no correlation between Mg/Ca ratios and $\delta^{18}O$ values. B). No correlation is observed between Sr/Ca and $\delta^{18}O$. However, when data from different taxa are combined, it can give a false correlation. Diamonds= *Hibolithes sp.*, circular= *Cylindroteuthis sp.*, square= *Lagonibelus sp*. From Wierzbowski and Rogov (2010).

6.4 Middle Jurassic Climates

6.4.1 Palaeotemperatures

The Jurassic is generally considered to have been dominated by greenhouse climate conditions with global average temperatures throughout the Jurassic being significantly warmer, by 5°C to 10°C, than at present and, for the most-part, humid (e.g., Hallam, 1991; Chandler *et al*., 1992; Berner, 1994; Huber *et al.*, 2000; Lécuyer *et al*., 2003; Sellwood and Valdes, 2008). More recently, however, a more detailed view of the Jurassic has emerged, with Kürschner (2001) suggesting the Jurassic was a relatively cool phase between the Permian and Cretaceous, though still warmer than today. Korte *et al.* (2015) also found evidence of cool, possibly even icehouse (cf. Kaplan, 1978; Price, 1999; Rogov and Zakharov, 2010), conditions called cool modes interspersed throughout the era (cf. Frakes *et al*., 1992). Evidence for warm and cool modes comes from oxygen isotope data and palaeobiogeographic ranges of fossil organisms (Dromart *et al*., 2003; Korte and Hesselbo, 2015). During the Jurassic, cold-intolerant organisms extended over a wider range of palaeolatitudes (Hallam, 1985; Barnard, 1973; Leinfelder *et al*., 2002). However, it must be stated that Jurassic fossils have been extinct too long to have close extant relatives whose climate tolerances are precisely known (Hallam, 1982).

Frakes *et al*. (1992) identified the Bathonian as a time of comparatively cool conditions globally. Evidence for cool conditions during the Middle Jurassic comes from glacial dropstones (Korte *et al*., 2015; albeit only at high palaeolatitudes), and a decrease in the size of calcareous nannofossils, which is interpreted as a product of low temperatures (Johnson, 1999).

As discussed previously, belemnites are thought to have secreted their calcite shells in isotopic equilibrium with seawater. Many authors (e.g., Sælen *et al*., 1996; Prince and Sellwood, 1997; Wierzbowski and Joachimski, 2007, 2009 and other references throughout this work) therefore assumed the $\delta^{18}O$ values of well-preserved belemnite rostra to be a reliable palaeothermometer.

When calculating palaeotemperatures from the Jurassic, a value of 1 needs to be added on for $\delta^{18}O$ values to account for the negative SMOW. Palaeotemperatures were calculated assuming that the belemnite calcite collected from Cabo Mondego and Albstadt-Pfeffingen that did not have elevated Fe and Mn ratios, are diagenetically unaltered, and were presumed precipitated in isotopic equilibrium with ambient seawater where oxygen isotope values and salinity remained unchanged throughout the succession. To calculate palaeotemperatures, an adapted version of Epstein (1953) was used as shown in Sharp (2007; chapter 6.3):

$$\text{Temperature (°C)} = 15.75 - 4.3\,(\delta c - \delta w) + 0.14\,(\delta c - \delta w)^2$$

To analyse palaeotemperature changes from the Upper Bajocian to the Lower Callovian, a combination of calculated palaeotemperature data based on $\delta^{18}O$ values from Cabo Mondego and Albstadt-Pfeffingen were used with the gap between the two being filled in with data from the Polish Jura Chain presented in Wierzbowski and Joachimski (2007).

The overall variation in calculated palaeotemperatures at Cabo Mondego is 11.8-19.5°C (when the results with Mn >0.5 mol/mmol are excluded), with overall variability being 7.7°C. The average palaeotemperature reported from Cabo Mondego was 14.2°C. These palaeotemperature estimates indicate cool climatic conditions considering the palaeolatitude of the study area (approximately 30°N). Belemnite $\delta^{18}O$ values from Cabo Mondego show considerable overlap with brachiopod $\delta^{18}O$ values, indicating a nekotobenthic habitat for belemnites. Such an interpretation is supported with isotope data from Wierzbowski (2002) and by Wierzbowski and Joachimski (2007). Overall, a cooling trend is observed from the *parkinsoni* Zone at Cabo Mondego with the Bathonian being cooler than the Bajocian, a view supported by other researchers (e.g., Frakes *et al*., 1992)

Data from the Polish Jura (Wierzbowski and Joachimski, 2007) was used to span the Lower and Middle Bathonian infill in the gap between Cabo Mondego and Albstadt-Pfeffingen. Colder palaeotemperature were reported from Poland than from the same biozones in Portugal. Such a result was expected given that Cabo Mondego (30°N) had a lower palaeolatitude than the Polish Jura (30°N

compared to 35°N) during the Middle Jurassic; thus, the average seawater temperature would be lower. Looking at figure 6.8, one can see that seawater temperatures decrease during the Late Bajocian *parkinsoni* Zone, just as they did in the Lusitanian Basin, and remained stable throughout the Bathonian. The data from Cabo Mondego and the Polish Jura agree with each other and those of Price (1999), who also suggested global cooling in the Bajocian and Bathonian based on the sedimentological evidence for glacial deposits in high palaeolatitudes (Gondwana, Siberia).

Wierzbowski and Joachimski (2007) found considerable variations in belemnite $\delta^{18}O$ values which they attributed to migration within the water column. Wierzbowski and Joachimski (2007), unlike this study, also collected $\delta^{18}O$ data from ammonites and bivalves. Average palaeotemperatures comparing belemnites with coeval bivalves indicates that belemnites were nekotobenthic. A nektonic habit for ammonites has also been supported by other authors (e.g., Anderson *et al*., 1994, Martill *et al*., 1994, Auclair *et al*., 2004; Lécuyer and Bucher, 2006) The lower variation in calculated palaeotemperatures between the two groups (8.3 °C for belemnites and 5.9 °C for ammonites) may be explained by ammonites having a more restricted depth range.

Calculated palaeotemperatures from Albstadt-Pfeffingen range from 8.2-15.9°C (when the results with Mn >0.2 mol/mmol are excluded), with overall variability being 7.7°C. The average palaeotemperatures reported from Albstadt-Pfeffingen was 10.9°C, more than 3°C lower than Cabo Mondego. Lower palaeotemperatures from Germany can be explained by a combination of having a higher palaeolatitude and cooler palaeotemperatures globally. The oxygen isotope values from Albstadt-Pfeffingen show a degree of scattering though a long-term warming trend can still be recognised throughout the succession. Declining $\delta^{18}O$ values are also recorded from other early Callovian successions, for example, the Isle of Skye (Nunn *et al.,* 2009) where the authors interpreted this result as a gradual increase in palaeotemperatures and a decrease in salinity, Yorkshire (Powell and Riding, 2016), and the Paris Basin (Brigaud *et al.,* 2009).

Each $\delta^{18}O$ record presented here shows a significant degree of scattering. Much of the noise in the belemnite records results from fractionation and a

cosmopolitan lifestyle of some belemnite species, rather than climate change, a conclusion reached by previous authors (e.g., McArthur *et al.,* 2007a) However, diagenesis should also be taken into account as it can remain unnoticed especially when proxies for diagenesis (such as the Fe and Mn) do not show a strong response.

Variations in $\delta^{18}O$ values within an individual rostrum may indicate that belemnites migrated between different positions in the water column. According to Hoffmann and Stevens (2020), belemnite migration patterns likely involved pathways along coastlines on the shelf but not directly over open ocean waters. *Sepia officinalis* populations in the Mediterranean Sea make seasonal migrations between shallower and deeper waters (inshore during spring and summer for reproduction; and offshore in autumn). Brigaud *et al*. (2009) noted similar $\delta^{18}O$ ranges from belemnite calcite from various sites in western and central Europe suggesting that bottom waters in the Tethys were well-mixed during the Middle-Upper Jurassic boundary.

The overall palaeotemperature trend for the Upper Bajocian to the Lower Callovian in the literature (see Price, 1999; Wierzbowski and Joachimski, 2007; Brigaud *et al.,* 2009; Powell and Riding, 2016) and the new data presented in this study is as follows (Figure 6.8):

- Decreasing calculated palaeotemperatures in the *parkinsoni* Zone,
- cool and stable palaeotemperatures throughout the Bathonian (*zigzag* to *discus* Zones),
- warming in the Lower Callovian (*herveyi* Zone).

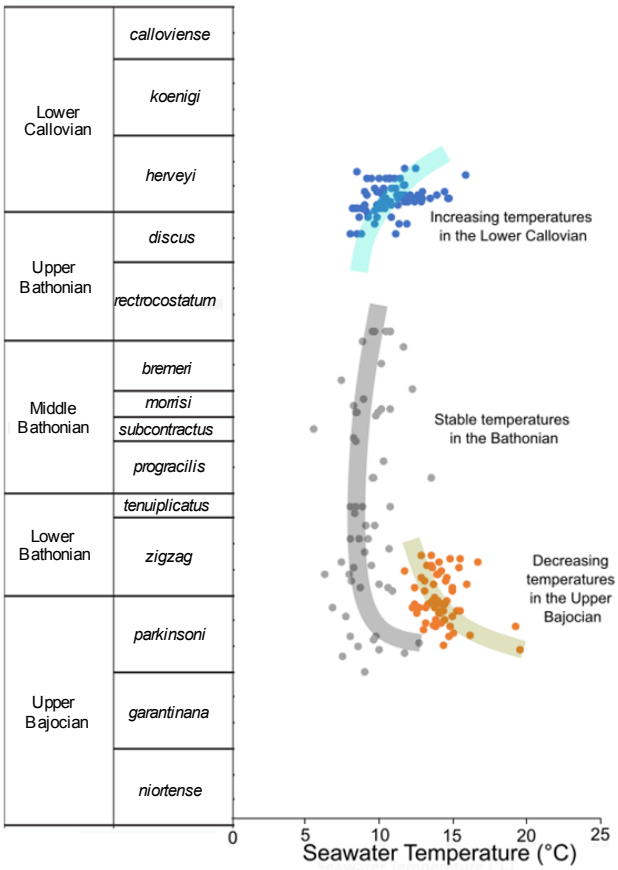

Figure 6.8: Palaeotemperature estimates from Cabo Mondego (orange), the Polish Jura Chain (grey), and Albstadt-Pfeffingen (blue). Polish data taken from Wierzbowski and Joachimski (2007) and stratigraphy based on Wierzbowski *et al*. (2017).

6.4.2 Carbon Isotope Trend

Variations in the $^{13}C/^{12}C$ values in marine carbonate rocks have long been used by researchers to date and correlate sediments (e.g., Scholle and Arthur, 1980; O'Dogherty *et al*. 2006; Saltzman and Thomas, 2012; Mette *et al*., 2019) and document changes in the $\delta^{13}C$ values in dissolved organic carbon (DIC; O'Dogherty *et al*. 2006; Hesselbo *et al*., 2007). The carbon-isotope curve has its highest potential as a high-resolution correlative tool at those stratigraphic levels characterised by distinctive shape and form. General trends in Jurassic $\delta^{13}C$ have been published by Bartolini *et al.* (1996), Podlaha *et al*. (1998), Gruszczyński (1998) and Bartolini and Cecca (1999).

The amount of scatter in all three localities, if Cabo Mondego is split into pre- and post-carbon isotope excursion, is considerable (pre-isotope excursion Cabo Mondego =1.96 ‰; post-isotope excursion Cabo Mondego = 3.11 ‰;

Polish Jura = 3.00 ‰; Albstadt-Pfeffingen = 2.50 ‰). Changes in $\delta^{13}C$ values may have arisen from both localised and temporal changes in the isotope composition in DIC from the Upper Bajocian-Lower Callovian seawater in the Tethys of Europe. Wierzbowski and Joachimski (2007) suggested that the lower $\delta^{13}C$ values reported from ammonites were caused by marine surface waters mixing with freshwater – which often has lower $\delta^{13}C$ values because of the oxidation of suspended terrestrial organic matter. However, such an explanation, and again as pointed out by the authors, cannot be sustained for long periods of time so cannot be the cause of the scatter in the carbon isotope data.

The Middle Jurassic $\delta^{13}C$ curve shows a series of major isotope events within the Aalenian, Lower-Middle Bajocian, Callovian, and middle Oxfordian Tethyan margin sediments (see Hoffman *et al.* 1991; Bill *et al*. 1995; Jenkyns, 1996; Weissert and Mohr 1996; Bartolini *et al*. 1996; Bartolini and Cecca, 1999; Rey and Delgado 2002; O'Dogherty *et al*. 2006; Sandoval *et al*., 2008; Nunn *et al.* 2009; Price *et al.*, 2018). The Middle Jurassic was a period of low carbonate platform production with Bartolini and Cecca (1999) reporting that the low carbonate platform production was induced by high eutrophication levels, which affected the Western Tethys during the Middle Jurassic (Bartolini *et al.,* 1996; Bartolini and Cecca, 1999). The $\delta^{13}C$ trends from the studied localities and Wierzbowski *et al*. (2017; Figure 6.9) shows that there was very little change in the global carbon cycle during the Bathonian.

Due to the limited exposure of the studied section and lack of notable changes in the $\delta^{13}C$ values at Albstadt-Pfeffingen, it would not be possible to use these results for stratigraphic correlation. The belemnite $\delta^{13}C$ records from Cabo Mondego, Albstadt-Pfeffingen and the Polish Jura do not indicate any major secular variations. The new data presented in this work agrees with whole rock samples from Spain (O'Dogherty *et al*., 2006). Nevertheless, $\delta^{13}C$ values from the Pfeffingen belemnites are consistent with what would be expected for the Bathonian-Callovian boundary (Bartolini *et al.,* 1996). The weak positive correlation between $\delta^{13}C$ and $\delta^{18}O$ values observed in both Cabo Mondego and Albstadt-Pfeffingen reflects the incorporation of metabolic CO_2 (or bicarbonate) (e.g. Li *et al*., 2012).

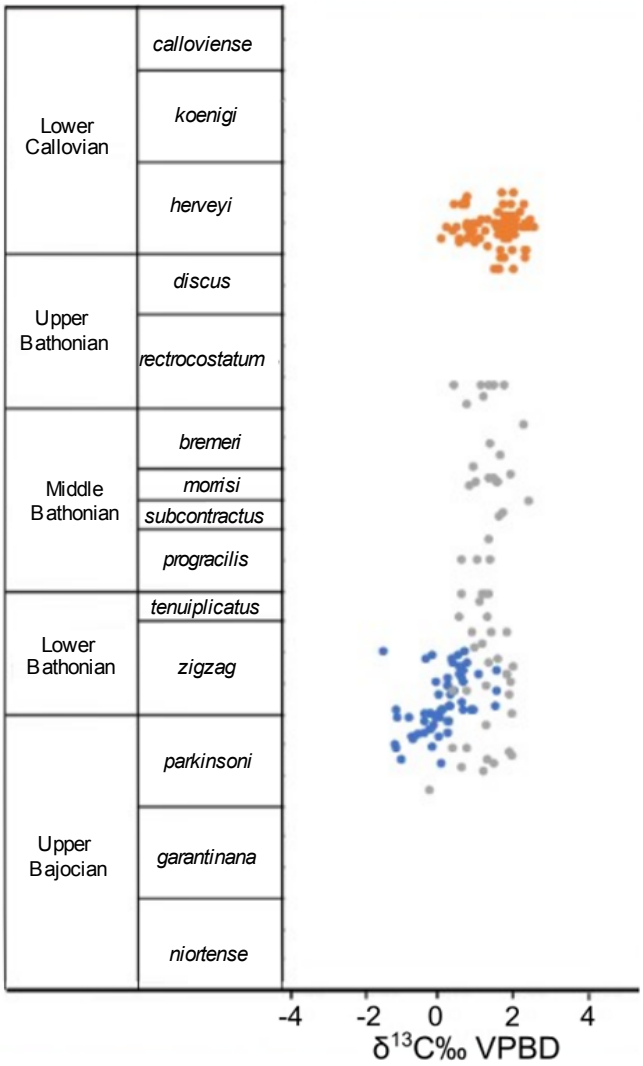

Figure 6.9: $\delta^{13}C$ values from Cabo Mondego (blue), the Polish Jura (grey), and Albstadt-Pfeffingen (orange). Polish data taken from Wierzbowski and Joachimski (2007) and stratigraphy based on Wierzbowski *et al*. (2017).

Chapter 7: Conclusions

- Strontium isotope ratios from Albstadt-Pfeffingen were used to identify a potential unconformity within the studied section which would compromise the site's candidacy as the GSSP for the base of the Callovian.

- The most likely explanation for the positive $\delta^{13}C$ excursion at Cabo Mondego is faunal turnover and not changes in the carbon cycle as changes in the carbon cycle would fail to account for the brachiopod record.

- The Mn/Ca ratios at both sites are a more suitable diagenetic marker in fossil calcite than Fe/Ca ratios due to showing a stronger correlation with $\delta^{18}O$ values. However, Mn still appears to be a poor marker for diagenesis as the covariation with is $\delta^{18}O$ weak and the power to discriminate between preserved and altered material is minimal.

- Belemnite $\delta^{18}O$ palaeotemperatures show cooling at the end of the Bajocian, a relatively cold climate during the Bathonian, and warming in the Lower Callovian.

- Belemnite $\delta^{13}C$ values at both studied locations do not show any prominent changes, supporting previous studies.

- Intra-specific fractionation in the studied belemnite rostra can be identified in carbon isotopes but not in oxygen isotopes.

- Mg/Ca and Sr/Ca ratios are not useful as palaeothermometers for Middle Jurassic belemnites at the two studied locations.

References

Ager, D. V. (1981) *The Nature of the Stratigraphical Record*, 2nd ed, Hong Kong: MacMillan.

Anders, E., and Ebihara, M. (1982) Solar-system abundances of the elements, *Geochimica et Cosmochimica Acta*, 46(11): 2363–2380.

Anderson, T.F. and Arthur, M.A. (1983) Stable isotopes of oxygen and carbon and their application to sedimentological and palaeoenvironmental problems, in Arthur, M.A. Anderson, T.F. Kaplan, I.R. Veizer, J. and Land, L.S. eds. (1983) *Stable isotopes in sedimentary geochemistry: Society of Economic Palaeontologists and Mineralogists Short course 10*, Dallas, Society for Sedimentary Geology: 1-151.

Anderson, T.F., Popp, B.N., Williams, A.C., Ho, L.Z. and Hudson, J.D. (1994) The stable isotopic records of fossils from the Peterborough Member, Oxford Clay Formation (Jurassic), UK: palaeoenvironmental implications, *Journal of the Geological Society,* 151: 125-128.

Armendáriz, M., Rosales, I., Bádenas, B., Aurell, M., García-Ramos, J.C. and Piñuela, L. (2012) High-resolution chemostratigraphic records from Lower Pliensbachian belemnites: Palaeoclimatic perturbations, organic facies and water mass exchange (Asturian basin, northern Spain), *Palaeogeography, Palaeoclimatology, Palaeoecology*, 333/334: 178-191.

Asmerom, Y., Jacobsen, S.B., Knoll, A.H., Butterfield, N.J. and Swett, K. (1991) Strontium isotopic variations of Neoproterozoic seawater: implications for crustal evolution, Geochimica et Cosmochimica Acta, 55(10): 2883-2894.

Auclair, A.-C., Lécuyer, C., Bucher, H. and Sheppard, S.M.F. (2004) Carbon and oxygen isotope composition of *Nautilus macromphalus*: a record of thermocline waters off New Caledonia, *Chemical Geology*, 207: 91-100.

Azerêdo, A.C. (1998) Geometry and facies dynamics of Middle Jurassic carbonate ramp sandbodies, West-Central Portugal, *Geological Society, London, Special Publications*, 149: 281-314.

Azerêdo, A.C. and Duarte, L.V. (2017) Stratigraphy, sedimentary patterns, and reservoir characteristics of Jurassic carbonate successions in the Lusitanian Basin, *Ciências da Terra*, 19(1): 13-33.

Azerêdo, A.C., Wright, V.P. and Ramalho, M.M. (2002) The Middle–Late Jurassic forced regression and disconformity in central Portugal: eustatic, tectonic and climatic effects on a carbonate ramp system, *Sedimentology,* 49(6): 1339-1370.

Azerêdo, A.C., Duarte, L.V., Henriques, M.H., Manuppella, G. and D, Dinâmica. (2003) *Continental no Triásico, Aos Mares do Jurássico Inferior e Médio. Cadernos de Geologia de Portugal*, Instituto Geológico Mineiro: Lisbon.

Badgley, C. and Gingerich, P. D. (1988) Sampling and faunal turnover in early Eocene mammals, *Palaeogeography, Palaeoclimatology, Palaeoecology,* 63(1-3): 141-157

Bailey, T.C., Rosenthal, Y., McArthur, J.M., van de Schootbrugge, B. and Thirlwall, M.F. (2003) Paleoceanographic changes of the Late Pliensbachian–Early Toarcian interval: a possible link to the genesis of an Oceanic Anoxic Event, *Earth and Planetary Science Letters,* 212(3-4):307-320.

Baker, P.A., Giesket, J.M. and Elderfield, H. (1982) Diagenesis of carbonates in deep-sea sediments - evidence from Sr/Ca ratios and interstitial dissolved Sr data, *Journal of Sedimentary Petrology*, 52(1): 71-82.

Bandel, K. and Spaeth, C. (1988) Structural differences in the ontogeny of some belemnite rostra, in Wiedmann, J. and Kullmann, J. eds. (1988) *Cephalopods Present and Past*, Stuttgart, Schweizerbart: 247-271.

Banner, J. L. and Hanson, G. N. (1990) Calculation of simultaneous isotopic and trace element variations during water-rock interaction with applications to carbonate diagenesis, *Geochimica et Cosmochimica Acta*, 54 (11): 3123–3137.

Barnard, P.D.W. (1973) Mesozoic floras, in Hughes, N.F. ed (1973) *Organisms and Continents Through Time Special Papers in Palaeontology 12,* London, Palaeontological Association: 175–188.

Bartolini, A. and Cecca, F. (1999) 20 My hiatus in the Jurassic of Umbria-Marche Apennines (Italy): carbonate crisis due to eutrophication, *Comptes Rendus de l'Académie des Sciences - Series IIA/Earth and Planetary Science*, 329: 587-595.

Bartolini, A., Baumgartner, P.O. and Hunziker, J.C. (1996) Middle and Late Jurassic carbon stable-isotope stratigraphy and radiolarite sedimentation of the Umbria–Marche Basin (Central Italy), *Eclogae Geologicae Helvetiae,* 89: 811-844.

Beher, E., Brand, E. and Franz, M. (2010) Bathonian and Lower Callovian ostracods of Albstadt-Pfeffingen (Middle Jurassic, Baden-Württemberg, Germany, *Palaeodiversity* 3: 43–57.

Bender, M. (2013) *Paleoclimate,* Princeton, Princeton University Press.

Benito, M. I. and Reolid, M. (2020) Comparison of the Calcareous Shells of Belemnitida and Sepiida: Is the Cuttlebone Prong an Analogue of the Belemnite Rostrum Solidum? *Minerals*, 10(3). Available at: <https://doi.org/10.3390/min10080713>. Accessed [12 February 2021].

Benito, M.I. and Reolid, M. (2012) Belemnite taphonomy (Upper Jurassic, Western Tethys) part II: Fossil-diagenetic analysis including combined petrographic and geochemical techniques, *Palaeogeography, Palaeoclimatology, Palaeoecology,* 358–360: 89–108.

Benito, M.I., Reolid, M. and Viedma, C. (2016) On the microstructure, growth pattern and original porosity of belemnite rostra: insights from calcitic Jurassic belemnites, *Journal of Iberian Geology*, 42(2): 201-226.

Berlin, T.S., Naidin, D.P., Saks, V.N., Teis, R.V. and Khabokov, A.V. (1967). Jurassic and Cretaceous climate in northern USSR from palaeotemperature determinations, *International Geological Review*, 9: 1080-1092.

Berner, R.A. (1994) GEOCARB II; a revised model of atmospheric CO_2 over Phanerozoic time, *American Journal of Science*, 294(1): 56-91.

Bettencourt, V. and Guerra, A. (1999) Carbon- and oxygen-isotope composition of the cuttlebone of Sepia officinalis: a tool for predicting ecological information? *Marine Biology*, 133: 651-657.

Bill, M., Baumgartner, P.O., Hunzikeer, J.C. and Sharp, Z.D. (1995) Carbon isotope stratigraphy of the Liesberg Beds Member (Oxfordian, Swiss Jura), *Eclogae Geologicae Helvetiae*, 88: 135-155.

Blum, J. D. and Eral, Y. (1995) A silicate weathering mechanism linking increases in marine 87Sr/ 86Sr with global glaciation, *Nature*, 373: 415-418.

Boggs, S. and Krinsley, D. (2006) *Application of cathodoluminescence imaging to study sedimentary rocks*, Cambridge, Cambridge University Press.

Brand, U. (1989) Biogeochemistry of late paleozoic American brachiopod and secular variation of seawater composition, *Biogeochemistry*, 7: 159-193.

Brand, U. and Veizer, J. (1980) Chemical diagenesis of a multicomponent carbonate system - 1. Trace elements, *Journal of Sedimentary Research*, 50(4):1219-1236.

Brand, U. and Veizer, J. (1981) Chemical diagenesis of a multicomponent carbonate system - 2, stable isotopes, *Journal of Sedimentary Research*, 51(3): 987-997.

Brand, U., Logan, A., Hiller, N. and Richardson, J. (2003). Geochemistry of modern brachiopods: applications and implications for oceanography and paleoceanography, *Chemical Geology*, 198(3): 305-334.

Brand, U., Azmy, K., Bitner, M.A., Logan, A., Zuschin, M., Came, R. and Ruggiero, E. (2013). Oxygen isotopes and MgCO3 in brachiopod calcite and a new paleotemperature equation, *Chemical Geology*, 359: 23-31.

Brand, W.A., Coplen, T. B., Vogl, J., Rosner, M. and Prohaska, T. (2014) Assessment of international reference materials for isotope-ratio analysis (IUPAC Technical Report), *Pure and Applied Chemistry*, 86(3): 425-467.

Brigaud, B., Durlet, C., Deconinck, J., Vincent, B., Pucéat, E., Thierry, J. and Touiller, A. (2009) Facies and climate/environmental changes recorded on a carbonate ramp: A sedimentological and geochemical approach on Middle

Jurassic carbonates (Paris Basin, France), *Sedimentary Geology*, 222(2009):181-206.

Bruckschen, P. and Veizer, J. (1997) Oxygen and carbon isotopic composition of Dinantian brachiopods: paleoenvironmental implications for the Lower Carboniferous seawater of western Europe, *Palaeogeography, Palaeoclimatology, Palaeoecology*, 132(1-4): 243-264.

Buck, E., Hahn, W. and Schädel, K. (1966) Zur Stratigraphie des Bajociums und Bathoniums (Dogger δ-ε) der Schwäbischen Alb, *Jahreshefte des Geologischen Landesamts in Baden-Württemberg*, 8: 23-46.

Callomon, J. and Dietl, G. (2007) Callovian working group, *ISJS Newsletter*, 34(2): 14-16.

Callomon, J.H. (1991) Callovian Boundary Working-Group. Proposals for the designation of a Basal Boundary Stratotype (GSSP) and the definition of the Callovian Stage. Field Symposium held in Stuttgart and Albstadt-Ebingen, southern Germany, September 1990, *Newsletter of the International Subcommission on Jurassic Stratigraphy*, 20: 5–9.

Callomon, J.H. and Dietl, G. (2000) On the proposed Basal Boundary Stratotype (GSSP) of the Middle Jurassic Callovian Stage, *GeoResearch Forum*, 6: 41-54.

Callomon, J.H. and Cope, J.C.W. (1995) The Jurassic Geology of Dorset, in Taylor, P.D. ed. (1995) *Field Geology of the British Jurassic*, London, Geological Society, London: 51-104.

Callomon, J.H. and Dietl, G. (1990). *Proposed definition of the Callovian Stage. Field Symposium in Swabia, Stuttgart/Albstadt (16–21 September, 1990).* – ISJS, Callovian Working Group. – XI + 20 pp.; Stuttgart.

Callomon, J.H., Dietl, G. and Page, K.N. (1988) On the ammonite faunal horizons and standard zonations of the Lower Callovian Stage in Europe, *2nd International Symposium on Jurassic Stratigraphy, Lisboa 1987,* 1: 359-376.

Canales, M.L. and Henriques, M.H. (2008) Foraminifera from the Aalenian and the Bajocian GSSP (Middle Jurassic) of Murtinheira section (Cabo Mondego, West Portugal): biostratigraphy and paleoenvironmental implications, *Marine Micropaleontology*, 67 (1-2): 155-179.

Canales, M.L. and Henriques, M.H. (2013) Foraminiferal assemblages from the Bajocian Global Stratotype Section and Point (Cape Mondego, Portugal), *Journal of Foraminiferal Research*, 43(2): 182-206.

Carpenter, S.J. and Lohmann, K.C. (1992) Sr/Mg ratios of modern marine calcite: empirical indicators of ocean chemistry and precipitation rate, *Geochimica et Cosmochimica Acta*, 56(5): 1837–1849.

Carpenter, S. J. and Lohmann, K. C. (1995) $\delta^{18}O$ and $\delta^{13}C$ values of modern brachiopod shells, *Geochimica et Cosmochimica Acta,* 59 (18): 3749-3764.

Catling, D.C. and Kasting, J. F. (2017) *Atmospheric Evolution on Inhabited and Lifeless Worlds*, Cambridge, Cambridge University Press.

Chandler, M.A., Rind, D. and Ruedy, R. (1992) Pangaean climate during the Early Jurassic: GCM simulations and the sedimentary record of paleoclimate. *Geological Society of America Bulletin,* 104: 543-559.

Clarkson, E.N.K. (1993). *Invertebrate palaeontology and evolution*, 3rd ed, London, Chapman & Hall.
Coggon, R. M., Teagle, D. A. H., Smith-Duque, C.E., Alt, J. C. and Cooper, M. J. (2010) Reconstructing past seawater Mg/Ca and Sr/Ca from Mid-Ocean Ridge flake calcium carbonate veins, *Science*, 327: 1114-1117.

Cohen, A.L., Owens, K.E., Layne, G.D. and Shimizu, N. (2002) The effect of algal symbionts on the accuracy of Sr/Ca paleotemperatures from coral, *Science*, 296 (5566): 331-333.

Cohen, K.M., Finney, S.C., Gibbard, P.L. and Fan, J.-X. (2013) The ICS International Chronostratigraphic Chart, *Episodes*, 36: 199-204.

Cohen, K.M., Finney, S.C., Gibbard, P.L. and Fan, J.-X. (2020) *The ICS International Chronostratigraphic Chart v2020/03.* Available at <https://stratigraphy.org/ICSchart/ChronostratChart2020-03.pdf. Accessed [20 June 2020].

Cowie, K. M. (1986) Guidelines for boundary stratotypes, *Episodes,* 9: 78-82.

Cowie, J. W., Ziegler, W., Boucot, A. J., Bassett, M. G., and Remane, J. (1986) Guidelines and statutes of the International Commission on Stratigraphy (ICS), *Courier Forschungsinstitut Senckenberg,* 83: 1-14.

Craig, H. (1953) The geochemistry of the stable carbon isotopes, Geochimica et Cosmochimica Acta, 3(2-3): 53-92.

Craig, H. (1957) Isotopic standards for carbon and oxygen and correction factors for mass-spectrometric analysis of carbon dioxide, *Geochimica et Cosmochimica Acta*, 12(1-2): 133-149.

d'Orbigny, A. (1842-1851) *Paléontologie Français. Description zoologiqueet ǵéologique de tous les animaux mollusques et rayonnés fossiles de France. Terrains oolitiques ou jurassiques. I. Céphalopodes,* Paris, Masson.

d'Orbigny, A. (1852) *Cours élémentaire de paléontologie et de géologiestratigraphique, Vol. 2,* Paris, Masson

Dance, M. A., Bello, G., Furey, N.B. and Rooker, J. R. (2014) Species-specific variation in cuttlebone $\delta^{13}C$ and $\delta^{18}O$ for three species of Mediterranean cuttlefish, *Marine Biology,* 161:489-494.

Dauphin, Y. (1984) Microstructures des Céphalopodes. IV Le"rostre" de Belosepia (Dibranchiata), *Paläontologische Zeitschrift,* 58: 99–117.

Dauphin, Y., Williams, C.T. and Barskov, I.S. (2007) Aragonitic rostra of the Turonian belemnitid *Goniocamax*: arguments from diagenesis, *Acta Palaeontologica Polonica,* 52: 85–97.

Davis, A.J. and John, C.M. (2019) The clumped (^{13}C single bond ^{18}O) isotope composition of echinoid calcite: Further evidence for “vital effects” in the clumped isotope proxy, *Geochimica et Cosmochimica Acta*, 245: 172-189.

Deines, P. (1980) The isotopic composition of reduced organic carbon, in Fritz, P. and Fontes, J. eds. (1980) *Handbook of environmental isotope geochemistry*, Amsterdam, Elsevier: 239-406.

Delaygue, G., Masson, V., Jouzel, J., Koster, R.D. and Healy, R.J. (2000) The origin of Antarctic precipitations: A modelling approach, *Tellus*, 52B: 19-36

DePaolo, D.J. (2011) Surface kinetic model for isotopic and trace element fractionation during precipitation of calcite from aqueous solutions, *Geochimica et Cosmochimica Acta*, 75: 1039-1056.

DePaolo, D.J. and Ingram, B.L. (1985) High-resolution stratigraphy with strontium isotopes, *Science*, 227(4689):938-941.

Dietl, G. (1981) Über Macrocephalites (Ammonoidea) aus dem Aspidoides-Oolith und die Bathonium/CalloviumGrenzschichten der Zollernalb (SW-Deutschland), *Stuttgarter Beiträge zur Naturkunde, (B),* 68: 1-15.

Dietl, G. (1990) *Procerites progracilis* COX & ARKELL und andere Ammoniten aus dem basalen Mittel-Bathonium (Mittl. Jura) der Zollernalb, Schwäb. Alb, SW-Deutschland, *Jahresberichte und Mitteilungen des oberrheinischen geologischen Vereins, Neue Folge*, 72: 329-340.

Dietl, G., Ebal, K. and Hugger, R. (1979) Zur Stratigraphie und Ammonitenfauna der Varians-Schichten (Mittle – und unterstes Ober Bathonian) von Talheim am Lupfen (südwestl. Schwäbische Alb), *Paläeontologische Zeitschrift*, 53: 182-197.

Dimter, A. and Smelror, M. (1990) Callovian (Middle Jurassic) marine microplankton from southwestern Germany: Biostratigraphy and paleoenvironmental interpretations, *Palaeogeography, Palaeoclimatology, Palaeoecology*, 80(3-4): 173-195.

Doyle, P. (1985) Sexual dimorphism in the belemnite *Youngibelus* from the lower Jurassic of Yorkshire, *Palaeontology,* 28:133-146.

Dromart, G., Garcia, J.-P., Picard, S., Atrops, F., Lécuyer, C. and Sheppard, S.M.F. (2003) Ice age at the middle-late Jurassic transition? *Earth and Planetary Science Letters*, 213: 205-220.

Dunca, E., Doguzhaeva, L., Schöne, B.R. and van de Schootbrugge, B. (2006) Growth patterns in rostra of the Middle Jurassic belemnite *Megateuthis giganteus*: controlled by the moon? *Acta Universitatis Carolinae, Geologica,* 49: 109-117.

Dutton, A., Huber, B.T., Lohmann, K. C. and Zinsmeister, W. J. (2007) High-resolution stable isotope profiles of a dimitobelid belemnite: implications for paleodepth habitat and Late Maastrichtian climate seasonality, *Palaios,* 22: 642-50.

Dzyuba, O.S., Goryacheve, A.A., Ruban, D.A., Gnezdilova, V.V. and Zayats, P.P. (2016) New data on Callovian (Middle Jurassic) belemnites and palynomorphs from the Northern Caucasus, southwest Russia, *Geologos*, 22(1):49-59.

Earle, S. (2019) *Physical Geology*, 2nd ed, Victoria, BC Campus.

Elderfield, H. (1986) Strontium isotope stratigraphy, *Palaeogeography, Palaeoclimatology, Palaeoecology*, 57(1): 71-90

Epstein, S., Buchsbaum, R., Lowenstam, H.A. and Urey, H.C. (1953) Revised carbonate-water isotopic temperature scale, *Bulletin of the Geological Society of America*, 64: 1315-1326.

Erba, E., Bottini, C., Weissert, H.J. and Keller, C.E. (2010) Calcareous nannoplankton response to surface-water acidification around Oceanic Anoxic Event 1a, *Science*, 329(5990): 428-432.

Farmer, G. and Baxer, M.S. (1976) Atmospheric carbon dioxide records levels as indicated by the stable isotope record in wood, *Nature*, 247: 273-275.

Faure, G. and Mensing, T.M. (2005) Isotopes: principles and applications, London, Wiley.

Fernández-López, S.R. and Henriques, M.H. (2002) Upper Bajocian-Lower Bathonian ammonites of Carbo Mondego Section (Portugal), *VI International Symposium on the Jurassic System*: 65-66.

Fernández-López, S.R., Henriques, M.H. and Mangold, C. (2006a) Ammonite succession at the Bajocian/Bathonian boundary in the Cabo Mondego region (Portugal), *Lethaia,* 39:253-264.

Fernández-López, S.R., Henriques, M.H. and Mangold, C. (2006b) Ammonite horizons at the basal Bathonian zone (*Parum* Subzone) in Cabo Mondego, Portugal, *Volumina Jurassica,* 4:161.

Fernández-López, S.R., Henriques, M.H., Mangold, C., and Pavia, G. (2007) New Early Bathonian Bigotitinae and Zigzagiceratinae (Ammonoidea, Middle Jurassic), *Rivista Italiana di Paleontologia e Stratigrafia*, 113: 383-399.

Fernández-López, S.R., Pavia, G., Erba, E., Guiomar, M., Henriques, M. H., Lanzam R., Mangold, C., Morton, N., Olivero, D. and Tiraboschi, D. (2009) The Global Boundary Stratotype Section and Point (GSSP) for base of the Bathonian Stage (Middle Jurassic), Ravin du Bès Section, SE France, *Episodes*, 32(4): 222-248.

Föllmi, K. B. (2016) Sedimentary condensation, *Earth-Science Reviews*, 152: 143-180.

Frakes, L.A., Francis, J.E. and Syktus, J.I. (1992) *Climate modes of the Phanerozoic*, Cambridge, Cambridge University Press.

Franz, M. and Knott, S.D. (2012) Foraminifera from the Callovian GSSP candidate section of Albstadt-Pfeffingen (Middle Jurassic, Southern Germany), *Neues Jahrbuch für Geologie und Paläontologie - Abhandlungen,* 264(3):263-282

Fujioka, H., Takayanagi, H., Yamamoto, K. and Iryu, Y. (2019) The effects of meteoric diagenesis on the geochemical composition and microstructure of Pliocene fossil *Terebratalia coreanica* and *Laqueus rubellus* brachiopod shells from northeastern Japan. *Progress in Earth and Planetary Science* 6(45). Available at <https://doi.org/10.1186/s40645-019-0289-7>. Accessed [12 October 2020].

Geyer, O.F. and Gwinner, M.P. (1984) *Die Schwäbische Jura und ihr Vorland*, 3rd ed, Berlin, Gebrüder Borntraeger Verlagsbuchhandlung.

Gradstein, F.M. and Ogg, J.G. (2012) The chronostratigraphic scale, in Gradstein, F.M., Ogg, J.G., Schmitz, M.D. and Ogg, G.M. eds. (2012) *The Geological Time Scale 2012*, Amsterdam, Elsevier: 31-42.

Gradstein, F., Ogg, J. and Smith, A.G. (2004) *A geological time scale 2004*, Cambridge, Cambridge University Press.

Gröcke, D.R. (2020) carbon isotope stratigraphy: principles and applications, in Montenari, M. eds. (2020) *Stratigraphy & Timescales, volume 5*, Cambridge, MA, Academic Press :1-40

Grossman, E. L. (2012a). Applying oxygen isotope paleothermometry in deep time, *The Paleontological Society Papers*, 18: 39-67.

Grossman, E.L. (2012b) Oxygen isotope stratigraphy, in Gradstein, F.M., Ogg, J.G., Schmitz, M.D. and Ogg, G.M. eds. (2012) *The Geological Time Scale 2012*, Amsterdam, Elsevier: 181-206.

Grossman, E.L., Zhang, C. and Yancey, T.E. (1991) Stable isotope stratigraphy of brachiopod from Pennsylvanian shales in Texas, *GSA Bulletin*, 103: 953-965.

Gruszczyński, M. (1998) Chemistry of Jurassic seas and its bearing on the existing organic life*, Acta Geologica Polonica*, 48(1): 1-29.

Gygi, R.A. and Persoz, F. (1986) Mineralostratigraphy, litho- and biostratigraphy combined in correlation of the Oxfordian (Late Jurassic) formations of the Swiss Jura range, *Eclogae Geologicae Helvetiae*, 79(2): 385-454.

Habermann, D., Neuser, R. D. and Richter, D. K. (1998) Low limit of Mn2+-activated cathodoluminescence of calcite: state of the art, *Sedimentary Geology*, 116 (1-2): 13-24.

Hall, A. and Kennedy, W. J. (1967) Aragonite in fossils, *Proceedings of the Royal Society of London. Series B, Biological Sciences,* 168(1013): 377-412.

Hallam, A. (1982). The Jurassic climate, in Berger, W.H and Crowell, J.C. eds. (1982) *Climate in Earth history: studies in geophysics*, Washington, DC, National Academy Press: 159-163.

Hallam, A. (1985) A review of Mesozoic climates, *Journal of the Geological Society of London*, 142: 433-445.

Hallam, A. (1991) Jurassic climates as inferred from the sedimentary and fossil records. *Philosophical Transactions of the Royal Society of London B*, 341: 287-296

Hallam, A. (2001) A review of the broad pattern of Jurassic sea-level changes and their possible causes in the light of current knowledge, *Palaeogeography, Palaeoclimatology, Palaeoecology*, 167(1-2): 23-37.

Hansen, J., Sato, M., Ruedy, R., Lo, K., Lea, D.W. and Medina-Elizade, M. (2006) Global temperature change, *PNAS*, 103(39): 14288-14293.

Harazim, D., van de Schootbrugge, B., Sorichter, K., Fiebig, J., Weug, A., Suan, G. and Oschmann, W. (2013) Spatial variability of watermass conditions within the European Epicontinental Seaway during the Early Jurassic (Pliensbachian–Toarcian), *Sedimentology,* 60(2): 359-390.

Henriques, M.H., Gardin, S., Gomes, C.R., Soares, A.F., Rocha, R.B., Marques, J.F., Lapa, M.R. and Montenegro, J.D. (1994) The Aalenian-Bajocian boundary at Cabo Mondego (Portugal), in Cresta, S. and Pavia, G. eds. (1994) *Proceedings of 3rd international meeting on Aalenian and Bajocian stratigraphy*: 63-77

Hermoso, M. and Lecasble, M. (2018) The effect of salinity on the biogeochemistry of the coccolithophores with implications for coccolith-based isotopic proxies, *Biogeosciences,* 15:6761-6772.

Hess, H. (1999) Lower Jurassic Posidonia Shale of Southern Germany, in Hess, H., Ausich, WI., Brett, B.E. and Simms, M.J. eds. (1999) *Fossil Crinoids*, Cambridge, Cambridge University Press: 183-196.

Hesselbo, S.P., Jenkyns, H.C., Duarte, L.V. and Oliveira, L.C.V. (2007) Carbon-isotope record of the Early Jurassic (Toarcian) Oceanic Anoxic Event from fossil wood and marine carbonate (Lusitanian Basin, Portugal), *Earth and Planetary Science Letters,* 253: 455-470.

Hilting, A.K., Kump., L.R. and Bralower, T.J. (2008) Variations in the oceanic vertical carbon isotope gradient and their implications for the Paleocene-Eocene biological pump, *Paleoceanography*, 23(3). Available at: < https://doi.org/10.1029/2007PA001458>. Accessed [20 May 2019].

Hoefs, J. (2008) *Stable isotope geochemistry*, Dordrecht, Springer.

Hoffmann, A., Gruszczyński, M., Malkowski, K., Halas, S., Matyja, B.A. and Wierzbowski, A. (1991) Carbon and carbon isotope curves for the Oxfordian of central Poland, *Acta Geologica Polonica*, 43: 157-164.

Hoffmann R., Richter, D.K., Neuser, R.D., Jöns, N., Linzmeier, B.J., Lemanis, R.E., Fusseis F., Xiao, X. and Immenhauser, A. (2016) Evidence for a composite organic–inorganic fabric of belemnite rostra: implications for palaeoceanography and palaeoecology, *Sedimentary Geology,* 341: 203-215.

Hoffmann, R. and Stevens, K. (2020) The palaeobiology of belemnites – foundation for the interpretation of rostrum geochemistry, *Biological Reviews,* 95: 94-123.

Howarth, R.J. and McArthur, J.M. (1997) Statistics for strontium isotope stratigraphy: a robust LOWESS Fit to the marine Sr-isotope curve for 0 to 206 Ma, with look-up chart for derivation of numerical age, *The Journal of Geology*, 105: 441-456.

Huang, C. (2018) Astronomical time scale for the Mesozoic, in Montenari, M. ed. (2018) *Stratigraphy & Timescales, Volume 3*, Cambridge, MA, Academic Press: 81-150.

Huber, B.T., MacLeod, K.G. and Wing, S.T. eds (2000) *Warm climates in Earth history*, Cambridge, Cambridge University Press.

Jenkyns, H.C. (1996) Relative sea-level change and carbon isotopes: data from the Upper Jurassic (Oxfordian) of central and southern Europe, *Terra Nova*, 8: 75-85.

Jenkyns, H.C. and Clayton, C.J. (1997) Lower Jurassic epicontinental carbonates and mudstones from England and Wales: chemostratigraphic signals and the early Toarcian anoxic event, *Sedimentology,* 44(4): 687-706.

Jenkyns, H.C., Jones, C.E., Gröcke, D.R., Hesselbo, S.P. and Parkinson, D.N. (2002) Chemostratigraphy of the Jurassic System: applications, limitations and implications for palaeoceanography, J*ournal of the Geological Society*, 159:351-378.

Johnson, A.L.A. (1999) Evidence and cause of small sixed in Bathonian (Middle Jurassic) marine bivalve of north-western Europe, *Palaeontology*, 42(4): 605-624.

Jones, C.E. and Jenkyns, H.C. (2001) Seawater strontium isotopes, oceanic anoxic events, and seafloor hydrothermal activity in the Jurassic and Cretaceous, *American Journal of Science*, 301(1): 112-149.

Jones, C. E., Jenkyns, H. C., Coe, A. J. and Hesselbo, S. P. (1994) Strontium isotopic variations in Jurassic and Cretaceous seawater, *Geochimica et Cosmochimica Act*, 58(14): 3061-3074.

Kabanov, G.K. (1967) Skeleton of belemnitids: morphology and biological analysis, *Transactions of the Paleontological Institute,* 114: 1-101.

Kaplan, M. E. (1978) Calcite pseudomorphoses in Jurassic and Lower Cretaceous deposits of the northern area of eastern Siberia, *Geol. Geofiz*, 19: 62–70.

Kaiho, K., Chen, Z.Q. and Sawada, K. (2009) Possible causes for a negative shift in the stable carbon isotope ratio before, during and after the end-Permian mass extinction in Meishan, South China, *Australian Journal of Earth Sciences*, 56:799-808.

Kim, S-T. and O'Neil, J.R. (1997) Equilibrium and nonequilibrium oxygen isotope effects in synthetic carbonates, *Geochimica et Cosmochimica Acta*, 61(16): 3461-3475.

Klug, C., Schweigert, G., Fuchs, D., Kruta, I. and Tischlinger, H. (2016). Adaptations to squid-style high-speed swimming in Jurassic belemnitids, *Biology Letters*, 12 (1): 20150877. Available at: <https://royalsocietypublishing.org/doi/10.1098/rsbl.2015.0877>. Accessed [10 March 2020].

Knauth, L. and Kennedy, M. (2009) The late Precambrian greening of the Earth, *Nature*, 460: 728-732.

Knott, S. (2010). *Die kalkschaligen Foraminiferen des Unter-Bathonium bis Unter-Callovium des Profils Albstadt-Pfeffingen (Zollernalb, Baden-Württemberg)*, Diplom-Arbeit, Universität Freiburg, Freiburg (unpublished).

Korte, C. and Hesselbo, S.P. (2011) Shallow marine carbon and oxygen isotope and elemental records indicate icehouse-greenhouse cycles during the Early Jurassic, *Paleoceanography*, 26: PA4219. doi:10.1029/2011PA002160.

Korte, C., Kozur, H.W., Bruckschen, P. and Veizer, J. (2003) Strontium isotope evolution of Late Permian and Triassic sea water, *Geochimica et Cosmochimica Acta,* 67: 47-62.

Korte, C., Hesselbo, S.P., Ullmann, C.V., Dietl, G., Ruhl, M., Schweigert, G. and Thibault, N. (2015) Jurassic climate mode governed by ocean gateway, *Nature Communications*, 6(10015). Available at: <http://doi. 10.1038/ncomms10015> [Accessed 12 March 2020].

Kürschner, W. (2001) Leaf sensor for CO_2 in deep time, *Nature*, 411: 247-248

Kuznetsov, A.B., Semikhatov, M.A. and Gorokhov, I.M. (2018) Strontium isotope stratigraphy: principles and state of the art, *Stratigraphy and Geological Correlation*, 26: 367-386.

Labails, C., Olivet, J.-L., Aslanian, D. and Roest, W.R. (2010) An alternative early opening scenario for the Central Atlantic Ocean*, Earth and Planetary Science Letters*, 297(3-4): 355-368.

Lécuyer, C. and Bucher, H. (2006) Stable isotope compositions of a late Jurassic ammonite shell: a record of seasonal surface water temperatures in the southern hemisphere? *eEarth Discussions*, 1(1): 1-19.

Lécuyer, C., Picard, S., Garcia, J.-P., Sheppard, S.M.F., Grandjean, P. and Dromart, G. (2003) Thermal evolution of Tethyan surface waters during the Middle–Late Jurassic: evidence from $\delta^{18}O$ values of marine fish teeth, *Paleoceanography* 18: 1076–1092.

Lee, X. and Wan, G. (2000) No vital effect on $\delta^{18}O$ and $\delta^{13}C$ values of fossil brachiopod shells, Middle Devonian of China, *Geochimica et Cosmochimica Acta*, 64(15): 2649-2664.

Leinfelder, R. R., Schmid, D.U., Nose, M. and Werner, W. (2002) Jurassic reef patterns-the expression of a changing globe, in Kiessling, W., Flügel, E. and Golonka, J. eds. (2002) *Phanerozoic reef patterns*, Broken Arrow, Society of Sedimentology: 465-520.

Lever, H. (2007) Review of unconformities in the late Eocene to early Miocene successions of the South Island, New Zealand: ages, correlations, and causes, *New Zealand Journal of Geology & Geophysics*, 50: 245-261.

Li, Q. (2011) *Belemnite paleo-proxies and dating of Mesozoic carbonates*, PhD Thesis, University College London.

Li, Q., McArthur, J.M. and Atkinson, T.C. (2012). Lower Jurassic belemnites as indicators of palaeo-temperatures, *Palaeogeography, Palaeoclimatology, Palaeoecology*, 315-316:38-45

Li, Q., McArthur, J.M., Doyle, P., Janssen, N., Leng, M.J., Müller, W. and Reboulet, S. (2013) Evaluating Mg/Ca in belemnite calcite as a palaeo-proxy, *Palaeogeography, Palaeoclimatology, Palaeoecology*, 388: 98-108.

Lohmann, G. P. (2006) A model for variation in the chemistry of planktonic foraminifera due to secondary calcification and selective dissolution, *Paleoceanography*, 10: 445-458.

Lowenstam, H.A. (1961) Mineralogy, O^{18}/O^{16} ratios, and strontium and magnesium contents of recent and fossil brachiopods and their bearing on the history of the oceans, *The Journal of Geology*, 69(3): 241-260

Lowenstam, H.A. and Epstein, S. (1954) Paleotemperatures of the Post-Aptian Cretaceous as Determined by the Oxygen Isotope Method, *The Journal of Geology*, 62(3): 207-248.

Lucas, S.G. (2018) The GSSP method of chronostratigraphy: a critical review, *Frontiers in Earth Science*, 6(191). Available at: <http://doi: 10.3389/feart.2018.00191>. Accessed [12 March 2019].

Lukeneder, A. (2015) Ammonoid habitats and life history, in Klug, C., Korn, D., De Baets, K., Kruta, I. and Mapes, R.H. eds. (2015) *Ammonoid paleobiology: from anatomy to ecology*, Dordrecht, Springer: 689-791.

Lyell, C. (1830) *Principles of geology, being an attempt to explain the former changes of the Earth's surface, by reference to causes now in operation. vol. 1,* London, John Murray.

Mabrouk, A., Belayouni, H., Jarvis, I. and Moody, R.T.J. (2006) Strontium, $\delta^{18}O$ and $\delta^{13}C$ as palaeo-indicators of unconformities: Case of the Aleg and Abiod formations (Upper Cretaceous) in the Miskar Field, southeastern Tunisia, *Geochemical Journal*, 40(4): 405-425.

Marshall, J.D. (1992) Climatic and oceanographic isotopic signals from the carbonate rock record and their preservation, *Geological Magazine*, 192:143-160

Martill, D. M., Taylor, M. A., Duff, K. L., Riding, J. B. and Bown, P. R. (1994). The trophic structure of the biota of the Peterborough member, Oxford clay formation (Jurassic), UK, *Journal of the Geological Society, London*, 151: 173-194.

Mason, R.A. (1987) Ion microprobe analysis of trace elements in calcite with an application to the cathodoluminescence zonation of limestone cements from the Lower Carboniferous of South Wales, U.K, *Chemical Geology*, 64: 209-224.

McArthur, J.M. (1994) Recent trends in strontium isotopes stratigraphy, *Terra Nova*, 6(4): 331-358.

McArthur, J.M., Howarth, R.J. and Bailey, T.R. (2001) Strontium isotope stratigraphy: LOWESS Version 3: best fit to the marine Sr-isotope curve for 0-509 Ma and accompanying look-up table for deriving numerical age, *The Journal of Geology*, 109(2): 155-170.

McArthur J.M., Howarth R.J. and Shields G.A. (2012) Strontium isotope stratigraphy, in Gradstein, F.M., Ogg, J.G., Schmitz, M.D. and Ogg, G.M. eds. (2012) *The Geological Time Scale 2012*, Amsterdam, Elsevier: 127-144.

McArthur, J.M., Donovan. D.T., Thirlwall, M.F., Fouke, B.W. and Mattey, D. (2000) Strontium isotope profile of the early Toarcian (Jurassic) oceanic anoxic event, the duration of ammonite biozones, and belemnite palaeotemperatures, *Earth and Planetary Science Letters*, 179 (2000): 269-285.

McArthur, J.M., Doyle, P., Leng, M.J., Reeves, K., Williams, C.T., Garcia-Sanchez, R. and Howarth, R.J. (2007a) Testing Palaeo-environmental Proxies in Jurassic Belemnites: Mg/Ca, Sr/Ca, Na/Ca, $\delta^{18}O$ and $\delta^{13}C$, *Palaeogeography, Palaeoclimatology, Palaeoecology*, 252 (3-4):464-480.

McArthur, J.M., Janssen, N.M.M., Reboulet, S., Leng, M.J., Thirlwall, B. and van de Schootbrugge, B. (2007b) Palaeotemperatures, polar ice-volume, and isotope stratigraphy (Mg/Ca, $\delta^{18}O$, $\delta^{13}C$, $^{87}Sr/^{86}Sr$): The Early Cretaceous (Berriasian, Valanginian, Hauterivian), *Palaeogeography, Palaeoclimatology, Palaeoecology,* 248 (3-4): 391-430.

McConnaughey, T.A (1989a) ^{13}C and ^{18}O isotopic disequilibrium in biological carbonates: I. Patterns, *Geochimica et Cosmochimica Acta*, 53(1): 151-162.

McConnaughey, T.A (1989b) ^{13}C and ^{18}O isotopic disequilibrium in biological carbonates: II. *In vitro* simulation of kinetic isotope effects, *Geochimica et Cosmochimica Acta*, 53(1): 163-171.

McConnaughey, T.A., Burdett, J., Whelan, J.F., Paull, C.K. (1997) Carbon isotopes in biological carbonates: Respiration and photosynthesis, *Geochimica et Cosmochimica Acta*, 61(1): 611-622.

Mette, W., Clemence, M.-E., Thibault, N., Korte, C., Konard, B. and Ullmann, C.V. (2019). Sedimentology, carbon isotope stratigraphy and micropalaeontology of the Rhaetian Zlambach Formation– Implications for the Dachstein carbonate platform development (Northern Calcareous Alps, Austria), *Sedimentary Geology*, 382: 47-60.

Meyer, A. and Martínez-Casasnovas, J.A. (1999) Prediction of existing gully erosion in vineyard parcels of the NE Spain: a logistic modelling approach, *Soil and Tillage Research*, 50(3-4): 319-331.

Miller, K. G., Feigenson, M. D., Wright, J. D. and Clement, B. M. (1991) Miocene isotope reference section, Deep Sea Drilling Project site 608: an evaluation of isotope and biostratigraphic resolution, *Paleoceanography*, 6: 33-52.

Monks, N., Hardwick, J. D. and Gale, A. S. (1996) The function of the belemnite guard, *Paläontologische Zeitschrift,* 70: 425– 431.

Mönnig, E. and Dietl, G. (2017) The systematics of the ammonite genus Kepplerites (upper Bathonian and basal Callovian, Middle Jurassic) and the proposed basal boundary stratotype (GSSP) of the Callovian Stage, *Neues Jahrbuch für Geologie und Paläontologie,* 286(3): 235-287.

Müller-Stoll, H. (1936) Beiträge zur Anatomie der Belemnoidea, *Nov. A. Leopold,* 4: 1-70

Naydin, D. P. and Teys, R. V. (1976) Oxygen isotope compositions of Eurasian Toarcian-Aalenian seas, *Geochemistry International*, 13: 163-173.

Neto, K.S., Henriques, M.H. and Antunes, R.L. (2011) Nanofósseis calcários da passagem Aaleniano-Bajociano do perfil do Cabo Mondego – Portugal (GSSP do Bajociano), *Boletim de Geociências da Petrobras*, 19(1-2): 235-250.

Norris, M.S. and Hallam, A. (1995) Facies variations across the Middle–Upper Jurassic boundary in Western Europe and the relationship to sea-level changes, *Palaeogeography, Palaeoclimatology, Palaeoecology*, 116(3-2): 189-245.

Norris, R.D., Kirtland Turner, S., Hull, P.M. and Ridgwell, A. (2013) Marine ecosystem responses to Cenozoic global change, *Science*, 341(6145): 492-498.

Nunn, E. V., Price, G.D., Hart, M.B., Page, K.N. and Leng, M.J. (2009) Isotopic signals from Callovian–Kimmeridgian (Middle–Upper Jurassic) belemnites and bulk organic carbon, Staffin Bay, Isle of Skye, Scotland, *Journal of the Geological Society*, 166: 633-641.

O'Dogherty, L., Sandoval, J., Bartolini, A., Bruchez, S., Bill, M. and Guex, J. (2006) Carbon–isotope stratigraphy and ammonite faunal turnover for the Middle Jurassic in the Southern Iberian palaeomargin, *Palaeogeography, Palaeoclimatology, Palaeoecology*, 239: 311–333.

O'Dogherty, L., Aguado, R., Baumgartner, P.O., Bill, M., Goričan, Š., Sandoval, J. and Sequeiros, L. (2018) Carbon-isotope stratigraphy and pelagic biofacies of the Middle–Upper Jurassic transition in the Tethys–Central Atlantic connection, *Palaeogeography, Palaeoclimatology, Palaeoecolog*y, 507: 129-144.

Ogg, J. G., Hinnov, L.A. and Huang, C. (2012) Jurassic, in Gradstein, F.M., Ogg, J.G., Schmitz, M.D. and Ogg, G.M. eds. (2012) *The Geological Time Scale 2012*, Amsterdam, Elsevier: 731-791.

Pandolfi, J.M., Connolly, S.R., Marshall, D.J. and Cohen, A.L. (2011). Projecting coral reef futures under global warming and ocean acidification, *Science*, 333(6041): 418-422.

Pavia, G. and Enay, R. (1997). Definition of the Aalenian-Bajocian Stage boundary, *Episodes,* 20(1): 16-22.

Pearson, P.N., Ditchfield, P.W., Singano, J., Harcourt-Brown, K.G., Nicholas, C.J., Olsson, R.K., Shackleton, N.J. and Hall, M.A. (2001) Warm tropical sea surface temperatures in the Late Cretaceous and Early Tertiary, *Palaeogeography, palaeoclimatology, Palaeoecology*, 222: 95-121.

Pederzani, S. and Britton, K. (2019) Oxygen isotopes in bioarchaeology: Principles and applications, challenges and opportunities, *Earth Science Reviews*, 188: 77-107.

Pieńkowski, G., Schudack, M.E., Bosák, P., Enay, R., Feldman-Olszewska, A., Golonka, J., Gutowski, J., Herngreen, G.F.W., Jordan, P., Krobicki, M., Lathuiliere, B., Leinfelder, R.R., MichalíK, J., Mönnig, E., Noe-Nygaard, N., Pálfy, J., Pint, A., Rasser, M.W., Reisdorf, A.G., Schmid, D.U., Schweigert, G., Sutlyk, F., Wetzel, A. and Wong, T.E. (2008) Jurassic, in McCann, T. ed. (2008) *The Geology of Central Europe, volume 2: Mesozoic and Cenozoic*, London, Geological Society of London: 823-922.

Pirrie, D. and Marshall, J.D. (1990) High-paleolatitude Late Cretaceous paleotemperatures: New data from James Ross Island, Antarctica, *Geology*, 18(1): 31-34.

Podlaha, O., Mutterlose, J. and Veizer, J. (1998) Preservation of $\delta^{18}O$ and $\delta^{13}C$ in belemnite rostra from the Jurassic/Early Cretaceous successions, *American Journal of Science,* 298: 324– 347.

Popp, B. N., F. A. Podosek, J. C. Brannon, T. F. Anderson, and J. Pier (1986). 87Sr/86Sr Ratios in Permo-Carboniferous seawater from the analyses of well preserved brachiopod shells, *Geochimica et Cosmochimica Acta*, 50: 1321– 1328.

Powell, J.H. and Riding, J.B. (2016) Stratigraphy, sedimentology and structure of the Jurassic (Callovian to Lower Oxfordian) succession at Castle Hill, Scarborough, North Yorkshire, UK, *Proceedings of the Yorkshire Geological Society*, 61: 109-133.

Prada, F., Yam, R., Levy, O., Caroselli, E., Falini, G., Dubinsky, Z., Goffredo, S. and Shemesh, A. (2019) Kinetic and metabolic isotope effects in zooxanthellate and non-zooxanthellate Mediterranean coral along a wide latitudinal gradient, *Frontiers in Marine Science*, 6(522) Available at <https://doi.org/10.3389/fmars.2019.00522>. Accessed [12 February 2021].

Price, G.D. (1999) The evidence and implication of polar ice during the Mesozoic, *Earth Science Reviews*, 48: 183–210.

Price, G. D. and Mutterlose, J. (2004) Isotopic signals from late Jurassic-early Cretaceous (Volgian-Valanginian) sub-Arctic belemnites, Yatria River, Western Siberia, *Journal of the Geological Society, London,* 161: 959-968.

Price, G.D. and Sellwood, B.W. (1997) "Warm" palaeotemperatures from high Late Jurassic palaeolatitudes (Falkland Plateau): Ecological, environmental or diagenetic controls? *Palaeogeography, Palaeoclimatology, Palaeoecology,* 129(3-4):315-327.

Price, G.D., Janssen, N.M.M., Martinez, M., Company, M., Vandevelde, J.H. and Grimes, S.T. (2018) A high-resolution belemnite geochemical analysis of Early Cretaceous (Valangian-Hauterivian) environmental and climatic perturbations, *Geochemistry, Geophysics, Geosystems*, 19(10): 3832-3843.

Purton, L.M.A., Sheilds, G.A., Brasier, M.D. and Grime, G.W. (1999) Metabolism controls Sr/Ca ratios in fossil aragonitic mollusks, *Geology*, 27(12): 1083-1086.

Qing, H. and Veizer, J. (1994) Oxygen and carbon isotope composition of Ordovician brachiopods: implications for coeval seawater, *Geochimica et Cosmochimica Acta*, 58(2): 4429-4442.

Railsback, L.B., Anderson, T.F., Ackerly, S.C. and Cisne, J.L. (1989) Paleoceanographic modelling of temperature-salinity profiles from stable isotopic data, *Paleoceanography*, 4: 585-591.

Rais, P., Louis-Schmid, B., Bernasconi, S.M. and Weissert, H. (2007) Palaeoceanographic and palaeoclimatic reorganization around the Middle–Late Jurassic transition, *Palaeogeography, Palaeoclimatology, Palaeoecology*, 251(3-4): 527-546.

Rasmussen, E.S., Lomholt, S., Andersen, C. and Vejbaek, O.V. (1998) Aspects of the structural evolution of the Lusitanian Basin in Portugal and the shelf and slope area offshore Portugal, *Tectonophysics*, 300: 199-225.

Ravelo, A. C. and Hillaire-Marcel, C. (2007) The use of oxygen and carbon isotopes of formainifera in paleoceanography, in Hillaire-Marcel, C. and De Vernal, A. eds. (2007) *Developments in marine geology, volume 1,* Amsterdam, Elsevier: 735-764.

Remane, J. (2003) Chronostratigraphic correlations: their importance for the definition of geochronologic units. *Palaeogeography, Palaeoclimatology, Palaeoecology,* 196: 7-18.

Remane, J., Bassett, M.G., Cowie, J.W., Gohrbandt, K.H., Lane, H.H., Michelsen, O. and Naiwen, W. (1996) Revised guidelines for the establishment of global chronostratigraphic standards by the International Commission on Stratigraphy (ICS), *Episodes*, 19(3): 77-81.

Rexfort, A. and Mutterlose, J. (2006) Stable isotope record from *Sepia officinalis* - a key to understanding the ecology of belemnites? *Earth and Planetary Science Letters,* 247:212-221.

Rexfort, A. and Mutterlose, J. (2009) The role of biogeography and ecology on the isotope signature of cuttlefishes (Cephalopoda, Sepiidae) and the impact on belemnite studies, *Palaeogeography, Palaeoclimatology, Palaeoecology,* 284: 153-163.

Richter, R. (1928) Aktuopaläontologie und Paläobiologie, eine Abgrenzung, *Senckenbergiana*, 10: 285-292.

Richter, D.K., Neuser, R.D., Schreuer, J., Gies, H. and Immenhauser, A. (2011). Radiaxial–fibrous calcites: a new look at an old problem, *Sedimentary Geology*, 239: 23–36.

Rocha, R., Henriques, M.H.P., Soares, A.F., Mouterde, R., Caloo, B., Ruget, C. and Fernández-López, S. (1990) The Cabo Mondego section as a possible Bajocian boundary stratotype, *Memorie Descrittive della Carta Geologica d'I*, XL: 49-60.

Rocha, J., Brilha, J. and Henriques, M.H. (2014) Assessment of the geological heritage of Cape Mondego Natural Monument (Central Portugal), *Proceedings of the Geologists' Association*, 125(1): 107-113.

Rogov, M. A., and V. A. Zakharov (2010), Jurassic and Lower Cretaceous glendonite occurrences and their implication for arctic paleoclimate reconstructions and stratigraphy, *Earth Science Frontiers*, 17: 345–347.

Rosales, I., Quesada, S. and Robles, S. (2004a) Paleotemperature variations of Early Jurassic seawater recorded in geochemical trends of belemnites from the Basque–Cantabrian basin, northern Spain, *Palaeogeography, Palaeoclimatology, Palaeoecology*, 203: 253-275.

Rosales, I., Robles, S and Quesada, S. (2004b). Elemental and oxygen isotope composition of Early Jurassic belemnites: salinity vs. temperature signals, *Journal of Sedimentalogical Research*, 74: 342-354.

Rosales, I., Barnolas, A., López-García, J.M. and Sevillano, A. (2021) Strontium isotope stratigraphy (SIS) dating of the Bathonian regression in western Tethys (Mallorca Island), *Journal of Iberian Geology*, Available at<https://doi.org/10.1007/s41513-020-00143-y> Access [6 January 2021].

Sælen, G. (1989) Diagenesis and construction of the belemnite rostrum, *Palaeontology*, 32(4): 765-798.

Sælen, G., Doyle, P. and Talbot, M. (1996) Stable-Isotope Analyses of Belemnite Rostra from the Whitby Mudstone Fm., England: Surface Water Conditions during Deposition of a Marine Black Shale, *Palaios,* 11(2): 97-117.

Saltzman, M.R. and Thomas, E. (2012). Carbon isotope stratigraphy, in Gradstein, F.M., Ogg, J.G., Schmitz, M.D. and Ogg, G.M. eds. (2012) The Geological Time Scale 2012, Amsterdam, Elsevier: 207-232

Salvador, A. (1994) *International Stratigraphic Guide: A Guide to Classification, Terminology, and Procedure*, 2nd ed, New York, John Wiley & Sons.

Sandoval, J. (1983) *Bioestratigrafía y paleontología (Stephanocerataceae y Perisphinctaceae) del Bajocense y Bathonense en las Cordilleras Béticas*, PhD Thesis, Granada University.

Sandoval, J. (1990) A revision of the Bajocian divisions in the Subbetic Domain (southern Spain), *Memoire descrittive della Carta Geologica d'Italia*, 40: 141-162.

Sandoval, J., O'Dogherty, L., Aguado, R., Bartolini, A., Bruchez, S. and Bill, M. (2008) Aalenian carbon-isotope stratigraphy: calibration with ammonite, radiolarian and nannofossil events in the Western Tethys, *Palaeogeography, Palaeoclimatology, Palaeoecology*, 267: 115-137.

Saruwatari, K., Satoh, M., Harada, N., Suzuki, I. and Shiraiwa, Y. (2016) Change in coccolith size and morphology due to response to temperature and salinity in coccolithophore *Emiliania huxleyi* (Haptophyta) isolated from the Bering and Chukchi seas, *Biogeosciences,* 13: 2743-2755.

Savard, M.M., Veizer, J. and Hinton, R. (1995) Cathodoluminescence at low Fe and Mn concentrations: a SIMS study of zones in natural calcites, *Journal of Sedimentary Research,* 65(1):208-213.

Schäfer, W. (1962) *Aktuo-paläontologie nach Studien in der Nordsee*, Frankfurt, Waldemar Kramer.

Schoeller, D.A. (1999) Isotope fractionation: why aren't we what we eat? *Journal of Archaeological Science*, 26: 667-673.

Sellwood, B.W. and Valdes, P.J. (2008). Jurassic climates, *Proceedings of the Geologists' Association,* 199(1): 5-17.

Shackleton, N.J. (1987) Oxygen isotopes, ice volume and sea level, *Quaternary Science Reviews*, 6(3-4): 183-190.

Shackleton, N.J. and Kennett, J.P. (1975) Paleotemperature history of the Cenozoic and initiation of Antarctic glaciation: oxygen and carbon isotope analyses in DSDP sites 277, 279 and 289, *Initial Reports of the Deep Sea Drilling Project*, 29: 743-755.

Shackleton, N., Hall, M., Line, J. and Shuxi, C. (1983) Carbon isotope data in core V19-30 confirm reduced carbon dioxide concentration in the ice age atmosphere, *Nature*, 306: 319-322.

Sharp, Z. (2007) *Principles of stable isotope geochemistry*, Princeton, Pearson Education.

Showers, W.J., Barrick, R. and Genna, B. (2002) Isotopic analysis of dinosaur bones: A new pyrolysis technique provides direct evidence that some dinosaurs were warm-blooded, *Analytical Chemistry,* 74: 142-150.

Silva, R.L., Mendonça Filho, J.G. Azerêdo, A.C. and Duartem L.V. (2013) Palynofacies and TOC analysis of marine and non-marine sediments across the Middle–Upper Jurassic boundary in the central-northern Lusitanian Basin (Portugal), *Facies*, 60: 255-276.

Sipple, R. F. and Glover, E. D. (1965) Structures in carbonate rocks made visible by luminescence petrography, *Science*, 150(3701): 1283-1287.

Smith, A. G., Barry, T., Bown, P., Cope, J., Gale, A., Gibbard, P., Gregory, J., Hounslow, M., Kemp, D., Knox, R., Marshall, J., Oates, M., Rawson, P., Powell, J. and Water, C. (2014) GSSPs, global stratigraphy and correlation, *Geological Society, London, Special Publications*, 404: 37-67.

Sørensen, A.M., Ullmann, C.V., Thibault, N. and Korte, C. (2015) Geochemical signatures of the early Campanian belemnite *Belemnellocamax mammillatus* from the Kristianstad Basin in Scania, Sweden, *Palaeogeography, Palaeoclimatology, Palaeoecology*, 433: 191-200.

Spaeth, C. (1971) Aragonitische und calcitische Primärstrukturen im Schalenbau eines Belemniten aus der englischen Unterkreide, *Paläontologische Zeitschrift*, 45: 33–40.

Spaeth, C. (1973) Weitere Untersuchungen der Primär- und Fremdstrukturen in calcitischen und aragonitischen Schalenlagen englischer Unterkreide-Belemniten, *Paläontologische Zeitschrift,* 47: 163–174.

Spaeth, C. (1975) Zur Frage der Schwimmverhältnisse bei Belemniten in Abhängigkeit vom Primärgefüge der Hartteile, *Paläontologische Zeitschrift,* 49: 321–331.

Spaeth, C.H.R., Hoefs, J. and Vetter, U. (1971) Some aspects of isotopic composition of belemnites and related paleotemperatures, *Geological Society of America Bulletin*, 82: 3139-3150.

Stanley, S.M. (2010). Relation of Phanerozoic stable isotope excursions to climate, bacterial metabolism, and major extinctions, *PNAS*, 107(45): 19185-19189.

Stevens, K., Griesshaber, E., Schmahl, W., Casella, L. A., Iba, Y. and Mutterlose, J. (2020) Belemnite biomineralization, development, and geochemistry: The

complex rostrum of *Neohibolites minimus, Palaeogeography, Palaeoclimatology, Palaeoecology*, 468: 388-402.

Stoll, H.M. and Schrag, D.P. (2001) Sr/Ca variations in Cretaceous carbonates: relation to productivity and sea level changes, *Palaeogeography, Palaeoclimatology, Palaeoecology*, 168(3-4): 311-336.

Tang, J., Köhler, S.J., and Dietzel, M. (2008) Sr^{2+}/Ca^{2+} and $^{44}Ca/^{40}Ca$ fractionation during inorganic calcite formation: I. Sr incorporation, *Geochimica et Cosmochimica Acta*, 72: 3718-3732.

Taylor, B.E. and Ward, P.D. (1983) Stable isotopic studies of *Nautilus macromphalus* Sowerby (New Caledonia) and *Nautilus pompilius* L. (Fiji), *Palaeogeography, Palaeoclimatology, Palaeoecology,* 41(1-2):1-16.

Terzidis, A. (1966) Der Braune Jura im Gebiet zwischen Eningen und Glems (Mittlere Schwäbische Alb, Württemberg), *Jahresberichte und Mitteilungen des oberrheinischen geologischen Vereins, Neue Folge*, 48: 31-68.

Thomas. C.D., Cameron, A., Green, R.E., Bakkenes, M., Beaumont, L.J., Collingham, Y.C., Erasmus, B.F.N., de Siqueirra, M.F., Grainger, A., Hannah, L., Huges, L., Huntley, B., van Jaarveld, A.S., Midgley, G.F., Miles, L., Ortega-Huerta, M.A., Peterson, T., Philips, O.L. and Williams, S.E. (2004). Extinction risk from climate change, *Nature*, 427:145-148.

Trincão, P., Lopes, E., de Carvalho, J., Ataide, S. and Perrolas, M. (2018) Beyond Time and Space—The Aspiring Jurassic Geopark of Figueira da Foz, *Geosciences*, 8(6). Available at: <https://doi.org/10.3390/geosciences8060190> [Accessed 12 May 2019].

Ullmann, C.V. and Korte, C. (2015) Diagenetic alteration in low-Mg calcite from macrofossils: a review, *Geological Quarterly,* 59(1):3-20.

Ullmann, C.V. and Pogge von Strandmann, P.A.E. (2017) The effect of shell secretion rate on Mg/Ca and Sr/Ca ratios in biogenic calcite as observed in a belemnite rostrum, *Biogeosciences*, 14:89-97.

Ullmann, C.V., Hesselbo, S.P. and Korte, C. (2013a) Tectonic forcing of Early to Middle Jurassic seawater Sr/Ca, *Geology*, 41(12):1211-1214.

Ullmann, C.V., Böhm, F., Rickaby, R.E.M., Wiechert, U. and Korte, C. (2013b) The Giant Pacific Oyster (*Crassostrea gigas*) as a modern analogy for fossil ostreoids: Isotopic (Ca, O, C) and elemental (Mg/Ca, Sr/Ca, Mn/Ca) proxies, G*eochemistry, Geophysics, Geosystems*, 14(10): 4109-4120.

Ullmann, C.V., Thibault, N., Ruhl, M., Hesselbo, S.P. and Korte, C. (2014) Effect of a Jurassic Oceanic Anoxic Event on belemnite ecology and evolution, *PNAS*, 111: 10073-10076.

Ullmann, C.V., Frei, R., Korte, C. and Hesselbo, S.P. (2015) Chemical and isotopic architecture of the belemnite rostrum, *Geochimica et Cosmochimica Acta*, 159: 231-243.

Ullmann, C.V., Frei, R., Korte, C. and Lüter, C. (2017). Element/Ca, C and O isotope ratios in modern brachiopods: Species-specific signals of biomineralization, *Chemical Geology*, 460: 15-24.

Ullmann, C., Boyle, R., Duarte, L.V., Hesselbo, S.P., Kasemann, S.A., Klein, T., Lenton, T.M., Piazza, V. and Aberhan, M. (2020) Warm afterglow from the Toarcian Oceanic Anoxic Event drives the success of deep-adapted brachiopods, *Scientific Reports*, 10. Available at < https://doi.org/10.1038/s41598-020-63487-6>. Accessed [15 October 2020].

Urey, H.C. (1947). The thermodynamic properties of isotopic substances, *Journal of the Chemical Society*, 1947: 562-581.

Urey, H.C., Lowenstam, H.A. and McKinney, C.R (1951). Measurement of paleotemperatures and temperatures of the Upper Cretaceous of England, Denmark, and the southeastern United-States, *Geological Society of America Bulletin*, 62: 399-416.

van de Schootbrugge, B., Föllmi, K.B., Bulot, L.G. and Burns, S.J. (2000) Paleoceanographic changes during the early Cretaceous (Valanginian–Hauterivian): evidence from oxygen and carbon stable isotopes, *Earth and Planetary Science Letters,* 181: 15-31.

Veizer, J. (1974). Chemical diagenesis of belemnite shells and possible consequences for paleotemperature determination, *Neues Jahrbuch für Geologie und Paläontologie, Abhandlungen*, 147: 91–111.

Veizer, J. (1983) Chemical diagenesis of carbonates: theory and application of trace element technique. *SEPM Short Course*, 10: 1-100.

Veizer, J. (1989) Strontium isotopes in seawater through time, *Annual Review of Earth and Planetary Sciences*, 17: 141-167.

Veizer, J., Fritz, P. and Jones, B. (1986) Geochemistry of brachiopods: oxygen and carbon isotopic records of Paleozoic oceans, *Geochimica et Cosmochimica Acta*, 50: 1679–1696.

Vervoort, P., Adloff, M., Greene, S.E. and Kirtland Turner, S. (2019) Negative carbon isotope excursions: an interpretive framework, *Environmental Research Letters*, 14 (8). Available at <https://iopscience.iop.org/article/10.1088/1748-9326/ab3318>. Accessed [18 January 2020].

Voigt, S., Wilmsen, M., Mortimore, R.N. and Voigt, T. (2003) Cenomanian palaeotemperatures derived from the oxygen isotopic composition of brachiopods and belemnites: evaluation of Cretaceous palaeotemperature proxies, *International Journal of Earth Sciences,* 92: 285–299.

Watkinson M. P. (1989) *Triassic to Middle Jurassic sequences from the Lusitanian Basin, Portugal, and their equivalents in other North Atlantic margin basins*, PhD thesis, The Open University.

Webber, D.M. and O'Dor, R.K. (1986) Monitoring the metabolic rate and activity of free-swimming squid with telemetered jet pressure*, Journal of Experimental Biology*, 126: 205-224.

Wefer, G. and Berger, W.H. (1991) Isotope paleontology: growth and composition of extant calcareous species, *Marine Geology*, 100(1-4): 207-248.

Westermann, G.E.G. and Callomon, J.H. (1988) The Macrocephalitinae and associated Bathonian and Early Callovian (Jurassic) ammonoids of the Sula Islands and New Guinea, *Palaeontographica*, 203: 1-90.

Wierzbowski, H. (2002) Detailed oxygen and carbon isotope stratigraphy of the Oxfordian in Central Poland, *Internal Journal of Earth Sciences*, 91(2): 304-314.

Wierzbowski, H. (2004) Carbon and oxygen isotope composition of Oxfordian-Early Kimmeridgian belemnite rostra: Palaeoenvironmental implications for Late Jurassic seas, *Palaeogeography. Palaeoclimatology. Palaeoecology,* 203: 153-168.

Wierzbowski, H. and Joachimski, M.M. (2007) Reconstruction of the Bajocian-Bathonian marine palaeoenvironments using carbon and oxygen isotope ratios of calcareous fossils from the Polish Jura Chain (central Poland), *Palaeogeography, Palaeoclimatology, Palaeoecology,* 254: 523-540.

Wierzbowski, H. and Joachimski, M.M. (2009). Stable isotopes, elemental distribution, and growth rings of belemnopsid belemnite rostra: proxies for belemnite life habitat, *Palaios,* 24(5-6):377-386.

Wierzbowski, H. and Rogov, M. (2010) Reconstructing the palaeoenvironment of the Middle Russian Sea during the Middle–Late Jurassic transition using stable isotope ratios of cephalopod shells and variations in faunal assemblages, *Palaeogeography, Palaeoclimatology, Palaeoecology*, 299 (2011): 250–264.

Wierzbowski, H., Dembicz, K. and Praszkier, T. (2009) Oxygen and carbon isotope composition of Callovian–Lower Oxfordian (Middle–Upper Jurassic) belemnite rostra from central Poland: A record of a Late Callovian global sea-level rise? *Palaeogeography, Palaeoclimatology, Palaeoecology*, 283(3-4): 182-194.

Wierzbowski, H., Anczkiewicz, R., Bazarnik, J. and Pawlak, J. (2012) Strontium isotope variations in Middle Jurassic (Late Bajocian–Callovian) seawater: implications for Earth's tectonic activity and marine environments, *Chemical Geology*, 334: 171–181.

Wierzbowski, H., Anczkiewicz, R., Pawlak, J., Rogov, M.A. and Kuznetsov, A.B. (2017) Revised Middle–Upper Jurassic strontium isotope stratigraphy, *Chemical Geology*, 466: 239-255.

Wilbur, K. M. (1972) Shell formation in mollusks, in Florkin M. and Scheer, B.T. eds. (1972) *Chemical Zoology Volume VII: Mollusca,* London, Academic Press: 103-146.

Wilkin, J.T.R. (2018) Isotopes and palaeoclimates, Geology Today, 34(6): 208-209.

Wilmsen, M. and Niebuhr, B. (2017) High-resolution Campanian–Maastrichtian carbon and oxygen stable isotopes of bulk-rock and skeletal components: palaeoceanographic and palaeoenvironmental implications for the Boreal shelf sea, *Acta Geologica Polonica,* 67(1): 47-74.

Zachos, J., Pagani, M., Sloan, L., Thomas, E. and Billups, K. (2001) Trends, rhythms, and aberrations in global climate 65 Ma to Present, *Science*, 292(5517): 686-693

Zakharov, Y.D., Shigeta, Y., Smyshlyaeva, O.P., Popov, A.M. and Ignatiev, A.V. (2006) Relationships between $\delta^{13}C$ and $\delta^{18}O$ values of the recent *Nautilus* and brachiopod shells in the wild and the problem of reconstruction of fossil cephalopod habitat, *Geosciences Journal,* 10: 331-345.

Zondervan, I., Zeebe, R.E., Rost, B. and Riebesell, U. (2001) Decreasing marine biogenic calcification: A negative feedback on rising atmospheric pCO_2, *Global Biochemical Cycles,* 15(2):507-516.